Metabolic subtyping and targeting of pancreatic ductal adenocarcinoma

Inaugural Dissertation

for

the doctoral degree of

Dr. rer. nat.

from the Faculty of Biology

University of Duisburg-Essen

Germany

Submitted by

Sinan Karakaya

Born in Mersin

August, 2020

The experiments underlying the present work were conducted at Institute for Developmental Cancer Therapeutics, West German Cancer Center, University Hospital Essen and at the Division of Solid Tumour Translational Oncology, German Cancer Consortium (DKTK) partner site Essen/Düsseldorf (Director: Prof. Dr. Jens Siveke).

1. Examiner: Prof. Dr. Jens Siveke

2. Examiner: Prof. Dr. Verena Jendrossek

3. Examiner:

Chair of the Board of Examiners: Prof. Dr. Joachim Foundrey

Date of the oral examination: 11.12.2020

DOI: 10.17185/duepublico/73673
URN: urn:nbn:de:hbz:464-20220131-073251-6

Table of Contents

List of abbreviations

Abbreviation	Description
A/A	Antibiotic-Antimycotic
ABCD3	ATP Binding Cassette Subfamily D Member 3
ACAA1/2	Acetyl-CoA Acyltransferase 1/2
ACACA/B	Acetyl-CoA Carboxylase Alpha/Beta
ACAD8	Acyl-CoA Dehydrogenase Family Member 8
ACAD9	Acyl-CoA Dehydrogenase Family Member 9
ACADL	Acyl-CoA Dehydrogenase Long Chain
ACADM	Acyl-CoA Dehydrogenase Medium Chain
ACADS	Acyl-CoA Dehydrogenase Short Chain
ACADSB	Acyl-CoA Dehydrogenase Short/Branched Chain
ACADVL	Acyl-CoA Dehydrogenase Very Long Chain
ACAT1/2	Acetyl-CoA Acetyltransferase 1/2
ACLY	ATP Citrate Lyase
ACOT1/2/4/6/7/8/9	Acyl-CoA Thioesterase 1/2/4/6/7/8/9
ACOX1/3	Acyl-CoA Oxidase 1/3
ACSBG1/2	Acyl-CoA Synthetase Bubblegum Family Member 1/2
ACSL1/3/4/5/6	Acyl-CoA Synthetase Long Chain Family Member 1/3/4/5/6
ACSM3/6	Acyl-CoA Synthetase Medium Chain Family Member 3/6
ACSS2	Acyl-CoA Synthetase Short Chain Family Member 2
ADEX	Aberrantly Differentiated Endocrine Exocrine Subtype
ADP	Adenosine Diphosphate
AKT	Protein Kinase B
ASNS	Asparagine Synthetase
ATM	ATM Serine/Threonine Kinase
ATP	Adenosine Triphosphate
BCA	Bicinchoninic Acid
BODIPY	4, 4-Difluoro-4-Bora-3a, 4a-Diaza-S-Indacene.
BRAF	B-Raf Proto-Oncogene, Serine/Threonine Kinase
BRCA1/2	Brca1/2 DNA Repair Associated
BSA	Bovine Serum Albumin
CARM1	Coactivator-Associated Arginine Methyltransferase 1

CDK6	Cyclin Dependent Kinase 6
CDKN2A	Cyclin Dependent Kinase Inhibitor 2A
cDNA	Complementary DNA
CoA	Coenzyme A
CPT1/2	Carnitine Palmitoyltransferase 1/2
CRAT	Carnitine O-Acetyltransferase
CS	Citrate Synthetase
DAB	3,3'-Diamine Benzidine
DAPI	4′,6-Diamidino-2-Phenylindole
DECR1	2,4-DiEnoyl-CoA Reductase 1
DG	Diacylglycerol
DMEM	Dulbecco's Modified Eagle Medium
DMSO	Dimethyl Sulfoxide
DNA	Deoxyribonucleic Acid
DTT	Dithiothreitol
ECAR	Extracellular Acidification Rate
ECH1	Enoyl-CoA Hydratase 1
ECHS1	Enoyl-CoA Hydratase, Short Chain 1
ECI1/2	Enoyl-CoA Delta Isomerase 1/2
EDTA	Ethylenediaminetetraacetic Acid
EGFR	Epidermal Growth Factor Receptor
EHHADH	Enoyl-CoA Hydratase And 3-Hydroxyacyl CoA Dehydrogenase
ELOVL1	ELOVL Fatty Acid Elongase 1
EMT	Epithelial–Mesenchymal Transition
ENO1/2	Enolase 1/2
ERK	Extracellular Signal Regulated Kinases
ETC	Electron Transport Chain
FA	Fatty Acid
FAD	Flavin Adenine Dinucleotide
FADS1	Fatty Acid Desaturase 1
FAO	Fatty Acid Oxidation
FASN	Fatty Acid Synthase
FBS	Foetal Bovine Serum

FBXW7	F-Box And Wd Repeat Domain Containing 7
FDR	False Discovery Rate
FFA	Free Fatty Acid
FFPE	Formalin-Fixed Paraffin-Embedded
FPP	Farnesyl Pyrophosphate
GAPDH	Glyceraldehyde-3-Phosphate Dehydrogenase
GATA6	Gata Binding Protein 6
GFPT1	Glutamine--Fructose-6-Phosphate Transaminase 1
GLS1	Glutaminase
GLUD1	Glutamate Dehydrogenase 1
GLUT1	Solute Carrier Family 2 Member 1/Slc2a1
GOT2	Glutamic-Oxaloacetic Transaminase 2
GSEA	Gene Set Enrichment Analysis
GSH	Glutathione
GUSB	Beta Glucuronidase
HADH	Hydroxyacyl-CoA Dehydrogenase
HADHA/B	HADHA Trifunctional Multienzyme Complex Subunit Alpha/Beta
HBP	Hexosamine Biosynthesis Pathway
HEPES	4-(2-Hydroxyethyl)-1-Piperazineethanesulfonic Acid
HER2	Human Epidermal Growth Factor Receptor 2 /Erbb2
HGF	Hepatocyte Growth Factor
HIF1A	Hypoxia Inducible Factor 1 Subunit Alpha
HK1/2	Hexokinase 1/2
HMDB	Human Metabolome Database
HMG-CoA	3-Hydroxy-3-Methylglutaryl Coenzyme A
HMGCR	3-Hydroxy-3-Methylglutaryl Coenzyme A Reductase
HRP	Horseradish Peroxidase
IC_{50}	Half Maximal Inhibitory Concentration
IF	Immunofluorescence
IHC	Immunohistochemistry
IPMN	Intraductal Papillary Mucinous Neoplasm
IVD	Isovaleryl-CoA Dehydrogenase
KEGG	Kyoto Encyclopedia Of Genes And Genomes

KRAS	V-Ki-Ras2 Kirsten Rat Sarcoma Viral Oncogene Homolog
KRT81	Keratin 81
LDHA/B	Lactate Dehydrogenase A/B
LDLR	Low Density Lipoprotein Receptor
LPA	Lysophosphatidic Acid
LPC	Lysophosphatidylcholine
LPE	Lysophosphatidylethanolamine
LPG	Lysophosphatidylglycerol.
LPI	Lysophosphatidylinositol
LPS	Lysophosphatidylserine
MCN	Mucinous Cystic Pancreatic Neoplasms
MCT1/SLC16A1	Monocarboxylate Transporter 1
MCT4/SLC16A3	Monocarboxylate Transporter 4
MDH1	Malate Dehydrogenase 1
ME1	Malic Enzyme
MECR	Mitochondrial Trans-2-Enoyl-CoA Reductase
MLL3	Lysine Methyltransferase 2c
MPC	Mitochondrial Pyruvate Carrier Complex
MPC1/2	Mitochondrial Pyruvate Carrier 1/2
mRNA	Messenger RNA
MUFA	Monounsaturated Fatty Acids
MYC	MYC Proto-Oncogene, BHLH Transcription Factor
NAD	Nicotinamide Adenine Dinucleotide
NADPH	Nicotinamide Adenine Dinucleotide Phosphate
NES	Negative Enrichment Score
NSCLC	Non-Small-Cell Lung Carcinoma
OCR	Oxygen Consumption Rate
OXPHOS	Oxidative Phosphorylation
P/S	Penicillin-Streptomycin
PALB2	Partner And Localizer Of Brca2
PanIN	Pancreatic Intraepithelial Neoplasia
PARP	Poly(ADP-Ribose) Polymerase
PBS	Phosphate-Buffered Saline

PC	Phosphatidylcholine
PCR	Polymerase Chain Reaction
PDAC	Pancreatic Ductal Adenocarcinoma
PDH	Pyruvate Dehydrogenase
PDK	Pyruvate Dehydrogenase Kinase
PDX	Patient Derived Xenograft
PE	Phosphatidylethanolamine
PEP	Phosphoenolpyruvate
PFA	Paraformaldehyde
PFK1	Phosphofructokinase 1
PI3Ks	Phosphoinositide 3-Kinases
PKLR	Pyruvate Kinase L/R
PKM1/2	Pyruvate Kinase Isoform M1/2
PLIN2	Perilipin 2
PNET	Pancreatic Neuroendocrine Tumours
PNPLA2	Patatin Like Phospholipase Domain Containing 2
PPP	Pentose Phosphate Pathway
PRODH1	Proline Oxidase
PUFA	Polyunsaturated Fatty Acid
QM	Quasi-Mesenchymal
RFU	Relative Fluorescence Unit
RNA	Ribonucleic Acid
ROI	Region Of Interest
ROS	Reactive Oxygen Species
RPE	Ribulose-5-Phosphate-3-Epimerase
RPIA	Ribose 5-Phosphate Isomerase A
RPMI	Roswell Park Memorial Institute
SCD	Stearoyl-CoA Desaturase
SCD5	Stearoyl-CoA Desaturase 5
SDS	Sodium Dodecyl Sulphate
SFA	Saturated Fatty Acid
SLC25A20	Solute Carrier Family 25 Member 20
SM	Sphingomyelin

SMAD4	SMAD Family Member 4
SMARCA4	SWI/SNF related, matrix associated, actin dependent regulator of chromatin, subfamily a, member 4
SREBP1/2	Sterol Regulatory Element Binding Protein 1/2
TBS	Tris-Buffered Saline
TCA	Tricarboxylic Acid
TCGA	The Cancer Genome Atlas
TNBC	Triple-Negative Breast Cancer
TP53	Tumour Protein P53
TRIS	Tris-(Hydroxymethyl)-Aminomethan
VEGF	Vascular Endothelial Growth Factor

List of figures

List of tables

Abstract

Pancreatic Ductal Adenocarcinoma (PDAC) is one of the deadliest malignancies in the world due to late diagnosis and lack of effective treatment. Thus, novel therapies are desperately needed. PDAC is presented in two molecular subtypes, Quasi-mesenchymal (QM, Basal-like) and classical (pancreatic progenitor). Recent studies showed that these subtypes clinically differ as well with classical subtype being more therapy responsive and with somewhat better prognosis.

This study aimed to identify which metabolic pathways are activated in one and the other subtype and whether these metabolic differences are functionally preserved in relevant preclinical PDAC models that may be further used for the development of subtype-specific metabolic therapies.

To this aim, established PDAC cell lines, Patient-Derived Xenografts, primary cells and patient samples were used as models. Gene expression analyses (RNA-seq, microarray, qPCR and GSEA) revealed that QM subtype is dominated by the metabolic transcripts involved in glycolysis and hypoxia whereas classical subtype is branded with gene sets involved in lipid and fatty acid metabolism. Functional seahorse metabolic flux assays also supported the transcriptome data that glycolysis and fatty acid oxidation are active metabolic processes in QM and classical subtype, respectively. Furthermore, immunohistological approaches identified lactate transporter MCT4 as a putative marker of glycolytic/QM PDACs in patient-related materials. However, functional heterogeneity and different levels of glycolysis and fatty acid oxidation usage were also present among members of the same subtype. Accordingly, analyzed chemical inhibitors of glycolysis and lipid metabolism did not present strong subtype dependent activity.

Even though glycolysis and fatty acid oxidation are dominant in QM and classical subtype respectively, identified functional heterogeneity indicates fine-tuning of metabolic dependencies and mixed usage of different metabolic pathways even in one transcriptional subtype. In a personalized approach, a patient with a transcriptional signature of QM and functionally active glycolysis would be an obvious candidate for metabolic targeting of glycolysis. However, due to the mixed usage of different metabolic pathways as well, further preclinical and clinical efforts are needed for evaluating the potential of combinatorial usage of metabolic inhibitors.

Zusammenfassung

Das duktale Adenokarzinom des Pankreas (*engl. PDAC*) ist, bedingt durch die meist späte Diagnosestellung und den Mangel an effektiven Behandlungen, eine der tödlichsten Tumorerkrankungen der Welt, weshalb neuartige Therapien dringend benötigt werden. PDAC liegt in zwei molekularen Subtypen vor, Quasi-Mesenchymal (QM, Basal-ähnlich) sowie klassisch (pankreatischer Vorläufer). Aktuelle Studien zeigen, dass diese Subtypen sich klinisch unterscheiden und der klassische Subtyp stärker auf Therapien anspricht und eine etwas bessere Prognosen hat.

Das Ziel dieser Arbeit war es zu identifizieren, welche metabolischen Signalwege in den jeweiligen Subtypen aktiv sind und ob diese metabolischen Unterschiede funktionell in relevanten präklinischen *PDAC* Modellen konserviert sind, um dadurch möglicherweise Subtyp-spezifische, metabolische Therapien zu entwickeln.

Mit diesem Ziel wurden etablierte *PDAC* Zelllinien, *patient derived xenografts* (PDX), primäre Zellen sowie Patientenproben als Modelle verwendet. Genexpressions-Analysen (RNA-seq, *microarray*, qPCR und GSEA) veranschaulichten, dass der QM-Subtyp primär durch metabolische Transkripte, welche in Glykolyse und Hypoxie involviert sind, bestimmt wird. Der klassische Subtyp hingegen ist gekennzeichnet durch Gene, welche im Lipid- und Fettsäure-Metabolismus eine wichtige Rolle spielen. Funktionelle *seahorse metabolic flux assays* unterstützen die Transkriptom-Daten und zeigten, dass die Glykolyse im QM-Subtyp und die Fettsäure-Oxidation im klassischen Subtyp jeweils aktive metabolische Prozesse sind. Zusätzlich wurde durch Immunhistologie-Experimente mit patientenbezogenem Material demonstriert, dass der Laktattransporter MCT4 als möglicher Marker für glykolytische QM-Subtypen in PDAC fungiert. Dennoch waren eine funktionelle Heterogenität und unterschiedliche Stufen von Glykolyse oder Fettsäure-Oxidation in verschiedene Tumormodellen des gleichen Subtyps nachweisbar. Darüber hinaus zeigten chemische Inhibitoren von Glykolyse und Fettsäure-Oxidation keine starken Subtyp-spezifischen Aktivitäten.

Auch wenn Glykolyse und Fettsäure-Oxidation im QM- bzw. klassischen Subtyp primär aktiv sind, deutet die identifizierte, funktionelle Heterogenität darauf hin, dass eine Art *fine tuning* von metabolischen Abhängigkeiten und eine kombinierte Nutzung von metabolischen Signalwegen vorliegt, selbst innerhalb eines transkriptionellen Subtyps. In einem personalisierten Therapieansatz wären Patienten mit Signaturen des QM-Subtyps offensichtliche Kandidaten für eine Behandlung, welche metabolisch die

Glykolyse adressiert. Dennoch sind, zusätzlich bedingt durch die kombinierte Nutzung mehrerer metabolischer Signalwege, weitere präklinische und klinische Bemühungen nötig, um das volle Potential von kombinierter Nutzung von metabolischen Inhibitoren beurteilen zu können.

1 Introduction

1.1 The Pancreas

The pancreas is both an exocrine and endocrine gland supporting digestion and systemic glucose balance, respectively (Shih, Wang, & Sander, 2013). It is located in the abdominal cavity and can be stratified into three macroscopic parts: the head that is connected to the duodenum, the body and pancreas tail that is close to the spleen (Hans G. Beger (Editor), 2018) (Figure 1.1.A). The exocrine part, which has a bigger volume than the endocrine portion, consists of acinar, centroacinar and ductal cells (Larsen & Grapin-Botton, 2017; Zhou & Melton, 2018). The acinar and centroacinar cells are clustered in an acinus and are responsible for the synthesis and secretion of digestive enzymes which are packed into vesicles called zymogens (Larsen & Grapin-Botton, 2017; Zhou & Melton, 2018). Ductal cells build connective branched ductal system through the gland and allow the flow of secreted enzymes (pancreatic juice) to the duodenum to support digestion (Larsen & Grapin-Botton, 2017; Zhou & Melton, 2018) (Figure 1.1.B). The endocrine portion, which comprises around 2 % of the pancreas, is made of Langerhans islets (Kleeff et al., 2016). These islets contain few to several thousand endocrine cells which belong to at least five different cellular subtypes that produce distinct peptide hormones (Brissova et al., 2005; Cabrera et al., 2006; Larsen & Grapin-Botton, 2017). The highest portion amongst endocrine cells in the pancreas belongs to beta cells (50-70%) which secrete insulin followed by glucagon secreting alpha cells (20-40%), somatostatin secreting delta cells (5-10%), ghrelin secreting epsilon cells (<1%) and pancreatic polypeptide cells (<5%) (Brissova et al., 2005; Cabrera et al., 2006; Dolensek, Rupnik, & Stozer, 2015; Hans G. Beger (Editor), 2018) (Figure 1.1.C). The hormones produced by these cells are secreted directly into the bloodstream and control the blood glucose levels (Bastidas-Ponce, Scheibner, Lickert, & Bakhti, 2017).

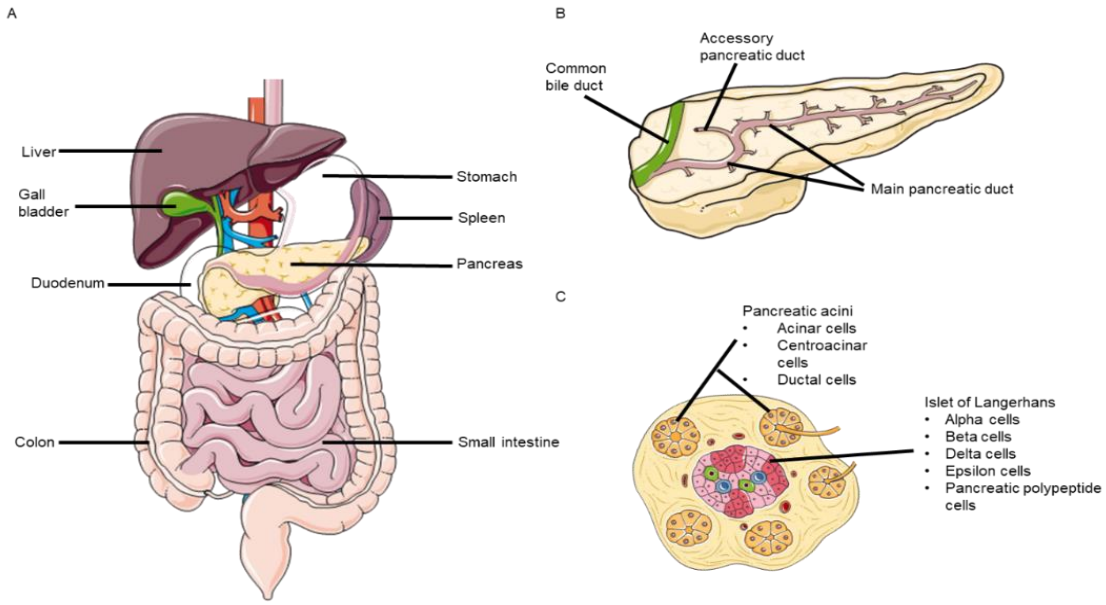

Figure 1.1 **Anatomy of the pancreas.** (A) Location of the pancreas in the body. (B) Gross anatomy of the pancreas. (C) A section from pancreatic tissue containing both endocrine (islet of Langerhans) and exocrine (pancreatic acini) parts. (Drawings obtained from https://smart.servier.com/)

1.2 Tumours of the pancreas

Different benign and malignant tumours of pancreas stemming from almost every pancreatic cell type have been identified with different incidence rates (Kleeff et al., 2016; Mann, Ying, Juan, Jenkins, & Copeland, 2016; Nagtegaal et al., 2020). The most frequently seen malignancies are pancreatic ductal adenocarcinoma (PDAC), pancreatic neuroendocrine tumours (PNET) and acinar cell carcinomas (ACC) (Kleeff et al., 2016). Pancreatic neuroendocrine tumours (deriving from endocrine cells) and acinar cell carcinoma (deriving from acinar cells) account for 2-5% and 1-2% of the cases, respectively, while pancreatic ductal adenocarcinoma (PDAC) constitutes almost 90% of the cases (Kleeff et al., 2016; Mann et al., 2016; Nagtegaal et al., 2020). Therefore, the term ‘pancreatic cancer’ generally refers to pancreatic ductal adenocarcinoma (Bastidas-Ponce et al., 2017; Nagtegaal et al., 2020) (Figure 1.2).

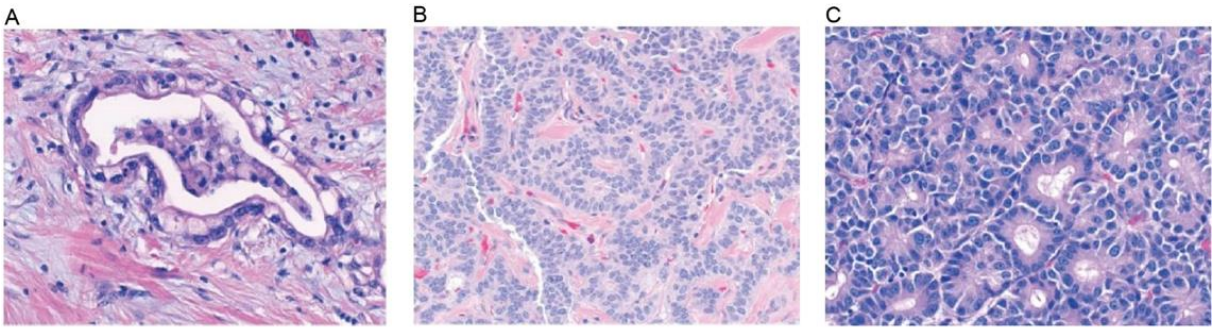

Figure 1.2 **Common tumours of the pancreas.** (A) Pancreatic ductal adenocarcinoma. (B) Pancreatic neuroendocrine tumours. (C) Acinar cell carcinoma. (Adapted from Kleeff et al., 2016 (Kleeff et al., 2016))

1.3 Pancreatic ductal adenocarcinoma (PDAC)

1.3.1 Epidemiology of PDAC

Pancreatic ductal adenocarcinoma is the 7th leading cause of cancer-related deaths worldwide (Bray et al., 2018) (Figure 1.3.A). Both incidence and mortality numbers are expected to be doubled by 2040 unless novel diagnostics and treatment options become available (Bray et al., 2018) (Figure 1.3.B). PDAC is mostly an age-related disease and most of the cases occur after the age of 60 (Bray et al., 2018; Kleeff et al., 2016; Ryan, Hong, & Bardeesy, 2014). Additionally, smoking(Bosetti et al., 2012), diabetes(Ben et al., 2011), obesity (Aune et al., 2012), chronic pancreatitis (Klein et al., 2004) and family history of PDAC (E. J. Jacobs et al., 2010) are cardinal risk factors of the disease and are responsible for one-third of the cases (Bray et al., 2018; Kleeff et al., 2016; Ryan et al., 2014). The five-year survival rate of PDAC, which is around 8%, has not changed much during the last decades (Grasso, Jansen, & Giovannetti, 2017; Ying et al., 2016). The main reasons for the fatal prognosis are late diagnosis due to lack of symptoms and reliable tumour markers, early distant metastasis and resistance to conventional chemotherapies (Biancur & Kimmelman, 2018; Hans G. Beger (Editor), 2018; Kleeff et al., 2016; Lerch et al., 2016).

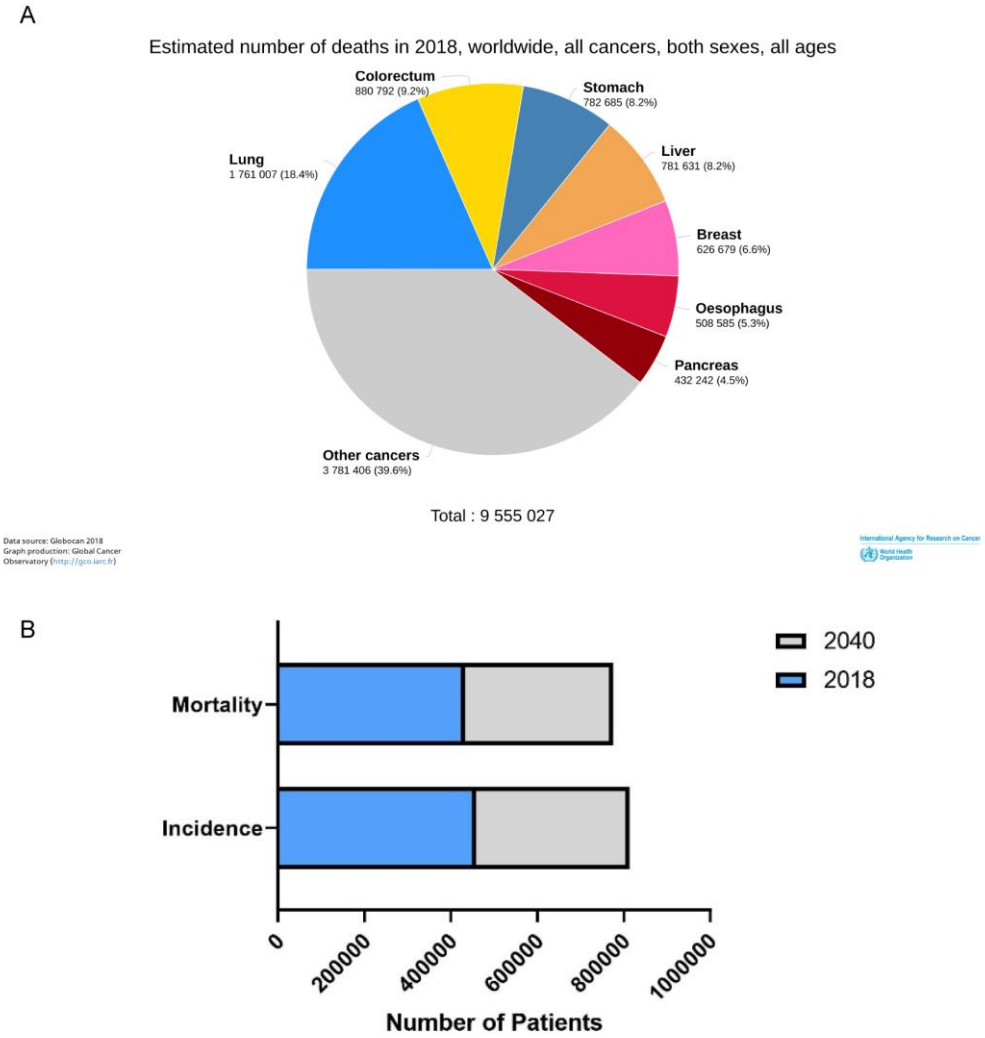

Figure 1.3 **Incidence and mortality rates of pancreatic cancer.** (A) Estimated numbers of cancer-related deaths in 2018. (B) Estimated numbers of PDAC incidence and mortality in 2040. (A, downloaded from Global Cancer Observatory, Cancer Today, http://gco.iarc.fr/; B, adapted from Cancer Tomorrow, http://gco.iarc.fr/)

1.3.2 Molecular pathology of PDAC

PDAC derives from three histologically distinct precursor lesions which are pancreatic intraepithelial neoplasia (PanIN), intraductal papillary mucinous neoplasm (IPMN), and mucinous cystic neoplasm (MCN) (Hans G. Beger (Editor), 2018). PanINs are the most prevalent one among them (Basturk et al., 2015; Kleeff et al., 2016; Oldfield, Connor, & Gallinger, 2017; Ying et al., 2016). The progression from PanIN, IPMN and MCN to advanced PDAC is a long-lasting, gradual process and each step has individual morphologic and genetic features (Distler, Aust, Weitz, Pilarsky, & Grutzmann, 2014; Hans G. Beger (Editor), 2018; Reddy et al., 2004; Zamboni, Hirabayashi, Castelli, & Lennon, 2013). Genomic studies indicate that an oncogenic *KRAS* mutation is the most

frequent genetic alteration found in around 95% of the patients (Aguirre & Collisson, 2017; Bryant, Mancias, Kimmelman, & Der, 2014; Hans G. Beger (Editor), 2018). Inactivation or deletion of tumour suppressor genes *CDKN2A, TP53* and *SMAD4* are the other common mutations seen in PDAC cases that are, together with *KRAS*, called 'the mountains' (Aguirre & Collisson, 2017; Bryant et al., 2014; Hans G. Beger (Editor), 2018) (Figure 1.4). Oncogenic *KRAS* seems to be the main regulator of PDAC and activation of KRAS plays role in both initiation and maintenance of the disease (Aguirre & Collisson, 2017; Hans G. Beger (Editor), 2018; Nagtegaal et al., 2020; Saiki & Horii, 2014). Preclinical studies with PDAC mouse models showed that initiating *KRAS* mutations are found in early precursor lesions and can be found even in healthy pancreatic cells (Bryant et al., 2014). Activation of *KRAS* via doxycycline in mice expressing pancreas-specific *KRAS* in a doxycycline-inducible manner is enough for PDAC development (Ying et al., 2012). On the other hand, *KRAS* extinction after PDAC development result in tumour regression, decreased tumour cell proliferation and increased cancer cell apoptosis as well as stromal modulation in the same mouse model (Ying et al., 2012). Once activated KRAS interacts with more than 80 downstream effector proteins and activates signalling pathways like RAS-RAF-MEK-ERK and PI3K-AKT-mTOR cascades as well as nuclear transcription factors such as HIF1A and MYC, controlling different processes like proliferation and survival (Buscail, Bournet, & Cordelier, 2020; Ying et al., 2012). Although around 8% of the patients have wild-type *KRAS*, RAS pathway is activated through alternative ways like BRAF mutations, emphasizing the significance of the activation of RAS signalling for PDAC (Aguirre & Collisson, 2017; Hans G. Beger (Editor), 2018). Inactivation of CDKN2A tumour suppressor, which occurs around 90% of the cases, is the second most frequent mutation that can be seen starting from low-grade PanINs and causes the loss of control over cell cycle (Bryant et al., 2014; Hans G. Beger (Editor), 2018). The other two mutated tumour suppressors TP53 and SMAD4, which are inactivated in 75 % and 55 % of the cases respectively, seem to occur in high-grade PanINs and invasive cancer (Bryant et al., 2014; Hans G. Beger (Editor), 2018; Saiki & Horii, 2014). Inactivation of TP53 protects the cancer cell from apoptosis and cell death even in the presence of DNA damage and causes accumulation of different mutations (Saiki & Horii, 2014). SMAD4 loss of activity leads to unregulated cellular growth that strongly correlates with metastatic phenotype (Saiki & Horii, 2014). In addition to 'the mountains', other genomic alterations with lower frequencies that are affecting

biological pathways like chromatin remodelling (*ARID1A, KDM6A, MLL3, SMARCA4*), cell cycle regulation (*MYC, CDK6, FBXW7*) and DNA repair (*ATM, BRCA2*) were identified and named as 'the hills' (Hans G. Beger (Editor), 2018; Nagtegaal et al., 2020; Saiki & Horii, 2014) (Figure 1.4). Even though the exact role of each genomic changes in tumour evolution and disease progression is still unclear, it is known that oncogenic KRAS dosage and distinct combination of identified genetic alterations, together with epigenome and tumour microenvironment, create diverse tumour phenotypes reflected in heterogeneous therapy response and clinical outcome (Chan-Seng-Yue et al., 2020; Mueller et al., 2018). Therefore, better understanding of molecular and physiological events is a prerequisite for a successful approach to disease therapy.

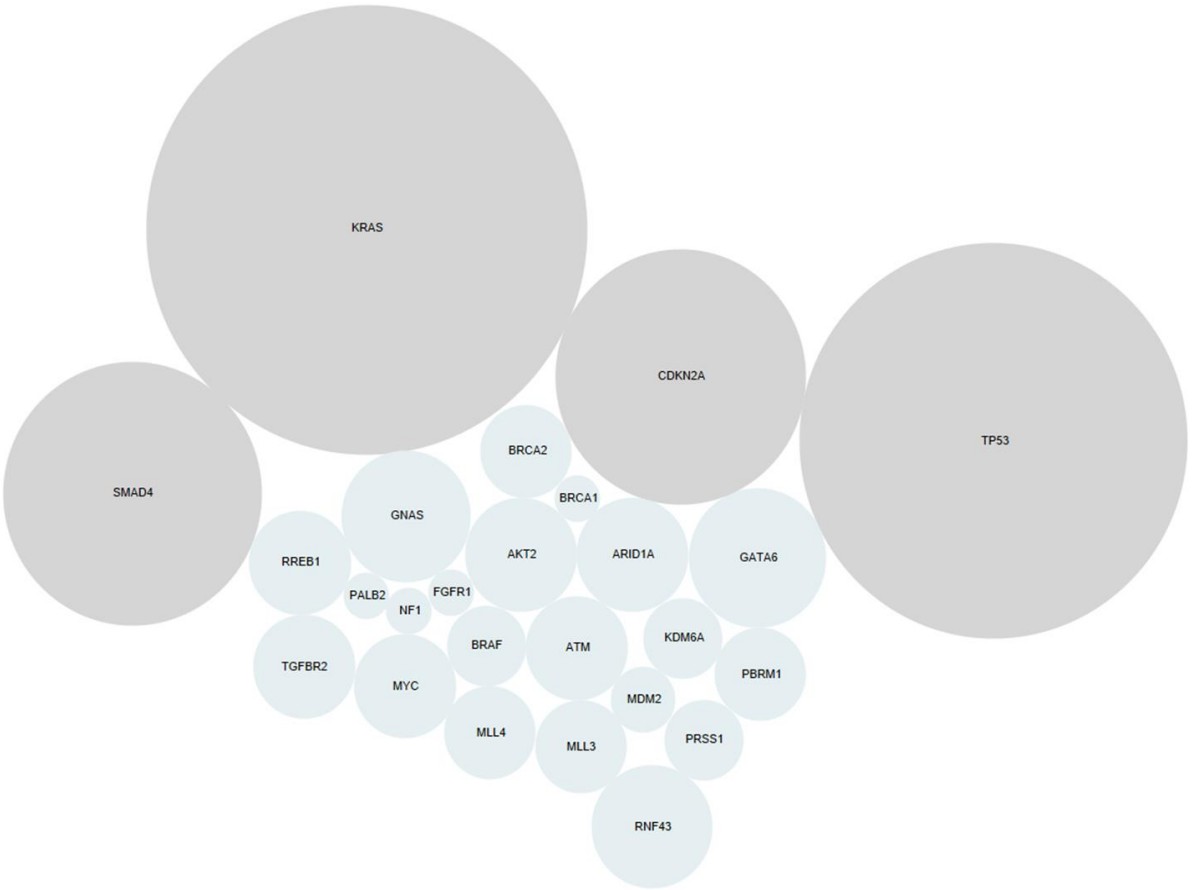

Figure 1.4 **Most frequent genetic alterations in PDAC.** Grey circles represent 'the mountains' which are the most frequently mutated genes in PDAC and blue circles represent 'the hills' which are less common mutations in PDAC with a lower frequency. The size of the circle is proportional to the mutation frequency of the respected gene in PDAC. (Data obtained from Raphael et al., 2017, (Cancer Genome Atlas Research Network. Electronic address & Cancer Genome Atlas Research, 2017))

1.3.3 Current and emerging therapies in PDAC

Despite the progress in THE understanding of pancreatic cancer development and pathology in the last decades, the 5-year survival has not changed substantially (Biancur & Kimmelman, 2018). The most effective available therapy is the surgical removal of the tumour (Orth et al., 2019; Saung & Zheng, 2017). However, only about 20% of the patients are eligible for surgery due to early development of systemic metastatic disease (Orth et al., 2019; Saung & Zheng, 2017). Systemic chemotherapy is the current first-line treatment for locally advanced and metastatic PDAC (Orth et al., 2019; Saung & Zheng, 2017). Nucleoside analogue Gemcitabine monotherapy has been used as a first-line therapeutic agent (Burris et al., 1997) until two other combination regimens, gemcitabine plus nanoparticle albumin-bound paclitaxel and FOLFIRINOX (the combination of folinic acid; thymidylate synthesis inhibitor, 5 fluorouracil; topoisomerase I inhibitor irinotecan; and DNA synthesis inhibitor, oxaliplatin), presented longer median overall survival in MPACT (Von Hoff et al., 2013) (8.5 vs 6.7 months, gemcitabine/nab-paclitaxel and gemcitabine monotherapy, respectively) and PRODIGE (Conroy et al., 2011) (11.1 vs 6.8 months, FOLFIRINOX and gemcitabine monotherapy, respectively) clinical trials compared to gemcitabine monotherapy (Orth et al., 2019; Saung & Zheng, 2017). Even though the efficacy of the two regimens has not been compared in a clinical trial, distinct patterns of therapy response in PDAC patient subgroups have been noticed (Aung et al., 2018; Kaissis et al., 2019; Muckenhuber et al., 2018). Some patients respond better to modified FOLFIRINOX and others to gemcitabine/nab-paclitaxel, indicating the significance of the identification of patient subgroups and predictive markers that can be used for subgroup identification and therapy selection (Aung et al., 2018; Kaissis et al., 2019; Muckenhuber et al., 2018).

Better understanding of the molecular mechanism underlying disease progression, therapy resistance, and metastasis as well as better stratification of patients via molecular profiling have enabled the identification of novel therapeutic targets for different cancers (Christenson, Jaffee, & Azad, 2020; Tsimberidou, 2015). With the introduction of therapies targeting specific tumour features such as growth factor receptors and signal transducers (molecular targeted therapy), improved therapy responses have been observed in specific molecular subgroups of patients with various cancers (Christenson et al., 2020; Tsimberidou, 2015). For example, the

combination of standard chemotherapy with epidermal growth factor receptor inhibitor (EGFR) erlotinib show improved response in EGFR overexpressing non-small-cell lung cancer patients (Rosell et al., 2012). Similarly, *BRAF*^{V600E} mutant metastatic melanoma patients respond better to the combination of standard chemotherapy with BRAF inhibitors vemurafenib (Chapman et al., 2011) and dabrafenib (Hauschild et al., 2012) than chemotherapy alone. In addition, human epidermal growth factor 2 (HER2) overexpressing breast cancer patients show improved therapy response when treated with a recombinant monoclonal antibody against HER2 trastuzumab in combination with standard chemotherapy (Slamon et al., 2001). However, resistance to these therapies commonly occurs in a short time after therapy and affecting the efficiency of these drugs in long term (Tsimberidou, 2015). So far, the combination of EGFR inhibitor erlotinib and gemcitabine is the only approved targeted therapy for PDAC which showed somewhat improved overall survival against gemcitabine monotherapy in both mutated *KRAS* and *KRAS* wild-type patients (6.2 vs 5·9 months with erlotinib/gemcitabine and gemcitabine monotherapy, respectively) (Moore et al., 2007). However, utilization of erlotinib/gemcitabine combination in clinical routine is limited due to better performance of current first-line therapies FOLFIRINOX and gemcitabine/nab-paclitaxel (Christenson et al., 2020; Orth et al., 2019). For most PDAC patients, effective targeted therapy options are still missing, even though the molecular profile of the disease is well known (Christenson et al., 2020; Orth et al., 2019). However, identification of small subsets of patients carrying actionable mutations like homologous recombination repair pathway mutations (*BRCA2, ATM, BRCA1, or PALB2*) (Waddell et al., 2015) emphasized the clinical value of molecular stratification of patients for therapy selection. BRCA mutated patients responded exceptionally well to platinum-based therapies (Golan et al., 2014) and showed increased sensitivity to poly (ADP-ribose) polymerase (PARP) inhibitors (Golan et al., 2019).

1.3.4 Molecular PDAC subtypes

The classification/stratification of cancer subtypes is not a very new concept (Collisson, Bailey, Chang, & Biankin, 2019; Hans G. Beger (Editor), 2018). Histological grading of the tumour tissue has been done according to tissue of origin and morphological/histological characteristics of malignant tissue for decades (Collisson et al., 2019; Hans G. Beger (Editor), 2018). The identified histological variants of ductal

adenocarcinoma are adenosquamous carcinoma, colloid adenocarcinoma, hepatoid carcinoma, medullary carcinoma, undifferentiated carcinoma and undifferentiated carcinoma with osteoclast-like giant cells (Collisson et al., 2019; Hans G. Beger (Editor), 2018; Nagtegaal et al., 2020) which are also graded as well-differentiated (resembles normal pancreatic duct), moderately differentiated and poorly differentiated (poorly formed glands and no glands, respectively) (Hans G. Beger (Editor), 2018). Together with morphological classification, histological grading is important in terms of prediction of disease prognosis since well and moderately differentiated PDACs show better prognosis compared to poorly differentiated PDACs (Collisson et al., 2019; Hans G. Beger (Editor), 2018). However, the use of morphological subtypes in determining treatment option is very limited due to different clinical features and therapy response of histologically similar tumours (Collisson et al., 2019; Hans G. Beger (Editor), 2018). For all the above reasons, molecular classification of PDAC is necessary for improvements in the management of the disease (Collisson et al., 2019; Singh, Hasselluhn, & Neesse, 2019). Much effort has been invested in identifying molecular subtypes of PDAC to establish molecular taxonomy that guides therapy development and treatment decisions (Collisson et al., 2019; Singh et al., 2019). After the success in identifying clinically-relevant molecular subtypes based on transcriptomics in other tumours like breast (Perou et al., 2000) and lymphoma (Alizadeh et al., 2000), transcriptome-based PDAC profiling has been performed by different groups in recent years (Collisson et al., 2019).

In 2011, Collisson et al., described three molecular PDAC subtypes termed classical, quasi-mesenchymal (QM-PDAC) and exocrine-like, according to gene expression data from 66 untreated primary PDAC samples (Collisson et al., 2011) (Figure 1.5). The Collisson's subtyping provided the first information about subtype-specific therapy response and relation to disease progression (Collisson et al., 2011). QM subtype is correlated with higher expression of mesenchymal genes and worse overall survival while classical subtype has higher expression of adhesion-related and epithelial genes and somewhat better prognosis (Collisson et al., 2011). Tumours (cancer cells) of QM subtype are more sensitive to nucleoside analogue gemcitabine whereas classical subtype responds better to EGFR targeting erlotinib treatment (Collisson et al., 2011). The third subtype, which is exocrine-like, shows overexpression of digestive enzyme

genes and it is still debated whether this subtype is influenced by tumour adjacent pancreatic tissue (Collisson et al., 2019; Collisson et al., 2011).

In 2015, Moffitt et al. used gene expression microarray data from primary tumours (n=145), metastasis (n=61) and normal tissue from both pancreas and the organ where metastasis occurs to separate the signals stemming from tumour, stroma and normal tissue (Moffitt et al., 2015) (Figure 1.5). They identified two tumour-specific (classical and basal-like subtypes) and two stroma-specific subtypes (normal and activated stroma) by using the segregated genomic data (Moffitt et al., 2015). The patients with classical subtype showed significantly better overall survival rates compared to the patients with QM tumours (Moffitt et al., 2015). Stroma-specific subtypes are also clinically relevant (Moffitt et al., 2015). Patients with normal stromal subtype have better prognosis and overall survival compared to patients with activated stromal subtype (Moffitt et al., 2015).

In 2016, Bailey et al. stratified 266 histopathologically classified, treatment-naïve primary bulk tumours into four subtypes named squamous, pancreatic progenitor, immunogenic, and aberrantly differentiated endocrine exocrine (ADEX) also based on gene expression data (Bailey et al., 2016) (Figure 1.5). All three classification overlap substantially (Collisson et al., 2019). The Collisson and Moffitt classical subtype are presented in the Bailey pancreatic-progenitor group while the QM subtype (Collisson) is overlapping with basal-like (Moffitt) and squamous (Bailey) subtypes (Bailey et al., 2016). Bailey's ADEX subtype correlates with Collisson's exocrine-like subtype and shares the expression patterns in exocrine/endocrine signatures (Bailey et al., 2016). The immunogenic subtype is dominated by expression signals coming from the immune infiltrates in the tumour and additionally shares many features with pancreatic progenitor subtype (Bailey et al., 2016; Collisson et al., 2019). All these findings have showed that molecular PDAC subtypes can be collected under two main subtypes as Classical and QM (Collisson et al., 2019). The multiple-layered analysis of genomics, transcriptomics and methylation data by The Cancer Genome Atlas Research Network (TCGA) also supports the idea of two main molecular PDAC subtypes as Classical and QM (Cancer Genome Atlas Research Network. Electronic address & Cancer Genome Atlas Research, 2017) (Figure 1.5).

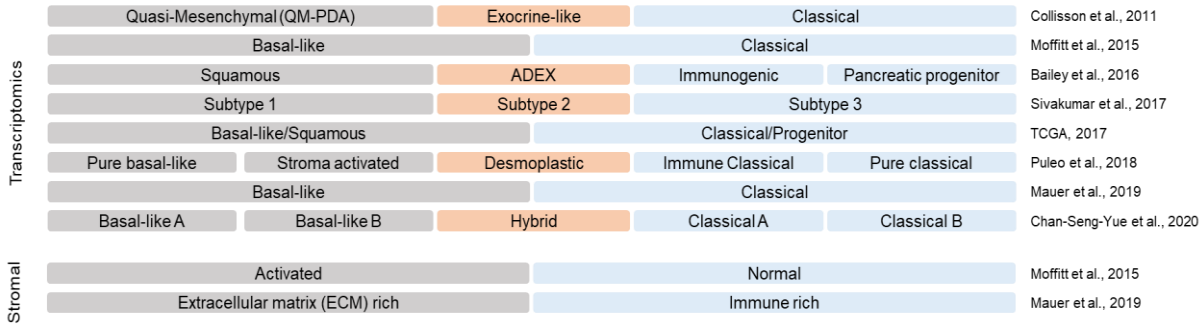

Figure 1.5 **Molecular Subtypes of PDAC.** Multiple transcriptomic subtypes of PDAC have been identified. Although each group uses different nomenclature, identified transcriptomic subtypes are correlated with each other and they can be collected under the umbrella of two main PDAC subtypes as QM-Squamous-Basal-like-Glycolytic and Classical-Pancreatic progenitor-Lipogenic. The debate about the stromal subtypes, whether they are individual subtypes or subgroups branching from the main subtypes still continues, however, there is a possible link between stromal subtypes and main transcriptomic PDAC subtypes. (Adapted from Le Large et al., 2017 (Le Large et al., 2017))

Importantly, the recently published COMPASS clinical trial confirmed the clinical relevance of the subtypes (Aung et al., 2018). Patients of classical subtype have better progression-free (6.4 months for Classical and 2.3 months for QM subtypes) and overall survival rates (10.4 months for Classical and 6.3 for QM subtypes) than QM patients when undergoing treatment with FOLFIRINOX (Aung et al., 2018). Recently, combinatorial analysis of whole genome sequencing and transcriptome data from 314 patients stratified PDAC into five molecular subtypes (basal-like1, basal-like 2, hybrid, classical 1 and classical 2) and show that two main subtypes, QM (basal-like) and classical, contains at least 2 more subgroups branching from each of them (Chan-Seng-Yue et al., 2020) (Figure 1.6).

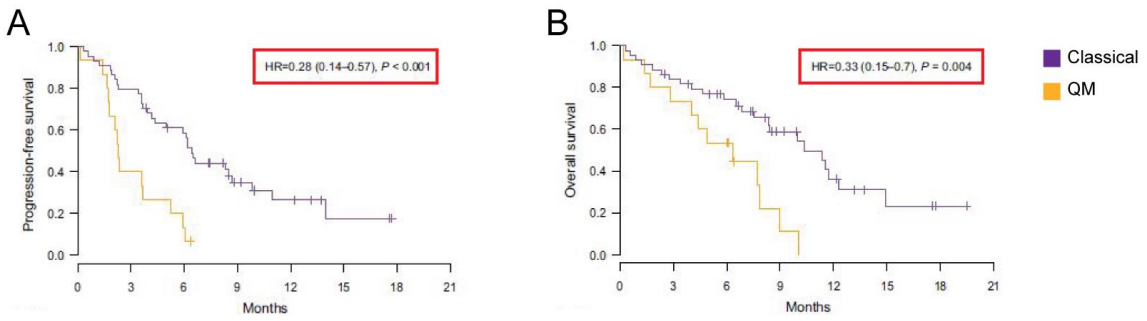

Figure 1.6 **Progression free and overall survival rates for patients of classical and QM subtypes.** Patients of classical subtype have better progression-free (A) and overall survival (B) rates than QM patients. Hazard ratios (HR) are shown with 95% confidence intervals and P values. (Adapted from Aung et al., 2017 (Aung et al., 2018))

1.3.5 PDAC metabolism

The molecular classification of PDAC into two major subtypes has been verified by multiple groups and is widely accepted (Collisson et al., 2019). However, metabolic aspects of the identified transcriptional differences are still largely unresolved. The transcriptome is functionally translated into proteome and metabolome (Lehninger, 2004). However, it is the protein activity, enzymatic actions and metabolic cycles that finally determine the phenotype of any cell, including cancer (Lehninger, 2004).

Metabolism consists of organized enzymatic reaction series called metabolic pathways that produce energy (catabolic pathways) from nutrients, synthesize macromolecules (anabolic pathways) from precursors and replenish the intermediate molecules necessary for anabolic and catabolic pathways (anapleurotic pathways) (DeBerardinis & Thompson, 2012; Metallo & Vander Heiden, 2013).

In differentiated non-proliferating cells, anabolic, catabolic and anapleurotic pathways are employed at optimal levels that cells only uptake necessary amounts of nutrients (carbohydrates, amino acids and lipids) and keep ATP and macromolecule production at a level that is sufficient for cellular homeostasis (Cantor & Sabatini, 2012; DeBerardinis, Lum, Hatzivassiliou, & Thompson, 2008). Under physiological conditions, quiescent cells use mostly glucose for energy production and macromolecule biosynthesis (Cantor & Sabatini, 2012; DeBerardinis et al., 2008). Therefore, glucose is, first, converted to pyruvate through a series of enzymatic reactions called glycolysis which in presence of oxygen ends with the production of pyruvate (Cairns, Harris, & Mak, 2011) (Figure 1.7). Later, glycolysis-derived pyruvate is transferred to mitochondria where it is oxidized to acetyl-CoA by pyruvate

dehydrogenase complex (PDH) to fuel tricarboxylic acid (TCA) cycle in which acetyl-CoA is oxidized to CO_2 (DeBerardinis et al., 2008; Lehninger, 2004; Schulze & Harris, 2012) (Figure 1.7). During acetyl-CoA oxidation in TCA cycle, electrons from TCA cycle intermediates are transported to nicotinamide adenine dinucleotide (NAD+) and flavin adenine dinucleotide (FAD++) that, later, NADH and $FADH_2$ join to electron transport chain (ETC) where they ultimately reduce oxygen (O_2) to water (H_2O) while catalysing the transition of ADP to ATP (Lehninger, 2004) (Figure 1.7). Consequently, sufficient basal energy for cells is generated in the form of ATP (38 ATP molecules) through oxidative phosphorylation (OXPHOS) (DeBerardinis et al., 2008). Besides bioenergetics, the TCA cycle is also in the centre of anabolic and anapleurotic pathways (Lehninger, 2004). During the acetyl-CoA oxidation in the TCA cycle, eight different intermediate metabolites are produced. Among them, oxaloacetate and α-ketoglutarate are used for protein and nucleic acid synthesis, while citrate is converted to acetyl-CoA by ATP citrate lyase (ACLY) in the cytoplasm and joins either fatty acid or sterol synthesis (Lehninger, 2004) (Figure 1.7).

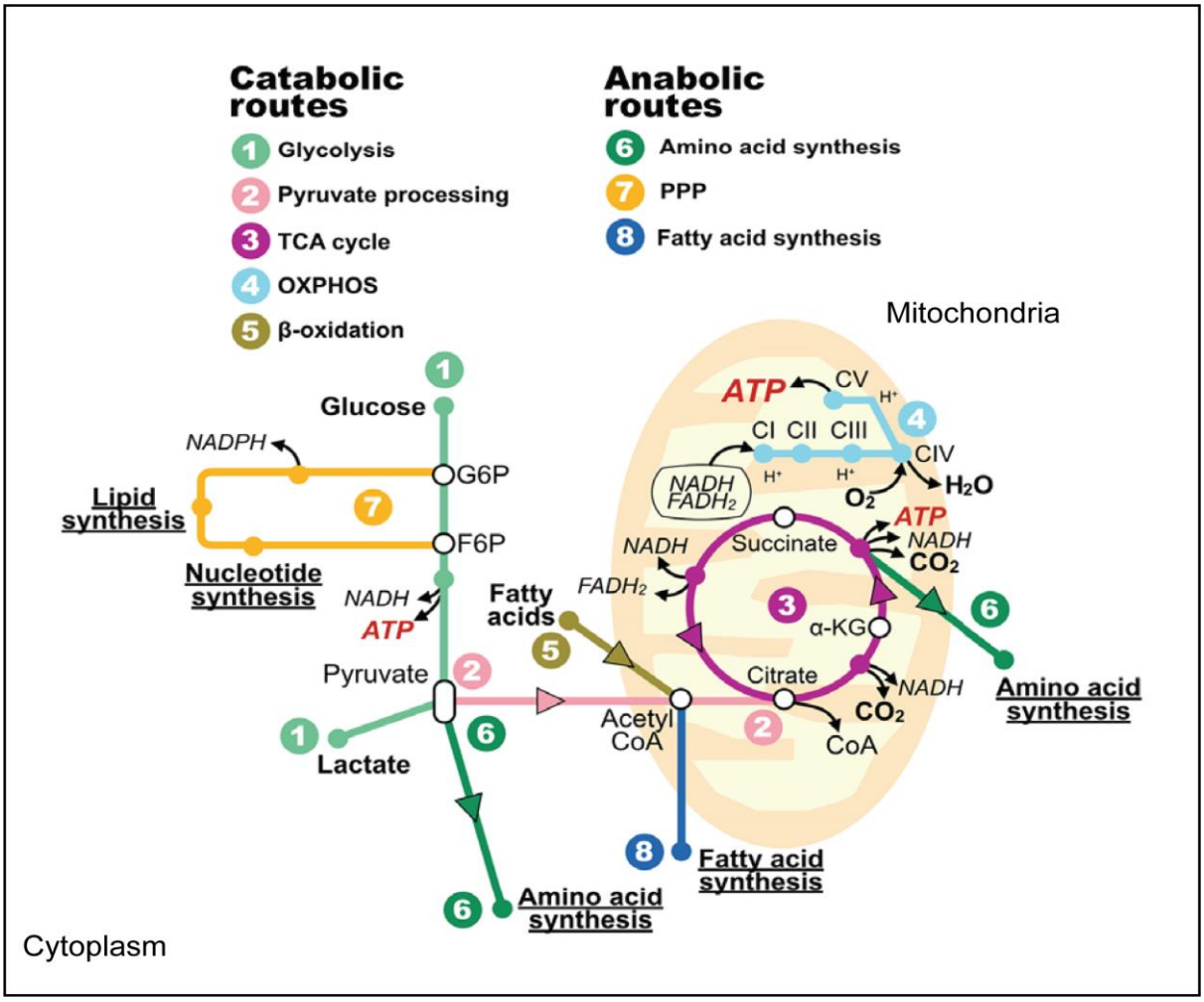

Figure 1.7 **Overview of cellular metabolism.** The main catabolic and anabolic processes utilized to produce ATP and macromolecules in the cell. F6P, fructose 6phosphate; G6P, glucose 6 phosphate; α-KG, alpha-ketoglutarate. (Adapted from Escoll et al., 2018, (Escoll & Buchrieser, 2018))

Differently, under low oxygen availability (hypoxia), cells preferably rely on glycolysis. Without entering the TCA cycle, pyruvate is converted into lactate (fermentation) via lactate dehydrogenase (LDH) activity (Cantor & Sabatini, 2012). As a result, cellular energy demand is mostly generated by glycolysis instead of oxidative phosphorylation to overcome the dearth of oxygen (Cantor & Sabatini, 2012). The shift in cellular bioenergetics from oxidative phosphorylation to glycolysis is regulated by hypoxia-inducible factor 1alpha (HIF1A), a transcription factor activated in response to hypoxia (Cantor & Sabatini, 2012). Once activated, HIF1A upregulates the expression of glucose transporters (GLUTs) and glycolytic genes such as lactate dehydrogenase A (*LDHA*) and hexokinases (*HK*s) to upgrade cellular glycolytic capacity (Cantor & Sabatini, 2012). Additionally, HIF1A enhances the expression of pyruvate dehydrogenase kinases (*PDK*s) which inhibit PDH complex to decrease the entry of

pyruvate to the TCA cycle instead of fermentation (Cantor & Sabatini, 2012). In this way, most of the glycolysis-derived pyruvate is channelled to lactate conversion that results in excessive glucose consumption and ample lactate production (Cantor & Sabatini, 2012).

Cancer cells under strong proliferation pressure increase their glucose uptake and convert most of the glucose to lactate via glycolysis regardless of oxygen availability (DeBerardinis et al., 2008). In 1931, Otto Warburg observed that cancer tissues in slice cultures produce large amounts of lactate in comparison to normal tissue (DeBerardinis et al., 2008; Warburg, 1956). Warburg suggested functional impairment of mitochondria in cancer cells as the reason for strongly upregulated glycolysis (DeBerardinis et al., 2008; Warburg, 1956) and even named upregulated glycolysis and defective mitochondria as one of the causes of cancer. This observation is known as 'the Warburg effect' (DeBerardinis et al., 2008; Warburg, 1956). Further studies with different malignant and non-malignant cells showed that utilization of aerobic glycolysis during proliferation is independent of mitochondrial defects and both malignant and non-malignant cells employ aerobic glycolysis to generate ATP during proliferation even though OXPHOS is more efficient (DeBerardinis et al., 2008; Lunt & Vander Heiden, 2011).

It is now known that aerobic glycolysis provides both bioenergetics and importantly biosynthetic advantages for proliferating cells (DeBerardinis et al., 2008). First, high glucose uptake and metabolism through glycolysis generates energy faster than OXPHOS (DeBerardinis et al., 2008). Secondly, conversion of pyruvate to lactate happens in parallel with NADH to NAD+ conversion what is necessary for cells control of challenged redox balance in the cancer cell (DeBerardinis et al., 2008). Lastly, the diversion of the glucose carbon to anabolic pathways such as pentose phosphate pathway and hexosamine biosynthesis provides metabolic precursors that are further used in the synthesis of macromolecules like nucleotides, amino acids and lipids (DeBerardinis et al., 2008). However, higher glycolytic rate reduces the contribution of glucose carbon to the TCA cycle, which is as well important metabolic hub for anabolic, and anapleurotic pathways. To compensate, proliferating cells also increase the uptake of glutamine and fatty acids to support the TCA cycle for macromolecule and energy production (Boroughs & DeBerardinis, 2015).

In healthy cells, proliferation and related metabolic processes are tightly regulated by various signalling pathways including RAS-RAF-MEK-ERK and PI3K-AKT-mTOR cascades (DeBerardinis et al., 2008). Even though, the same signalling pathways control the cancer cell growth and proliferation, oncogenic activating mutations in these cascades and loss of tumour suppressor genes enable cancer cells to overcome cellular control mechanisms that lead to unrestrained cell proliferation(DeBerardinis et al., 2008). Moreover, rapid and unconstraint proliferation of cancer cells and consequent improper vascularization create hypoxic and nutrient-deprived microenvironment even in the early phases of tumour development (Marchiq & Pouyssegur, 2016). As a result, cancer cells change and adapt their metabolic phenotype to be able to grow and survive in this harsh tumour microenvironment (DeBerardinis et al., 2008). The rewired intracellular metabolism of glucose, glutamine and lipids, increased nutrient acquisition via pinocytosis, autophagy and metabolic crosstalk with the stromal cells are the adaptive metabolic mechanisms that are known to be used by cancer cells to support their proliferation and survival (Pavlova & Thompson, 2016). Metabolic changes supporting cancer cell growth and proliferation are orchestrated by aberrantly activated signalling cascades, especially PI3K-AKT-mTOR signalling pathway (Cairns et al., 2011; DeBerardinis et al., 2008). Activation of PI3K-AKT-mTOR pathway by oncogenes induces upregulation of transcription factors MYC, HIF1A and sterol regulatory element-binding proteins (SREBPs) (Cairns et al., 2011; DeBerardinis et al., 2008; Snaebjornsson, Janaki-Raman, & Schulze, 2020). As a result, MYC and HIF1A enhanced aerobic glycolysis and glutaminolysis via increasing glucose (Cairns et al., 2011; DeBerardinis et al., 2008) and glutamine uptake and upregulating expression of regulating transcription factors such as SREBPs that regulates fatty acid and cholesterol synthesis (Snaebjornsson et al., 2020).

Aerobic glycolysis is a well-studied metabolic phenomenon detected in various cancers including non-small-cell-lung cancer, colorectal cancer and pancreatic cancer (Kimmelman, 2015). In murine PDAC, together with hypoxic microenvironment, oncogenic *KRAS* activation orchestrates the establishment of glycolytic phenotype via inducing RAS-RAF-MEK-ERK and PI3K-AKT-mTOR signalling pathways that promote transcription factors MYC and HIF1A (Blum & Kloog, 2014; Buscail et al., 2020). Activation of respective transcription factors results in increased glucose uptake and

upregulation of the expression of multiple glycolytic enzymes, e.g. glucose transporter GLUT1 (SLC2A1), hexokinase 1 (HK1), and lactate dehydrogenase A (LDHA) (Blum & Kloog, 2014; Buscail et al., 2020) (Figure 1.8.A). Increased glycolytic capacity due to continuous activation of growth signalling, enhances ATP generation through glycolysis and amplifies the flux of glucose carbon to the anabolic processes such as pentose phosphate pathway (PPP) and hexosamine biosynthesis pathway (HBP) (DeBerardinis et al., 2008). The PPP which consists of two branches as oxidative arm and non-oxidative arm is responsible for the synthesis of nucleotide precursor ribose-5-phosphate and plays a role in cellular redox balance through nicotinamide adenine dinucleotide phosphate (NADPH) production (Patra & Hay, 2014). Within the oxidative arm, glucose-derived glucose-6-phosphate is converted to ribulose-5-phosphate, concomitantly generating two molecules of NADPH (Patra & Hay, 2014). Later, non-oxidative arm converts ribulose-5-phosphate into either xylulose-5-phosphate or ribose-5-phosphate which can be further utilized to generate nucleotide precursors by the enzymes ribose-5-phosphate isomerase (RPIA) and ribulose-5-phosphate-3-epimerase (RPE), respectively (Patra & Hay, 2014) (Figure 1.8.A). In murine PDAC, the non-oxidative arm is promoted by oncogenic KRAS signalling via increased expression of RPIA and RPE enzymes, indicating increased nucleotide synthesis, whereas oxidative arm of the pathways is not regulated by oncogenic KRAS suggesting alternative routes for NADPH production in PDAC (Ying et al., 2012). Another anabolic pathway where glucose carbon is diverted is the HBP that generates uridine diphosphate-N-acetylglucosamine (UDP-GlcNAc), a precursor molecule for protein glycosylation (Biancur & Kimmelman, 2018).

Glycosylation is a posttranslational modification that stabilizes various proteins having a role in cancer cell viability like MYC (Guillaumond et al., 2013). Therefore, upregulation in the pathway is detected in many tumours as well as in PDAC (Guillaumond et al., 2013). Accordingly, KRAS dependent elevation in the expression of rate-limiting enzyme glutaminefructose-6-phosphate aminotransferase 1 (GFPT1) and increased protein glycosylation has been observed in PDAC (Bryant et al., 2014; Guillaumond et al., 2013; Ying et al., 2012) (Figure 1.8.A). In line with the increased activity in anabolic pathways, MYC regulated overexpression of pyruvate kinase isoform M2 (PKM2) enzyme, instead of pyruvate kinase isoform M1 (PKM1) like in normal cells, slows down the last step of glycolysis that possibly allow ample

production of anabolic intermediates from glucose carbon (Cairns et al., 2011; Vander Heiden et al., 2010). Even though glucose carbon is shifted to anapleurotic pathways branching from glycolysis, a good part of the glucose is still converted to lactate (DeBerardinis et al., 2008). The conversion of pyruvate to lactate by LDHA generates NAD+ that is a cofactor used by glyceraldehyde-3-phosphate dehydrogenase (GAPDH) through glycolysis and is essential for the continuation of glycolysis (de Bari & Atlante, 2018). Moreover, higher glycolytic rate causes increased cytoplasmic acidosis, which is balanced via lactate export to microenvironment (de Bari & Atlante, 2018). The lactate transport is performed by monocarboxylate transporters (MCTs) 1 and 4 that are upregulated in various cancers (de Bari & Atlante, 2018). Extracellular lactate, then, acts as a signalling molecule and changes the metabolism of stromal cells in favour of tumour cells (Marchiq & Pouyssegur, 2016). For example, increased extracellular lactate concentrations lead to activation of vascular endothelial growth factor (VEGF) in endothelial cells resulting in neovascularization in tumour tissue while increasing the cancer cell migration that may cause increased metastasis (Marchiq & Pouyssegur, 2016). Furthermore, increased acidity in microenvironment limits the cytotoxic activity of T cells (Fischer et al., 2007; S. R. Jacobs et al., 2008) and promotes macrophage polarization towards immune-suppressive M2-like phenotype (Colegio et al., 2014; Ye et al., 2018) that supports immune evasion of cancer cells (Marchiq & Pouyssegur, 2016) (Figure 1.8.B). Furthermore, it has been recently shown that lactate locally produced by the cancer cells is exported but then again important into cancer cell where is then being converted back to pyruvate by lactate dehydrogenase B (LDHB) enzyme and is actively used in the TCA cycle (Hui et al., 2017; Zdralevic et al., 2018). In murine PDAC and lung cancer, lactate seems to be the second-best fuel used in the TCA cycle, just after glutamine (Hui et al., 2017).

In addition to changes in glucose metabolism, cancer cells reprogram glutamine metabolism in order to meet their increased energetic and biosynthetic demands (L. Yang, Venneti, & Nagrath, 2017). Glutamine is an anapleurotic carbon and nitrogen source that fuels the TCA cycle for energy and macromolecule production (Son et al., 2013). MYC-mediated upregulation of glutamine transporters (SLC1A5 and SLC38A5) and glutaminase enzyme (GLS1) has been detected in various cancers (L. Yang et al., 2017). In most malignant and non-malignant cells glutamine is metabolized via the canonical pathway which is enhanced in a variety of different tumour entities (L. Yang

et al., 2017). Through canonical pathway, glutamine is, first, converted to glutamate by glutaminase enzyme (GLS1) in the mitochondrial matrix (Son et al., 2013). Following, glutamate is either transformed into α-ketoglutarate by glutamate dehydrogenase (GLUD1) and incorporated into TCA cycle or used for the synthesis of glutathione (GSH), an antioxidant necessary for the maintenance of cellular redox homeostasis (Son et al., 2013). PDAC is also dependent on non-canonical utilization of glutamine which is orchestrated by oncogenic KRAS through overexpression of glutamic-oxaloacetic transaminase 1 (GOT1) and repression of GLUD1 (Biancur & Kimmelman, 2018; Son et al., 2013) (Figure 1.8.B). Within the non-canonical glutamine metabolism, glutamine-derived glutamate is transformed into acetate with glutamic-oxaloacetic transaminase 2 (GOT2) in mitochondria and transferred to cytoplasm, where it is converted to oxaloacetate by glutamic-oxaloacetic transaminase 1 (GOT1) (Son et al., 2013). Following, oxaloacetate is converted to malate and subsequently to pyruvate via malate dehydrogenase (MDH1) and malic enzyme (ME1), respectively (Son et al., 2013). The conversion of oxaloacetate to pyruvate generates NADPH and NAD+, again protecting pancreatic cancer cells against reactive oxygen species (ROS) (Son et al., 2013).

Another common metabolic change observed in cancer, PDAC as well, is deregulation in lipid metabolism (Biancur & Kimmelman, 2018) (Figure 1.8.C). Lipids provide building blocks like phospholipids and cholesterol for membrane biogenesis, energy via fatty acid oxidation and precursors for signalling molecules that all together support cancer cell growth and proliferation (Biancur & Kimmelman, 2018). Lipids are mostly synthesized from fatty acids and non-malignant cells mainly uptake fatty acids for lipid synthesis from blood circulation (Menendez & Lupu, 2007). Conversely, cancer cells promote *de novo* fatty acid synthesis to be less dependent on extracellular lipids whose availability is low in tumour tissue with improper vascularization (Snaebjornsson et al., 2020). For fatty acid synthesis, cancer cells utilize cytoplasmic acetyl-CoA which can be derived from glucose (via TCA cycle), glutamine (via glutaminolysis) or acetate (converted by Acyl-coenzyme A synthetase short-chain family member 2, ACSS2) depending on substrate and oxygen availability (Snaebjornsson et al., 2020). Cytoplasmic acetyl-CoA is converted to malonyl-CoA by acetyl-CoA carboxylase A and B (ACACA/B) (Snaebjornsson et al., 2020). Malonyl-CoA is, then, converted into 16-carbon saturated fatty acid palmitate with a multi-step condensation catalysed by fatty

acid synthase (FASN) (Snaebjornsson et al., 2020). From palmitate, cells create non-essential fatty acid pool via elongation catalysed by fatty acid elongases (ELOVL1-7) and desaturation catalysed by stearoyl-CoA desaturases (SCD and SCD5) and fatty acid desaturases (FADS1-3) (Snaebjornsson et al., 2020). Increase in *de novo* fatty acid synthesis also changes cellular lipid composition due to inability of human desaturases to synthesize most of the polyunsaturated fatty acids and leads to saturation of membrane phospholipids (Snaebjornsson et al., 2020). The saturation of membrane lipids protects cancer cells from endoplasmic reticulum stress and mitochondrial dysfunction due to higher stability of saturated and monounsaturated fatty acids against lipid peroxidation caused by high concentrations of reactive oxygen species (Rysman et al., 2010).

Besides *de novo* fatty acid synthesis, cholesterol synthesis through the mevalonate pathway is also increased in cancers. Together with cholesterol, mevalonate pathway intermediates farnesylpyrophosphate (FPP) and squalene play an important role in cancer cell signalling, growth and survival (Mullen, Yu, Longo, Archer, & Penn, 2016; Snaebjornsson et al., 2020). The enhancement in both fatty acid and cholesterol synthesis in cancer cells is regulated by PI3K-AKT-mTOR signalling pathway and its downstream target SREBPs (Mullen et al., 2016; Snaebjornsson et al., 2020). The expression of fatty acid synthesis related genes is generally controlled by SREBP1 whereas SREBP2 regulates the expression of mevalonate pathway enzymes (Mullen et al., 2016; Snaebjornsson et al., 2020). Accordingly, the overexpression in the rate-limiting enzymes of both *de novo* fatty acid synthesis (e.g. ACLY, FASN and SCD) (Furuta et al., 2008; Qin et al., 2020) and cholesterol synthesis (HMGCR) (Guillaumond et al., 2015) are also observed in pancreatic cancer (Baenke, Peck, Miess, & Schulze, 2013; Beloribi-Djefaflia, Vasseur, & Guillaumond, 2016; Hauschild et al., 2012; Snaebjornsson et al., 2020; Sunami, Rebelo, & Kleeff, 2017) (Figure 1.8.C). Additionally, upregulation in extracellular fatty acid (via increased lysophospholipid scavenging,) and cholesterol uptake (via upregulated low-density lipoprotein receptor, LDLR, expression,) are also detected in PDAC (Auciello et al., 2019; Guillaumond et al., 2015). Different factors such as nutrient availability and hypoxia determine by which way cancer cells maintain and utilize the intracellular fatty acid pool (Rohrig & Schulze, 2016). For example, hypoxia and low nutrient availability cause upregulation in *de novo* fatty acid synthesis what increases intracellular saturated to monounsaturated fatty

acids ratio (Baenke et al., 2013; Beloribi-Djefaflia et al., 2016; Munir, Lisec, Swinnen, & Zaidi, 2019; Snaebjornsson et al., 2020; Sunami et al., 2017). Furthermore, under hypoxic conditions, HIF1A promotes the storage of fatty acids in form of triacylglycerol in lipid droplets by increasing expression of lipid droplet membrane protein perilipin 2 (PLIN2) (Bensaad et al., 2014; Munir et al., 2019) and decreasing the expression of phospholipase domain-containing 2 (PNPLA2) (Bensaad et al., 2014; Zhang et al., 2017). This results in inhibition of fatty acid usage in energy production (Bensaad et al., 2014; Zhang et al., 2017) thus simultaneously protecting cancer cells from lipotoxicity since beta-oxidation produces reactive oxygen species (Huang et al., 2014; Munir et al., 2019). However, functional fatty acid oxidation is also shown to be essential for tumour growth and survival in various cancers (Carracedo, Cantley, & Pandolfi, 2013; Ma et al., 2018). Fatty acid oxidation (FAO) is a multi-step catabolism of fatty acids into acetyl-CoA, which further fuels the TCA cycle in the mitochondria (Carracedo et al., 2013; Ma et al., 2018). FAO starts with the activation of fatty acids to fatty acyl-CoA by long-chain fatty acyl-CoA synthetases (ACSLs) in the cytoplasm (Carracedo et al., 2013; Ma et al., 2018). Following the activation, fatty acyl-CoA is converted to fatty acyl-carnitine by carnitine palmitoyltransferase 1 (CPT1) on the outer mitochondrial membrane and it is shuttled to the mitochondrial matrix via carnitine/acylcarnitine translocase (SLC25A20) activity (Carracedo et al., 2013; Ma et al., 2018). On the matrix side of the inner mitochondrial membrane, acyl-carnitine is reconverted to acyl-CoA by carnitine palmitoyltransferase 2 (CPT2) and acyl-CoA enters the fatty acid oxidation cycle which is a 4-step cycle cleaving two carbons in the form of acetyl-CoA from fatty acids (Carracedo et al., 2013; Ma et al., 2018). In addition to generating acetyl-CoA, which is further oxidized in TCA cycle, every fatty acid oxidation cycle creates NADH and FADH2 that are used by ETC for ATP production (Carracedo et al., 2013; Ma et al., 2018). Fatty acid oxidation provides the energy necessary for cancer cells and feeds TCA cycle with acetyl-CoA and is upregulated through overexpression of key enzymes like ACSL3 and CPT1A in many different cancer types including KRAS mutant mouse non-small cell lung cancer and human NSCLC cells (Padanad et al., 2016) and MYC-overexpressing triple-negative breast cancer cells as well as TNBC patient-derived xenograft (Camarda et al., 2016), respectively (Carracedo et al., 2013; Ma et al., 2018).

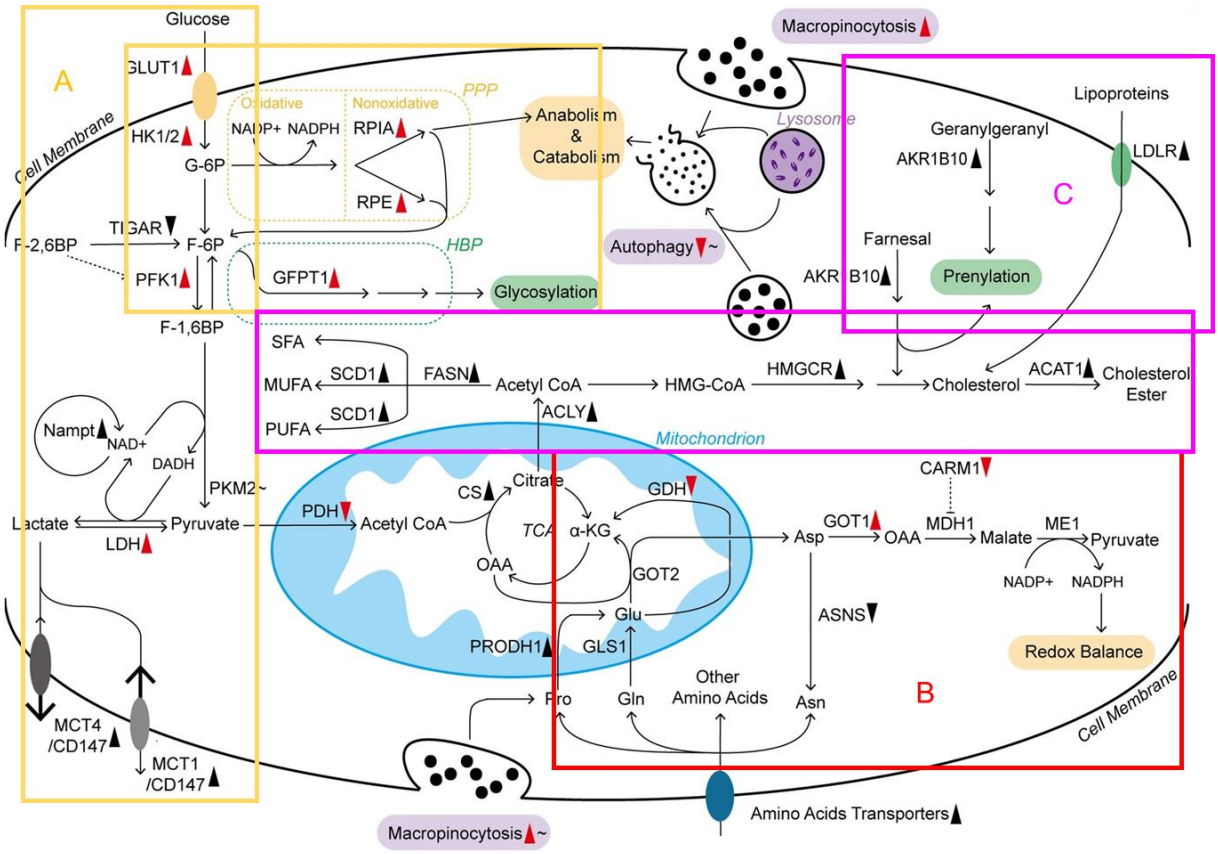

Figure 1.8 **Metabolic rewiring of PDAC**. Oncogenic KRAS-driven reprogramming of glucose (A), glutamine (B) and fatty acid metabolism (C) induced by changes in rate-limiting enzymes and transporters and increased macropinocytosis and autophagy in PDAC. Long solid arrows point to shifts or bioconversions. The dotted arrow means positive regulation, dotted arrow with blunt end indicates negative regulation. Red arrowheads following the enzymes, transporters, and processes represent the effects induced by mutant KRAS: upward means upregulation; downward means downregulation. The black symbols represent the changes induced by other or unknown reasons. In addition, those following tildes indicate dual regulation under different conditions. ACLY, ATP citrate lyase; ASNS, asparagine synthetase; CARM1, Coactivator-associated arginine methyltransferase 1; CS, citrate synthetase; F-6P, fructose 6-phosphate; F- 1,6BP, fructose 1,6-bisphosphate; F-2,6BP, fructose 2,6-bisphosphate; GFPT1, glutamine:fructose 6-phosphate amidotransferase 1; G-6P, glucose 6- phosphate; HK1/2, hexokinase 1/2; HMGCR, 3-hydroxy-3-methylglutaryl coenzyme A reductase; HMG-CoA, 3-hydroxy-3-methylglutaryl coenzyme A; ME1, malic enzyme; MUFA, monounsaturated fatty acid; PFK1, phosphofructokinase 1; PRODH1, proline oxidase; PUFA, polyunsaturated fatty acid; RPE, ribulose-5-phosphate epimerase; SCD1, stearoyl-CoA desaturase; SFA, saturated fatty acid; TCA, tricarboxylic acid. (Adapted from Qin et al., 2020 (Qin et al., 2020))

In addition to rewiring of intracellular nutrient metabolism, opportunistic modes of nutrient acquisition such as selective autophagy and macropinocytosis and metabolic crosstalk between cells within the tumour play an important role for cancer cell growth and survival (Pavlova & Thompson, 2016). Autophagy can be described as recycling

of cytosolic components and it has been shown in various cancers that it supports cancer cell progression and survival via providing nutrients, controlling reactive oxygen species and sustaining oxidative phosphorylation (Kimmelman & White, 2017). In PDAC, autophagy has a contradictory role in tumour initiation and progression (A. Yang et al., 2014; S. Yang et al., 2011). Initial autophagy restricts the tumour initiation while inhibition of autophagy suppress tumour progression in PDAC xenografts and mouse models (A. Yang et al., 2014; S. Yang et al., 2011) (Figure 1.8). Besides autophagy, extracellular scavenging process such as macropinocytosis, an internalization of extracellular fluid trough membrane ruffling, is actively used by KRAS driven cancers including PDAC (Commisso et al., 2013) (Figure 1.8). In this process, pancreatic stellate cells secrete amino acids (alanine) (Sousa et al., 2016), extracellular proteins like albumin (Davidson et al., 2017; Kamphorst et al., 2015) and collagen (Olivares et al., 2017) and extracellular lipids, especially lysophosphatidylcholines (Auciello et al., 2019) which are internalized and digested in the lysosome of the cancer cell to support tumour growth (Blum & Kloog, 2014; Cohen et al., 2015; Halbrook & Lyssiotis, 2017; Qin et al., 2020) (Figure 1.8 and Figure 1.9). Metabolic interactions between cancer cells and tumour microenvironment also support tumour growth and survival (Halbrook & Lyssiotis, 2017; Qin et al., 2020; Yao, Maitra, & Ying, 2020). Access to nutrient and oxygen in the tumour microenvironment is dependent on the closeness to blood vessels (Lyssiotis & Kimmelman, 2017). Cells, which are close to the vasculature, have better access to nutrients and oxygen compared to counterparts, which are distant to blood vessels (Lyssiotis & Kimmelman, 2017). Cancer cells developed a metabolic symbiosis with the microenvironment what supports tumour growth and proliferation (Lyssiotis & Kimmelman, 2017). For example, it has been shown in different cancer entities including lung, colon and pancreas cancer that lactate secreted by hypoxic cancer cells is used by normoxic neighbours as mitochondrial fuel and available glucose in tumour microenvironment is either transported to or imported by hypoxic cancer cells (Lyssiotis & Kimmelman, 2017). In PDAC mouse models, high extracellular lactate concentrations and hypoxic areas of the tumours are coincident and PDAC cells in the hypoxic regions release lactate via monocarboxylate transporter 4 (MCT4) which is upregulated in hypoxic cancer cells (Guillaumond et al., 2013; Lyssiotis & Kimmelman, 2017) (Figure 1.8 and Figure 1.9). The extracellular lactate derived from hypoxic PDAC cells is, then, imported by normoxic cancer cells via monocarboxylate transporter 1 (MCT1) and metabolized in

mitochondria (Guillaumond et al., 2013). Similar metabolic symbiosis also occurs between ovarian cancer cells and stromal cells like cancer-associated fibroblasts (CAFs) and adipocytes that stromal cells consume lactate as metabolic fuel and spare the glucose for cancer cells (Lyssiotis & Kimmelman, 2017) (Figure 1.9).

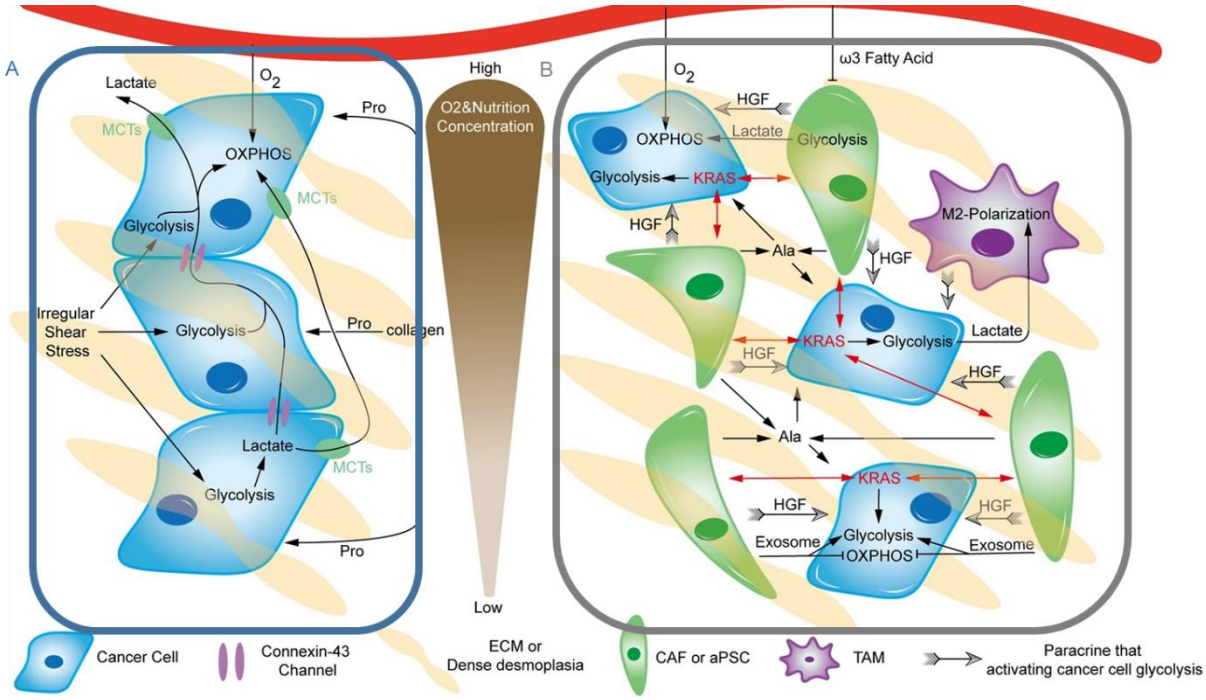

Figure 1.9 **Metabolic crosstalk within the microenvironment.** Pancreatic cancer cells interact with both neighbour cancer cells (A) and stromal cells (B) in different ways. Signalling molecules released from cancer cells can metabolically reprogram stromal cells and stimulate stromal cells to secrete metabolites via exosomes. Lactate produced by hypoxic cells is used as mitochondrial fuel by normoxic cancer cells. The extracellular matrix-derived collagen converted to proline and used as a nutrient by cancer cells. Black arrows imply shift, positive regulation or fuelling, whereas blunt ends indicate inhibition. Ala, alanine; HGF, hepatocyte growth factor. (Adopted from Qin et al., 2020 (Qin et al., 2020))

1.3.6 Metabolic PDAC subtypes

In 2015, Daemen et al. performed large-scale metabolite profiling of 38 established pancreatic cancer cell lines (Daemen et al., 2015). Metabolic profiling segregated the cells into three different metabolic patterns: cells with accumulation of carbohydrate-glycolytic metabolites, cells with accumulation of miscellaneous lipids, fatty acids and cholesterol derivatives and cells with a low abundancy of all metabolites (Daemen et al., 2015). Based on these data, the authors proposed existence of 3 different metabolic subtypes of PDAC, glycolytic, lipogenic and slow proliferating (Daemen et al., 2015) (Figure1.10). The authors suggested that PDAC cells of different subtypes use different metabolic strategies and depend on distinct metabolic pathways for

disease progression (Daemen et al., 2015). Cells of the glycolytic subtype force glucose in aerobic glycolysis and supply the mitochondrial TCA cycle preferably with glutamine, whilst cells of the lipogenic subtype use glucose-derived pyruvate in TCA cycle and glucose-derived carbons for lipid synthesis (Daemen et al., 2015). As a result, cell lines show different responses to inhibition of glycolysis and lipid biosynthesis (Daemen et al., 2015). Comparison of gene expression pattern to the previously published Collisson's gene set assigners correlated the glycolytic cell lines to the quasi-mesenchymal transcriptional subtype and the lipogenic cell lines to classical subtype (Daemen et al., 2015). The importance of glycolysis for PDAC has been noticed not only on the cell line level but also in PDAC patients (Baek et al., 2014). Expression analysis of lactate exporter MCT4 in patient biopsy samples supported correlation of MCT4 and survival. Namely, patients with high MCT4 expression present worse prognosis and shorter survival (Baek et al., 2014). In the same study, MCT4 knockdown experiments in human PDAC cell line MiaPaCa2 led to the deregulation of glycolysis in these cells and compensatory metabolic rewiring to oxidative phosphorylation (Baek et al., 2014). Additionally, downregulation of MCT4 did sensitise the cells to MCT1 inhibition supporting the notion that active inhibition of glycolysis through MCT1/MCT4 lactate transport blockage is a relevant metabolic target in PDAC (Baek et al., 2014). Very recently, in 2020 another group of authors analysed gene expression in a very large collection of patient samples (>300) and noticed a segregation of metabolic genes into four subtypes: slow, glycolytic, cholesterogenic and hybrid (Karasinska et al., 2020) (Figure 1.10). Similarly as observed by Daemen et al*.,* in cell lines, major glycolytic genes were found to be upregulated in one subtype termed glycolytic while genes necessary for cholesterol synthesis and homeostasis were upregulated in PDACs of another group of patients, consequently termed cholesterolgenic subtype (Karasinska et al., 2020). The authors also find correlations among glycolytic genes and mesenchymal transcriptional programme of the QM (or basal-like) and cholesterogenic genes with the classical (or progenitor-like) gene programmes (Karasinska et al., 2020). Once again, the patients with the glycolytic transcriptional programme have worse prognosis and survival than those rich in cholesterogenic transcripts (Karasinska et al., 2020). Furthermore, 56 PDAC liver metastases were analysed by Law et al., with quantitative proteomics and four different subgroups, proliferative, inflammatory, progenitor-like and metabolic, were determined based on the quantification of 916 proteins in each sample (Law et

al., 2020) (Figure 1.10). Proteins related to mitochondrial beta-oxidation and ethanol oxidation pathways are highly expressed in metabolic and progenitor-like subtypes whereas proliferative subtype displays enrichment in proteins associated with cell proliferation and telomere maintenance (Law et al., 2020). On the other hand, the inflammatory subtype is recognized with high expression of proteins adaptive immune response and complement activation (Law et al., 2020). Further comparison of proteomics subtypes with Bailey's transcriptional subtypes revealed that proliferative and inflammatory subtypes are associated with QM/squamous subtype whereas progenitor-like subtype overlaps with Bailey's classical/progenitor subtype (Law et al., 2020). Altogether, it is reasonable to assume that a correlation between transcriptional PDAC subtypes and metabolic features exists. However, all of the metabolic characterisations performed so far is restricted to gene expression data (Karasinska et al., 2020) and is done using commercially available PDAC cell lines (Daemen et al., 2015) that have been kept for a long time in 'artificial' cell culture conditions. Whether the gene expression is indeed translated into functionally relevant metabolic differences and whether these differences can be used for detection and especially for the development of subtype-specific metabolic targeting strategies is largely unknown.

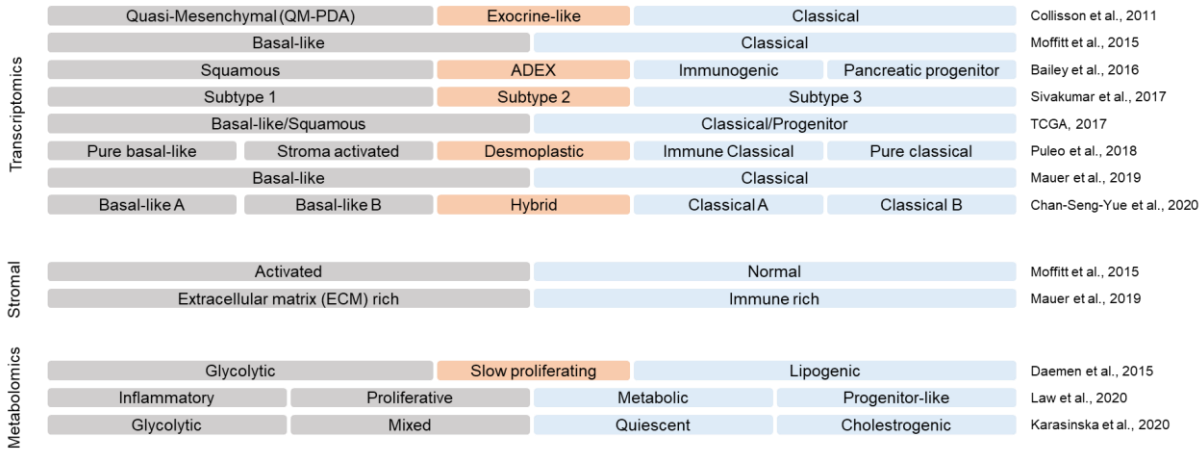

Figure 1.10 **Metabolic subtypes correlate with transcriptional PDAC subtypes.** Three different groups have been described metabolic subtypes of PDAC according to metabolite profiling (Daemen et al., 2015), proteomics (Law et al., 2020) and metabolic gene expression (Karasinska et al., 2020). It has been shown that metabolic subtypes overlap with previously suggested molecular subtypes on transcriptome level. (Adapted from Le Large et al., 2017 (Le Large et al., 2017))

1.4 Aim of the study

The aim of this thesis was to investigate which metabolic pathways are functionally relevant and active in the two major transcriptional subtypes of PDAC identified so far and provide a detailed functional characterisation of metabolic pathways particularly active in a subtype-specific manner, especially in the patient-relevant preclinical models such as primary patient-derived cells and patient-derived xenografts.

To this aim, I analysed a large collection of established PDAC cell lines, Patient-Derived Xenografts (PDX), PDX-derived primary cells and patient data and experimentally evaluated the following:

a) which metabolic pathways are differentially regulated on gene expression level between subtypes and how preserved are the metabolic pathways among different models?

b) are the identified metabolic pathways functionally evident and phenotypically relevant in preclinical models?

Together with PDACs heavy dependence on metabolic adaptations to survive and progress in challenging tumour microenvironment, the overall failure of conventional and molecular therapies against PDAC has rendered metabolism as one of the prime targets for therapy development. Preservation and functionality of metabolic peculiarities in the relevant preclinical models create a basis for future use of these models for development and evaluation of subtype-specific metabolic therapies.

Better understanding of metabolism of PDAC subtypes contribute to current knowledge of PDAC biology and pave the way for identification of novel, possibly subtype-specific, detection methods and metabolic targets in future.

2 Materials and methods

2.1 Cell culture

2.1.1 Established PDAC cell lines

Eight different established cell lines representing PDAC subtypes were used as a model and maintained in 1:1 mixture of Dulbecco's Modified Eagle Medium (DMEM) no glucose (11966025, ThermoFisher Scientific, Waltham, USA) and DMEM no glucose, no glutamine, no phenol red (A1443001, ThermoFisher Scientific, Waltham, USA), containing 5mM D-glucose (A2494001, ThermoFisher Scientific, Waltham, USA), 2mM L-glutamine (G7513, Sigma-Aldrich, St. Louis, USA), 5% v/v foetal bovine serum (10500064, ThermoFisher Scientific, Waltham, USA) and 1% v/v penicillin-streptomycin (P/S)(15140122, ThermoFisher Scientific, Waltham, USA). This medium is called ‘low glucose DMEM’. Cells were cultured in 75 cm2 cell culture flasks (G200FF-75, Kisker Biotech, Steinfurt, Germany) at 37˚C in a humidified atmosphere containing 5 % CO2 (HERACell 240i, ThermoFisher Scientific, Waltham, USA). Cells were passaged when they reached 70-80% confluency and culture media were changed every 48 hours to preserve physiological nutrient levels.

Table 2-1 Established PDAC cell lines

Name	Reference	Molecular Subtype
HPAC	CVCL_3517	Classical PDAC cell line
HPAF II	CVCL_0313	Classical PDAC cell line
PaTu8988S	CVCL_1846	Classical PDAC cell line
HupT4	CVCL_1300	Classical PDAC cell line
KP4	CVCL_1338	QM PDAC cell line
MiaPaca2	CVCL_0428	QM PDAC cell line
PSN1	CVCL_1644	QM PDAC cell line
PaTu8988T	CVCL_1847	QM PDAC cell line

2.1.2 Patient-derived xenograft-derived primary cell lines (PDCs)

Patient-derived xenograft (PDX) tumour establishment and primary cell isolation from PDX tumours were done by Dr. Sven T. Liffers. Eleven different primary cell lines isolated from patient derived-xenografts (PDXs) were used in the transcriptomic and metabolic analysis. The classification of cell lines into subtypes was kindly performed by Dr. Smiths S. Lueong as described in section 2.3.4. Cells were propagated in the mixture of (1:1) Keratinocyte serum-free medium (17005042, ThermoFisher Scientific,

Waltham, USA) and RPMI 1640 no glucose medium (11879020, ThermoFisher Scientific, Waltham, USA) containing 4.5 mM glutamine, 5 mM D-glucose, 0.26 mM sodium pyruvate, 6% v/v foetal bovine serum, 1% v/v penicillin-streptomycin and 0,5% v/v antibiotic-antifungal (15240062, ThermoFisher Scientific, Waltham, USA). This medium is called 'low glucose RPMI'. Cells were cultured in 75 cm2 cell culture flasks at 37˚C in a humidified atmosphere containing 5 % CO2. Cells were passaged when they reached 90% confluency and culture media were changed every 48 hours to preserve physiological nutrient levels.

Table 2-2 Primary cells derived from patient derived xenografts (PDCs)

Name	**Molecular Subtype**
PDC44	Classical PDAC cell line
PDC58	Classical PDAC cell line
PDC59	Classical PDAC cell line
PDC62	Classical PDAC cell line
PDC70	Classical PDAC cell line
PDC89	Classical PDAC cell line
PDC34	QM PDAC cell line
PDC57	QM PDAC cell line
PDC69	QM PDAC cell line
PDC78	QM PDAC cell line
PDC80	QM PDAC cell line

2.2 Metabolic assays

2.2.1 Seahorse XF96 metabolic flux assays

2.2.1.1 Cell number optimization

Seahorse basal measurement assays with a different number of cells/well were conducted for established and primary PDAC cell lines to determine optimum cell seeding density for each established and primary cell lines. Cultured cells were collected by using 0.05% Trypsin-EDTA (25300054, ThermoFisher Scientific, Waltham, USA) and counted with an automated cell counter (TC20TM, Bio-Rad, Hercules, USA). One day prior to the assay, cells were plated as triplicates in their respective growth medium to an Agilent Seahorse XF Cell Culture Microplate (102416-100, Agilent Technologies, Santa Clara, USA) with cell densities between 7500 and 45000 cells/well (established cell lines) or densities between 2000 and 20000 cells/well

(PDCs), respectively. The cells were incubated overnight at 37˚C in a humidified atmosphere containing 5 % CO2. One sensor cartridge was hydrated with 200 µl/well Agilent Seahorse XF Calibrant and incubated at 37˚C in a non-CO2 incubator overnight (102601-100, Agilent Technologies, Santa Clara, USA). Additionally, the Agilent Seahorse XF Analyser (101991-100, Agilent Technologies, Santa Clara, USA) was turned on to establish a stable temperature of 37°C. The assay media were prepared by adding 5 mM D-glucose and 2 mM L-glutamine to Seahorse XF Base Medium (DMEM based, 103334-100, Agilent Technologies, Santa Clara, USA) and Seahorse XF RPMI medium (RPMI based, 103575-100, Agilent Technologies, Santa Clara, USA) for established cell lines and PDCs, respectively. The assay medium was warmed up to 37˚C and pH was adjusted to 7.4 with 0.1 N NaOH. Then, the assay medium was sterile filtered with Steriflip-HV (SE1M003M00, MERCK, Darmstadt, Germany). Prior to the assay, the growth medium in the wells was changed to assay medium (final volume of 180 µl/well) and the cells were incubated at 37˚C in a non-CO2 incubator (Ecotron, Infors HT, Bottmingen, Switzerland) for one hour. During the incubation period, the hydrated cartridge was loaded to the XF analyser for calibration. After the calibration, the microplate containing cells was loaded and the basal measurement assay was performed. After each assay, the results were normalized to the nuclear DNA content per well. For normalization, 150 µl medium was aspirated from each well and the wells were washed with 150 µl Phosphate Buffered Saline (PBS) (14190250, ThermoFischer Scientific, Waltham, USA). For fixation, cells were, then, incubated in 4% paraformaldehyde solution in PBS (150 µl/well) (30525-89-4, Santa Cruz Biotechnology, Dallas, USA) for 10 minutes. Following the fixation, cells were washed 3x10 minutes with PBS (150 µl/well) and were stained with DAPI nucleic acid stain (1:2000 in PBS, 100 µl/well) (D1306, ThermoFischer Scientific, Waltham, USA) for 10 minutes at room temperature. After staining, cells were washed two times with PBS (100 µl/well) and the fluorescent signal was measured at Ex/Em 350/460 using the microplate reader (Spark 10M, Tecan, Männedorf, Switzerland). Results were analysed with Wave 2.6.0 software (Agilent Technologies, Santa Clara, USA).

2.2.1.2 Seahorse XF Mito Fuel Flex Test Kit

To determine the dependencies of each cell line on different mitochondrial fuels (glucose, glutamine and long-chain fatty acids), Seahorse XF Mito Fuel Flex Test Kit was used. For this, the optimum cell numbers from each established PDAC cell line

were seeded (five replicate wells x 6 conditions x 1 cell line) in the Agilent Seahorse XF Cell Culture Microplate one day before the assay. Also, one sensor cartridge was hydrated with 200 µl Agilent Seahorse XF Calibrant and incubated at 37˚C in a non-CO2 incubator overnight. On the assay day, DMEM based assay medium containing 5mM glucose and 2mM glutamine was prepared and pH was adjusted to 7.4 with 0.1 N NaOH. The low glucose DMEM in the wells was replaced with freshly prepared Seahorse assay medium and cells were incubated 37˚C in a non-CO2 incubator for one hour. Meanwhile, the inhibitors were loaded into previously hydrated sensor cartridge as described in the Agilent Seahorse XF Mito Fuel Flex Test Kit User Manual (103260-400, Agilent Technologies, Santa Clara, USA) and sensor calibration was performed. Then, the assay was performed as described by the manufacturer's instructions and normalization of the results were performed as described in 2.2.1.1. The results were analysed with Wave 2.6.0 software.

2.2.1.3 Seahorse XF Glycolytic Rate Assay Kit

To calculate the basal and compensatory glycolytic rates of each cell line, Seahorse XF Glycolytic Rate Assay Kit was used. For this assay, optimum cell numbers of both established and PDCs were seeded (six replicate wells x 1 condition x 1 cell line) in a microplate one day prior to assay. Also, one sensor cartridge was hydrated with 200 µl Agilent Seahorse XF Calibrant and incubated at 37˚C in a non-CO2 incubator overnight. On the assay day, glycolytic rate assay medium was prepared based on Seahorse XF DMEM medium with 5mM HEPES (103575-100, Agilent Technologies, Santa Clara, USA) and Seahorse XF RPMI medium for established cell lines and PDCs, respectively. If necessary, further supplements were added to achieve final concentrations of 5mM glucose, 2mM glutamine and 5mM HEPES (15630080, ThermoFisher Scientific, Waltham, USA). As described before, the assay medium was warmed up to 37˚C and pH was adjusted to 7.4 with 0.1 N NaOH. Then, low glucose DMEM and low glucose RPMI medium in the wells were changed to the respective glycolytic rate assay medium and cells were incubated 37˚C in a non-CO2 incubator for one hour. In the meantime, inhibitors were loaded into previously hydrated sensor cartridge as described in the Agilent Seahorse XF Glycolytic Rate Assay Kit User Manual (103344-400, Agilent Technologies, Santa Clara, USA). The cartridge with inhibitors was loaded into the Seahorse XF Analyzer for sensor calibration. The glycolytic rate assay medium in wells was replaced with fresh glycolytic rate assay

medium just prior to assay. Then, the plate was loaded and the assay was performed according to the manufacturer's manual. The normalization of results was done as described in section 2.2.1.1 and the results were analysed with Wave 2.6.0 software.

2.2.2 Metabolic inhibitor screening

To determine the half-maximal inhibitory concentration (IC_{50}) of different metabolic inhibitors, in vitro cytotoxicity assays were performed. As a first step, the optimum cell numbers were determined for established and primary cell lines. With densities between 1000 and 6000 cells/well, all cell lines were seeded as triplicates in both 96-well white flat-bottom plates (3917, Corning, New York, USA) for luminescent and a 96-well clear flat-bottom plates (655101, Greiner Bio-One, Kremsmünster, Austria) for visual inspection. The plates were incubated at 37˚C in a humidified atmosphere containing 5 % CO2 for 72 hours. The optimum seeding density for each cell line was determined according to the luminescent signal created by CellTiter-Glo Luminescent Cell Viability reagent (G7573, Promega, Mannheim, Germany) and visual inspection of each well under the microscope (Primovert, Zeiss, Oberkochen, Germany). All drugs were dissolved in dimethyl sulfoxide (DMSO) (A3672, AppliChem, Darmstadt, Germany) (Table 2-1). 96-well white flat-bottom plates were printed with 10 different concentrations of each drug (drug concentrations between either 50-0.01 µM or 25-0.01 µM were logarithmically distributed) using the digital dispenser (D300e, TECAN, Männedorf, Switzerland). Using the reagent dispenser (Multidrop™ Combi, ThermoFisher Scientific, Waltham, USA), established cell lines, as well as PDCs, were seeded as triplicates to the inhibitor-printed 96-well plates in their previously determined optimum densities. The plates were incubated at 37˚C in a humidified atmosphere containing 5 % CO2 for 72 hours. Then luminescent signal proportional to the number of viable cells were measured with Tecan Spark microplate reader after addition of 100 µl luminescent reagent to each well, 2 minutes shaking and 8 minutes incubation at room temperature, respectively. The results were normalized to DMSO control for each inhibitor. The inhibitor concentrations were transformed to a logarithmic scale with the equation 'x=log(X)' and dose-response curves for each cell line and inhibitor were generated by using 'log (inhibitor) vs. normalized response – variable slope' equation. Finally, from these curves, the half-maximal inhibitory concentrations (IC_{50}) for each cell line and each inhibitor was calculated with GraphPad Prism 8 software (GraphPad Software, San Diego, USA).

Table 2-3 Inhibitors

Name	Catalogue #	Supplier
AZD 3965	19912	Cayman Chemicals, Ann Arbor, USA
Cerivastatin	ab142853	Abcam, Cambridge, UK
GSK 2194069	5303	Tocris, Bristol, UK
Ingenol-3-angelate	16207	Cayman Chemicals, Ann Arbor, USA
Lovastatin	ab120614	Abcam, Cambridge, UK
Orlistat	S1629	Selleckchem, Houston, USA
Perhexiline	16982	Cayman Chemicals, Ann Arbor, USA
Shikonin	14751	Cayman Chemicals, Ann Arbor, USA
Simvastatin	S6196	Sigma-Aldrich, St. Louis, USA
Syrosingopine	SML1908	Sigma-Aldrich, St. Louis, USA
TriascinC	Cay10007448	Biomol, Hamburg, Germany
Trimetazidine dihydrochloride	S454301	Selleckchem, Houston, USA

2.2.3 Free fatty acid quantification assay kit

Free fatty acid quantification assay kit (ab65341, Abcam, Cambridge, UK) enables to calculate the intracellular free fatty acid amount for each cell line. For this, both PDCs and established PDAC cell lines were seeded in their normal growth medium (low glucose RPMI and low glucose DMEM, respectively) in 15 cm cell culture dishes and were incubated at 37˚C in a humidified atmosphere containing 5 % CO2. When cells reached 70-80 % confluency, media were changed to FBS-free low glucose RPMI or low glucose DMEM and cells were incubated for lipid starvation for 24 hours. Then cells were washed twice with ice-cold PBS on ice and collected by scratching in 1 ml PBS. 1 x 10^6 cells were collected from each cell line for the free fatty acid quantification. Lipids were extracted and the assay was performed according to the kit protocol. The absorbance proportional to the amount of free fatty acids in standard and sample wells were measured at 570 nm wavelength with Tecan Spark microplate reader and used for calculation of free fatty acid content in each cell line.

2.2.4 Fatty acid uptake assay

BODIPY™ FL C16 (D3821, ThermoFisher Scientific, Waltham, USA) was used to identify the difference in fatty acid uptake between established PDAC cell lines belonging to different PDAC subtypes. The cells were seeded in black, clear-bottom

96 well plates (CLS3603, Corning, New York, USA) with a cell density of 40000 cells/well in low glucose DMEM and incubated overnight for attachment. The next day, low glucose DMEM was changed to a phenol red and FBS-free starvation medium containing 5mM glucose, 2mM glutamine and 1% v/v penicillin-streptomycin and the cells were incubated overnight for lipid starvation. Then, the experimental medium containing 5mM glucose, 2mM glutamine, 25 µM BODIPY™ FL C16 and 25 µM fatty acid-free bovine serum albumin (A8806, Sigma-Aldrich, St. Louis, USA) was prepared and incubated at 37˚C for 30 minutes for attachment of BODIPY™ FL C16 to BSA. Then, the starvation medium on the cells was replaced with the experimental medium containing BODIPY-labelled fatty acid and the cells were incubated with this medium at 37˚C in a humidified atmosphere containing 5 % CO2 for one hour. Subsequently, trypan blue dye solution with a final concentration of 1mM was added to extinguish BODIPY signal outside the cells. The fluorescent signal was measured with Tecan Spark microplate reader at Ex/Em 485/525. For normalization, cells were lysed with 20 µl RIPA buffer per well and protein concentrations measured as described in 2.4.1.

To confirm the import of BODIPY™ FL C16, cells were also seeded in 8-well culture slides (3 wells, 2 experimental and 1 control, for each cell line with 40000 cells/well) (354108, Corning, New York, USA) and incubated overnight for attachment. The next day, low glucose DMEM on the cells was exchanged with phenol red and FBS-free starvation medium containing 5mM glucose, 2mM glutamine and 1% v/v penicillin-streptomycin and the cells were incubated overnight for lipid starvation. Then, the aforementioned experimental medium was added in 2 wells from each cell line and cells were incubated one more hour with this medium. For fixation, the cells were incubated with 4% PFA for 10 minutes at room temperature. Then, cells washed three times with PBS and slides mounted with DAPI-containing mounting medium. Imported BODIPY™ FL C16 was visualised with a fluorescent microscope (Axio Imager.A2, Zeiss, Oberkochen, Germany) at 488 nm wavelength. To calculate the percentage of the cells having BODIPY™- labelled lipid droplets, three representative pictures (with 40x magnification) were taken per well. The total number of cells (DAPI) and the number of cells with BODIPY™- labelled lipid droplets (DAPI+BODIPY) in each picture were counted manually to calculate the percentage of cells with BODIPY™- labelled lipid droplets in each picture. Then, the means of percentages from three pictures of each cell line were calculated to obtain the final result.

2.3 DNA/RNA related methods

2.3.1 RNA isolation

Both established PDAC cell lines and primary cells were seeded on 10 cm cell culture dishes and incubated at 37˚C in a humidified atmosphere containing 5 % CO2 until each one of them reached 70-80 % confluence. Cells were washed twice with ice-cold PBS and collected in 1 ml PBS by scratching on ice. Then, the cell suspensions were centrifuged (Heraeus™ Fresco™ 17, ThermoFisher Scientific, Waltham, USA) at 400 x g and 4˚C for 5 minutes. RNA isolation was done with the Maxwell® RSC simplyRNA Cells Kit (AS1390, Promega, Mannheim, Germany) by using an automated nucleic acid purification system (Maxwell® RSC Instrument, AS4500, Promega, Mannheim, Germany) according to the manufacturer's instructions. The RNA yield and the quality were measured using NanoDrop 2000c spectrophotometer (ND-2000, ThermoFisher Scientific, Waltham, USA) at 260 nm wavelength.

2.3.2 cDNA synthesis

Invitrogen™ SuperScript™ IV First-Strand Synthesis System (18091050, ThermoFisher Scientific, Waltham, USA) was used to synthesize cDNA from isolated RNAs. Total of 2 µg template RNA, 50 µM oligo d(T)20 primer and 10mM dNTP mix (10mM each) were mixed and nuclease-free water up to 13 µl was added to the mixture. The mixture was vortexed (Vortex-Genie 2, Scientific Industries, Bohemia, USA) and heated at 65˚C for 5 minutes for annealing in a thermal cycler (T100, Bio-rad Laboratories, Hercules, USA) and then incubated on ice for one minute to stop the reaction. Reverse transcription mix containing 5x SSIV buffer, 100 mM DTT, RNaseOUT recombinant RNase inhibitor and SuperScript IV reverse transcriptase (200 U/µl) was prepared and added to annealed RNA. The mixture was incubated at 55 ˚C for 10 minutes for reverse transcription and subsequently heated to 80 ˚C for 10 minutes to inactivate reverse transcriptase. cDNA was used either directly or stored at -20 ˚C for further use.

2.3.3 Quantitative Real-Time PCR

Relative gene expression of the genes of interest from each sample were determined with the LightCycler 480 instrument (05015278001, Roche, Basel, Switzerland). Both the standard curve method and the delta-delta CT method were used for calculating the relative gene expression. For the standard curve, standard dilutions were prepared by diluting the cDNA three-fold first and then preparing the dilution series from the first

standard by diluting it tenfold at a time. For sample dilutions, cDNA was diluted for 4-fold. Primers were designed by using Primer 3 software (https://primer3plus.com/) and product specificity were checked with the University of California Santa Cruz in silico PCR (https://genome.ucsc.edu/cgi-bin/hgPcr) and with melting curve analysis. 100 µM primer stock solutions were prepared by following manufacturers' instructions (addition of suggested volume of water to lyophilized primers). Primer mix containing the forward and reverse primers for a specific gene was prepared by diluting 100 µM stock solution 200 times in water (5 µl from each primer stock solution + 990 µl water). In the end, 20 µl of reaction mix consisting of 10 µl the SYBR GREEN PCR Master Mix (04707516001, Roche, Basel, Switzerland), 6 µl primer mix and 4 µl cDNA was prepared for each reaction and loaded into a PCR plate (04729692001, Roche, Basel, Switzerland) as triplicates for each cDNA sample. Beta-glucuronidase (GUSB) gene was used as a reference in every qPCR assay. Each qPCR assay was run for 40 cycles and student's t-test was used for statistical analysis.

Table 2-4 Primer list

Gene ID	Forward Primer	Reverse Primer	Product Size
MYC	CAGCTGCTTAGACGCTGGATT	GTAGAAATACGGCTGCACCGA	131bp
ENO1	GCTCCGGGACAATGATAAGAC	ACCAGGGCAGGCGCAATA	90bp
ENO2	CGGGAACTCAGACCTCATCC	GGAGGATCATGAACTCCTGCA	101bp
GUSB	TGCAGGTGATGGAAGAAGTG	TTGCTCACAAAGGTCACAGG	172bp
HIF1A	GCCGCTGGAGACACAATCAT	TGGGTGAGGGGAGCATTACA	112bp
HK1	CCAACATTCGTAAGGTCCATTCC	CCTCGGACTCCATGTGAACATT	139bp
HK2	GAGCCACCACTCACCCTACT	CCAGGCATTCGGCAATGTG	249bp
LDHA	GCCGTCTTAATTTGGTCCAG	TCTTCCAAGCCACGTAGGTC	135bp
SLC16A1 / MCT1	CACCAGCGAAGTGTCATGGA	ATCAAGCCACAGCCTGACAA	141bp
SLC16A3 / MCT4	ATCACTGGCTTCTCCTACGC	CTGTAGCCGATCCCAAACTC	83bp

2.3.4 Microarray, RNA sequencing and gene set enrichment analysis

RNA samples from established PDAC cell lines, primary cells and PDX samples were sent to DKFZ Genomics and Proteomics Core Facility for transcriptome analysis (Illumina HT12 v4 expression bead chip). The obtained raw data were loaded on a

DKFZ server (HUSAR), which is accessible from DKTK Essen and were analysed on a local server in our lab by Dr Smiths S. Lueong (established cell lines, PDCs, PDX and Patient samples) and Dr. Sven T. Liffers (PDXs) as described below.

Gene expression profiling was performed on patient-derived primary cells and patient-derived xenografts using the Illumina HT12v4 bead chip arrays. Bead intensity information was extracted using the Bioconductor package illuminaio and the limma package was used for background correction. Using the necq function, quantile normalization was performed followed by log transformation. Low expression features were filtered and the probes were collapsed to the highest. The normalized expression values were then exported for downstream analysis.

For established PDAC cell lines, gene expression was achieved by means of 100 bp paired-end mRNA sequencing on an Illumina Novaseq 600. Reads were preprocessed by using CASAVA, Cutadapt and Skewer v.0.2.2 and mapped to the hg38 reference genome using STAR v.2.7.1a. Quantification was performed during alignment using STAR with the --quantMode GeneCounts parameter. A gene expression count matrix was generated with raw read counts using edgeR and stored in s DGEList object containing sample phenodata. All genes with less than 2 count per million reads (cpm) in more than 20% of all samples considered were filtered out. Reads were normalized using the normalization function in edgeR and the normalized read count matrix was used for downstream analysis.

For subtype determination, the normalized expression values were imported in R and the top 3000 most variable features were then selected by calculating the median absolute deviation. The selected features were centered relative to the median and unsupervised clustering was performed using the ConcensusClusterPlus algorithm and validated using a non-negative matrix factorization approach. Gene set enrichment analysis (GSEA) was performed to determine the subtype of each sample by comparing with data from previously published pioneering subtyping studies. Moreover, GSEA with Hallmark, REACTOME and KEGG gene set databases were performed on the identified groups for subtype-specific gene networks determination with the data from established and primary PDAC cell lines PDXs and patient samples.

Single gene expression analyses were performed with the normalized gene expression values from the aforementioned data sets. Mann-Whitney test was used to determine

statistical significance in gene expression levels between PDAC subtypes as well as between PDAC patients, pancreatitis patients and healthy samples.

2.4 Protein related methods

2.4.1 Protein isolation and quantification

Established PDAC cell lines and PDCs were seeded to 10 cm cell culture dishes and incubated at 37˚C in a humidified atmosphere containing 5 % CO2 until each cell line reach 70-80 % confluence. Dishes were washed with ice-cold PBS twice and then cells were collected with 1 ml PBS containing phosphatase (4906845001, Roche, Basel, Switzerland) and proteinase (4693124001, Roche, Basel, Switzerland) inhibitors by scratching on ice. Cells were centrifuged at 400 x g for 5 minutes at 4 ˚C to obtain the cell pellet. For cell lysis, cells were resuspended in 50-100 µl RIPA buffer (9806S, Cell Signalling Technology, Danvers, USA) and incubated for 20 minutes on ice, then centrifuged at 10000 rpm for 10 minutes at 4 ˚C. Supernatant containing proteins from each cell line was transferred to a new Eppendorf tube for storage at -80 ˚C. For quantification of the protein concentration in each sample, the Pierce™ BCA Protein Assay Kit (23225, Thermo Fisher Scientific, Waltham, USA) was used according to manufacturer's instructions. After 30 minutes incubation of samples and different concentrations of albumin standards with bicinchoninic acid (BCA) solution at 37 ˚C, the colorimetric measurement was performed at 490 nm wavelength with the Tecan Spark microplate reader and calculations of protein concentrations were done with Microsoft Excel (Microsoft, Redmond, USA).

2.4.2 Western blot analysis

As a first step, a western blot working solution containing 10 µg protein (in RIPA buffer), the appropriate amount of 10mM Tris-HCl solution and 1x loading buffer was prepared for each sample and incubated at 95 ˚C for five minutes for protein denaturation. Physical separation of the proteins of interest was performed with 10 % (proteins of interest have a molecular weight between 30 – 110 kDa) SDS polyacrylamide gel with Mini-PROTEAN® Tetra Handcast Systems (1658006FC, Bio-Rad, Hercules, USA). Then, separated proteins were transferred to a nitrocellulose membrane via Trans-Blot® Turbo™ RTA Mini Nitrocellulose Transfer Kit (1704270, Bio-Rad, Hercules, USA). After transfer, membranes were cut according to the molecular weight of the protein of interest and were then blocked against unspecific binding in 5% bovine serum albumin (BSA) in 0,1 % Tween 20 (Carl Roth, 9127.1, Carl Roth, Karlsruhe,

Germany) in TBS (TBST) solution for one hour at room temperature. For protein-specific detection, membranes were incubated with the appropriate primary antibody solution (in 5% BSA in TBST) overnight at 4 ˚C. Next, membranes were washed 3 x 10 minutes with TBST and incubated for one hour at room temperature with either anti-rabbit or anti-mouse secondary antibody according to primary antibody's host species. After washing the membrane 2 x 10 minutes with TBST and 1 x 10 minutes with TBS, the protein bands were detected with SuperSignal™ West Dura Extended Duration horseradish peroxidase substrate (34076, ThermoFisher Scientific, Waltham, USA) and ChemiDoc™ MP imaging system (Bio-Rad, Hercules, USA). Image Lab version 6.0.0 software (Bio-Rad, Hercules, USA) were used for the analysis of the detected protein bands.

Table 2-5 Primary and secondary antibodies for western blot

Primary Antibodies				
Target	**Species**	**Dilution**	**Catalogue #**	**Supplier**
β-actin	Rabbit	1:15000	ab8227	Abcam
LDHA	Rabbit	1:1000	3582	Cell Signalling
HIF1A	Mouse	1:500	610958	BD Biosciences
SLC16A3/MCT4	Rabbit	1:1000	HPA021451	Atlas antibodies
MYC	Rabbit	1:1000	ab32072	Abcam
Secondary Antibodies				
Target	**Species**	**Dilution**	**Catalogue #**	**Supplier**
Anti-rabbit	Goat	1:50000	111-035-003	Jackson ImmunoResearch
Anti-mouse	Goat	1:10000	115-035-003	Jackson ImmunoResearch

2.4.3 Immunohistochemistry

Formalin-fixed paraffin-embedded (FFPE) PDAC patient samples were stained against metabolic targets with primary antibodies (Table 2-4). The embedded tumour tissue was sectioned at 3 µm and sections were prepared for further analysis. First, FFPE slides were deparaffinised and rehydrated with Leica ST5010 Autostainer XL (ST5010, Leica Biosystems, Wetzlar, Germany): 3 x Xylene, 2 x 100% ethanol, 2 x 96% ethanol, 2 x 70% ethanol, and ddH_2O. Then, slides were incubated in either Tris-based or

Citrate-based antigen unmasking solution (H-3300 and H-3301, respectively, Vector Laboratories, Burlingame, USA) at 110 ˚C in a decloaking chamber (DC2012, Biocare Medical, Pacheco, USA) for 15 minutes. After the slides cooled down for 30 minutes, the tissues on each slide were circled with a hydrophobic pen (H-4000, Vector Laboratories, Burlingame, USA) and incubated with 3% hydrogen peroxide (1072091000, Merck, Darmstadt, Germany) for 15 minutes to block endogenous peroxides. Then slides were incubated 5 minutes with blocking solution (ZUC007, Zytomed systems, Berlin, Germany) to prevent unspecific primary antibody binding. Next, the respective antibody was diluted with SignalStain® Antibody Diluent (8112L, Cell Signalling Technology, Danvers, USA) to desired concentration and slides were incubated with antibody solutions for one hour at room temperature. After the incubation with a primary antibody, slides were incubated with ZytoChem Plus (HRP) One-Step Polymer anti-Mouse/Rabbit/Rat (ZUC053, Zytomed systems, Berlin, Germany) secondary antibody for 30 minutes at room temperature. Then, signals were developed with Liquid DAB+, 2-component Immunohistochemistry Visualization system (K346811-2, Agilent Technologies, Santa Clara, USA). Counterstaining of the tissue was performed with haematoxylin (1092491000, Merck, Darmstadt, Germany) and the slides were washed under running tap water for 10 minutes. Between the aforementioned steps, all slides were washed 3 x 5 minutes with 0.1 % Triton-X 100 (Carl Roth, 3051.3) in TBS and rinsed with TBS when it was necessary. Then, slides were dehydrated in the autostainer (2 x 70% ethanol, 2 x 96% ethanol, 2 x 100% ethanol, and xylene.) and mounted with Medite Pertex xylene based mounting medium (MEDITE, Orlando, USA). Lastly, slides were incubated overnight and scanned with Zeiss Axio Scan.Z1 slide scanner (Zeiss, Oberkochen, Germany) by using 10x bright-field filters.

2.4.4 Multiplex immunofluorescence

Co-expression of metabolic marker proteins with either Cyto-keratin 81 (KRT81, QM marker) or GATA6 (Classical marker) on therapy naïve, resected FFPE patient samples were evaluated with immunofluorescent multiplexed staining. For this, Opal 7-Color Automation IHC Kit (NEL811001KT, Perkin Elmer, Waltham, USA) was used. Since the protocol consists of the repetition of immunohistochemical staining and fluorescent labelling of proteins of interest with different Opal fluorophores until all targets detected, immunohistochemical staining protocol for each antibody were

optimized prior to multiplex staining. Then, the antibodies were paired with different Opal fluorophores and the consecutive staining order for each antibody were determined to obtain the best result for multiplex staining. When optimized IHC conditions, antibody-fluorophore pairs and staining order were determined, the protocol below was followed. First, FFPE slides were dewaxed with Leica ST5010 Autostainer XL (3 x Xylene, 2 x 100% ethanol, 2 x 96% ethanol, 2 x 70% ethanol, and ddH_2O). After deparaffinization, slides were fixed with 4 % PFA for 20 minutes at room temperature. Then, slides were incubated in either Tris-based or Citrate-based antigen unmasking solution (Vector Laboratories, H-3300 and H-3301, respectively) in a microwave (NN-E201 WM, Panasonic, Kadoma, Japan) at maximum power for 5 minutes and at 360 watts for 20 minutes. After the slides cooled down for 30 minutes, tissues on each slide were circled with a hydrophobic pen and incubated with 3% hydrogen peroxide to block endogenous peroxides. Slides were incubated 5 minutes with blocking solution and 30 minutes with antibody diluent/blocking solution (ARD1001EA, Perkin Elmer, Waltham, USA) to prevent unspecific primary antibody binding. Next, the respective antibody was diluted in antibody diluent/blocking (ARD1001EA, Perkin Elmer, Waltham, USA) to desired concentration and slides were incubated with antibody solutions for one hour at room temperature or 4°C overnight. After incubation with primary antibody, slides were incubated with Opal Polymer HRP Ms+Rb (Perkin Elmer; ARH1001EA) secondary antibody for 30 minutes at room temperature. For fluorescent labelling, the slides were incubated with the respective Opal fluorophore, which was prepared according to the manufacturer`s instructions and diluted 200 times before use for 10 minutes at room temperature. Slides were washed 2 x 5 minutes with TBS-T and 1 x 5 minutes with TBS between each step. This protocol was repeated starting from the antigen retrieval step for each antibody but with different Opal Fluorophores. After the last staining cycle, antigen retrieval step was performed with citrate-based buffer. Then, slides were cooled down and mounted with VECTASHIELD® Antifade Mounting Medium with DAPI (H-1200-10, Vector Laboratories, Burlingame, USA). During the staining process, all steps were performed under light protection.

Table 2-6 Primary antibodies for immunohistochemistry and multiplex immunofluorescence

Primary antibodies				
Target	**Species**	**Dilution**	**Catalogue #**	**Supplier**
LDHA	Rabbit	1:600	3582	Cell Signalling
GLUT1	Rabbit	1:800	ab652	Abcam
ENO1	Rabbit	1:800	ab85086	Abcam
PKM2	Rabbit	1:200	4053	Cell Signalling
ACACA	Rabbit	1:50	3662	Cell Signalling
ACACB	Rabbit	1:300	HPA006554	Atlas Antibodies
SLC25A20	Rabbit	1:25	HPA016862	Atlas Antibodies
FASN	Rabbit	1:100	3180	Cell Signalling
ACSL5	Rabbit	1:100	HPA007162	Atlas Antibodies
ACSL4	Rabbit	1:100	HPA005552	Atlas Antibodies
MCT1	Rabbit	1:200	ab85021	Abcam
KRT81	Rabbit	1:100	ab197356	Abcam
SLC16A3/MCT4	Rabbit	1:400	HPA021451	Atlas Antibodies
Pan-cytokeratin	Mouse	1:100	ab6401	Abcam
GATA6	Goat	1:50	AF1700	R&D systems

2.4.5 Image analysis

The whole-slide quantification analysis of immunohistochemically and immunofluorescently stained FFPE patient samples was done with Definiens Tissue Studio 4.3 software (Definiens AG, Munich, Germany). First, images obtained from immunohistochemistry or immunofluorescent analyses were uploaded to the software. Region of interest (ROI) containing tumour and stromal parts of each slide was separately determined. Then, twelve representative fields from each slide were selected for setting the signal thresholds. The signal threshold for haematoxylin staining and nucleus diameter was set for cellular detection. Three different signal thresholds for the protein of interest were determined to detect low, medium and highly stained cells. The software detects and counts every cell in the ROI according to pre-set thresholds. The number of positive cells (low, medium and high) in the ROI of each slide were used to calculate the percentage of positive cells. Finally, the differences in expression between different samples were analysed by comparing the percentage of positive cells.

For immunofluorescent image analysis, determination of the ROI and the detection of nucleus and cells in the ROI were performed as described above. Different from IHC analysis, one threshold (low) was determined for each protein of interest. Therefore, the software can detect and count every positive and negative cell for each protein in the ROI. Additionally, the software also calculated the number of cells co-expressing at least two proteins. With these numbers, the percentage of cells expressing each protein separately and/or simultaneously was calculated and used for co-expression analyses.

2.5 Metabolite profiling

2.5.1 Targeted metabolite profiling

2.5.1.1 Targeted lipid profiling

Both primary and established PDAC cell lines were seeded in 10 cm tissue culture dishes as triplicates. The low glucose growth media in every dish were changed after overnight incubation. After further incubation at 37˚C in a humidified atmosphere containing 5% CO_2 for 48 hours, cells were collected on ice by scratching after a two-time wash with ice-cold PBS. The number of cells from each dish were counted with TC20 automated cell counter. Then, 1 x 10^6 cells from each dish were collected for metabolite analysis and 3 x 10^5 cells from the same dish transferred to a separate tube for protein content measurement for the normalization of the results. The cells were centrifuged at 400 x g at 4 ˚C for 5 minutes and supernatants were aspirated and cell pellets were frozen with dry ice and stored at -80 ˚C for further analysis. Then samples were sent in dry ice to Prof. Dr. Thomas Hankemeier's group at the University of Leiden, the Netherlands for analysis and lipid profiling was performed by Wei Yang and Dr. Amy Harms as described below.

For each cell pellet, 600 µL ice-cold 80% methanol in water was added to lyse the cells followed by vortexing in a bullet blender with beads at speed of 6 for 2 minutes. 150 µL cell suspension was transferred to a new Eppendorf tube for sample preparation of positive lipids platforms. Bligh & Dyer method was applied with Chloroform: MeOH: H_2O (1:2:2 in volume). The aqueous phase and organic phase (with lipids) were transferred to a new tube respectively and the solvents were dried in the Speedvac. The dried lipids were reconstituted with isopropanol according to SOP 101 version 10 in house and all samples then were transferred to vials to be ready for analysis. The lipids were analysed with ultra-performance liquid chromatography- electrospray

ionization-quadrupole time-of-flight (UPLC-ESI-Q-TOF6530) method. Acquired data were evaluated using MultiQuant Software for Quantitative Analysis (AB SCIEX, Version 3.0.2), by the integration of assigned MRM peaks and normalization using proper internal standards. Response ratio (RR) of each metabolite was then corrected with protein concentration. 230 µL cell suspension was transferred to a new Eppendorf tube for sample preparation of signalling lipid platform. The sample was spike with 5 µL antioxidant, 10 µL internal standards, 150 µL buffer (pH 4.6) and 1mL extraction solvent (BuOH:MTBE 1:1). After sample vortex in the bullet blender, all the samples were centrifuged for 10min at 158000 rcf. The supernatant was transferred and dried and then was reconstituted for analysis. The samples were analysed by ultra-performance liquid chromatography-tandem mass spectrometer (UPLC-MS/MS) using a Kromasil Eternity XT C18 column (Akzo Nobel) for high pH and an Acquity BEH C18 column (Waters) for the low pH method. The Triple quadrupole MS was used in polarity switching mode and all analytes were monitored in dynamic Multiple Reaction Monitoring (dMRM). The acquired data was evaluated using LabSolutions software (Shimadzu), by the integration of assigned MRM peaks and normalization using accordingly selected internal standards. When available, a deuterated version of the target compound was used as an internal standard. For the other compounds, the closest-eluting internal standard was employed. Response ratio (RR) of each metabolite was then corrected with protein concentration. The acquired data for each platform was analysed with MetaboAnalyst 4.0 (https://www.metaboanalyst.ca/) (Chong et al., 2018).

2.5.1.2 Biocrates AbsoluteIDQ® p180 Kit

Both primary and established PDAC cell lines were seeded in 10 cm tissue culture dishes as quadruple. The low glucose growth media in every dish were changed after overnight incubation. Then cells further were incubated at 37˚C in a humidified atmosphere containing 5% CO2 for 48 hours. Cells from 2 dishes were washed with 15 ml room temperature- warm PBS containing $MgCl_2$ and $CaCl_2$ (D8662, Sigma-Aldrich, St. Louis, USA) once and 1 ml ice-cold 100% methanol was added. Then, cells were collected by scratching on ice. Collected cells were frozen immediately and preserved at -80˚C. The two remaining dishes were used to measure the protein concentration which is then, used for normalization of the results. Cell pellets were then sent to Biocrates Life Sciences, Innsbruck, Austria and targeted lipid profiling was

performed with the Biocrates AbsoluteIDQ p180 (Biocrates Life Sciences, Innsbruck, Austria) kit and UPLC-MS/MS. The acquired data for each platform was analysed with MetaboAnalyst 4.0 (https://www.metaboanalyst.ca/) (Chong et al., 2018).

2.6 Statistical analysis

GraphPad Prism 8 software was used for statistical analysis. Two-tailed heteroscedastic t-test was used to determine statistical significance and p-value was employed as; $p<0.05$ (*), $p<0.01$(**), $p<0.001$(***) and $p<0.0001$(****). Kaplan-Meier survival analysis and Mantel-Cox test were used to prepare and compare survival curves, respectively.

3 Results

3.1 Hypoxia/glycolysis and lipid metabolism related gene sets are differently regulated in quasi-mesenchymal and classical PDAC subtypes

To identify subtype-specific metabolic features on transcriptome level, a large collection of gene expression data from different PDAC models was established and analysed (Table 3-1). For this purpose, total RNA was collected from 8 established cell lines and 11 PDX-derived primary cells (PDCs) and RNA-seq as well as Illumina HT-12 v4 bead chip arrays were performed, respectively. For 48 patient-derived xenografts (PDX), data from Illumina HT-12 v4 bead chip arrays were kindly provided by Prof. Stephan Hahn (University of Bochum). In addition, transcriptome data (Illumina Sentrix Human-6v3 Whole Genome Expression BeadChips) of 204 PDAC patient samples was kindly provided by Prof. Jörg Hoheisel (DKFZ Heidelberg) (E-MTAB-1791 (Jandaghi et al., 2016)).

Table 3-1 Data sets and obtained platforms

Data Set	Platform
Established PDAC cell lines	RNA-seq
PDX derived primary cell lines	Illumina HumanHT-12 v4 expression beadchip array
Patient derived xenografts	Illumina HumanHT-12 v4 expression beadchip array
Patient samples	Illumina Sentrix Human-6v3 Whole Genome Expression BeadChips

After data collection, patient, PDX and PDC data sets were successfully clustered into two major PDAC subtypes, classical and QM. The classification of samples into subtypes was kindly conducted by Dr. Smiths S. Lueong via using a developed classification system based on transcriptional data from publicly available datasets with known subtypes (PDAC cell lines, GSE21654, (Maupin et al., 2010); PDAC xenograft, E-MTAB-4029, (Noll et al., 2016) and PDAC tumours, GSE16515, (Pei et al., 2009) and GSE15471, (Badea, Herlea, Dima, Dumitrascu, & Popescu, 2008)). For established PDAC cell lines, the classification done by Daemen et al. was used and 4 cell lines from each subtype were selected for further analyses (QM: Kp4, MiaPaca2,

PaTu8988T, PSN1 and classical: HPAC, HPAFII, HUPT4, PaTu8988S, PaTu8988S) (Daemen et al., 2015).

Table 3-2 Stratification of PDAC models into subtypes

Data set	Sample size	Classical	QM
Established cells	8	4	4
PDCs	11	6	5
PDXs	48	28	20
Patient Samples	204	88	116

Following the subtyping, gene set enrichment analysis (GSEA Broad institute; HALLMARK, KEGG and REACTOME collections) was performed to compare gene expression patterns of classical and QM subtypes in all datasets. In patient, PDX and PDC data sets, QM subtype demonstrated an enrichment of epithelial-to-mesenchymal transition gene set (HALLMARK_EMT) correlating with mesenchymal features of the subtype (Bailey et al., 2016). In classical samples, an enrichment of transcripts related to epithelial organizations such as cell-cell organization and tight junctions (HALLMARK Apical Junction) was observed in established, PDC and PDX data sets (Figure 3.1). This observation suggesting mesenchymal and epithelial phenotype for QM and classical subtype, respectively, correlated with the literature (Bailey et al., 2016; Collisson et al., 2011) and supported our internally-developed classification system.

The analysis of subtype-specific metabolic transcripts revealed that specific metabolic processes are remarkably preserved in one or the other subtype throughout different models. Gene sets of glycolysis, hypoxia, MYC targets were frequently enriched in QM samples of investigated PDAC models, whereas transcripts related to different facets of lipid metabolism dominated classical samples in all data sets (Figure 3.1). Although, PDCs were cultured in typical laboratory normoxic conditions and thus, were exposed to completely different microenvironment than patient and PDX tumours, enrichment of hypoxia gene set (HALLMARK_HYPOXIA) was detected in QM subtype of PDX, PDC and patient data sets (Figure 3.1). Similarly, glycolysis/glucose metabolism gene sets in QM subtype were preserved in PDX, patient and established cell line data sets together with the enrichment of ‘MYC-targets’ gene sets despite the

microenvironmental distinctions (Figure 3.1). Interestingly, glycolysis gene set was not enriched in QM PDC cells, probably due to higher heterogeneity in patient-derived cells and low number of samples.

The enrichment of transcripts related to glycerolipid metabolism was detected in classical samples of patient, PDX and established cells while glycosphingolipid metabolism gene set was upregulated in classical group of PDCs and established cells. Moreover, classical group of PDX and patient data sets correlated with fatty acid metabolism gene set. In addition, cholesterol metabolism gene set was refined in classical PDX, PDC and established cell lines (Figure 3.1).

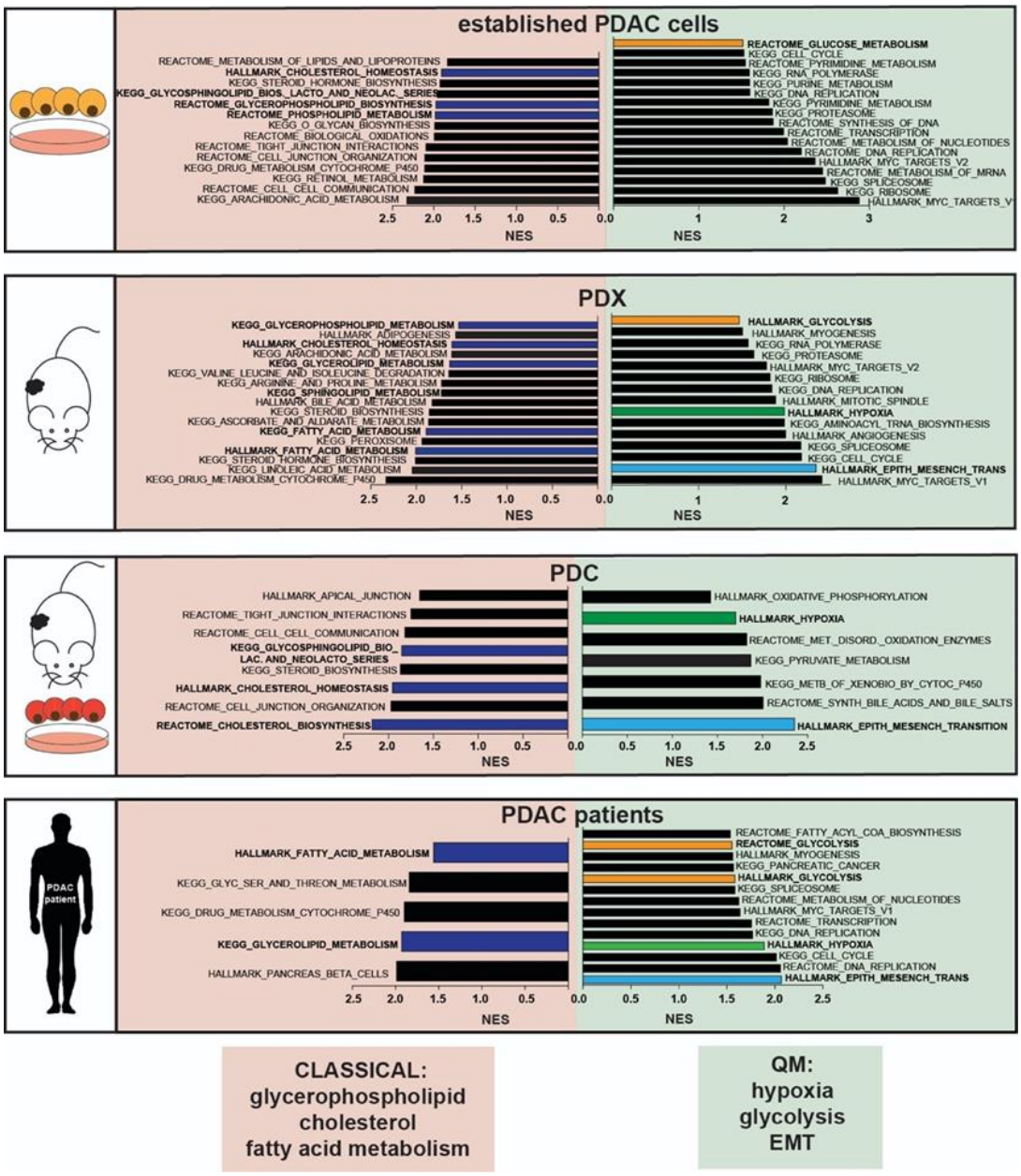

Figure 3.1 **Gene Set Enrichment Analysis (GSEA) identifies glycolysis/hypoxia and lipid/fatty acid metabolism as enriched in QM and classical PDAC samples respectively**. GSEA analysis was performed for established cells (n=8, 4QM, 4 classical), Patient-Derived Xenografts (PDX; n=48, 20 QM and 28 classical), Patient-Derived Cells (PDC; n=11, 5 QM and 6 classical) and Patient Samples (N=204; 116 QM, 88 classical). Presented are Normalized Enrichment Scores (NES>1.5) for selection of metabolic gene sets identified as significantly enriched (FDR q value <0.05) in QM or classical subtypes. Gene set databases HALLMARK, REACTOME and KEGG were used for analysis. In the QM dataset, Epithelial to Mesenchymal Transition (EMT, blue), Glycolysis/Glucose Metabolism (orange), Hypoxia (green) and MYC targets are commonly enriched in most of the datasets. Gene sets typical for the cellular organization (tight junctions, cell-cell communication) together with lipid/cholesterol/fatty acid metabolism (dark blue) are enriched in classical subtype.

3.2 Functional evaluation of glycolysis in pre-clinical PDAC models

3.2.1 Highly glycolytic cells present high *HIF1A/MYC* expression

Global enrichment of glycolysis and hypoxia-related gene sets in QM groups of all investigated PDAC models indicated that glycolysis might be metabolically active in this subtype. However, gene expression is not necessarily directly translated into active metabolic processes. Metabolic processes are largely regulated by different factors such as substrate and co-factor availability, microenvironmental conditions, post-translational modifications, etc. Therefore, to evaluate whether glycolysis identified in the transcriptome is physiologically relevant, glycolytic activity was first assessed with Seahorse metabolic flux assays in established and PDX-derived primary PDAC cell lines. Seahorse assays are performed with living cells and provide more comprehensive image of cells' actual metabolic activity. The two major energy-producing processes in the cell, glycolysis and OXPHOS, are evaluated and their activities are estimated with Seahorse metabolic flux assays by measuring the proton (H+) concentration and oxygen pressure in media in the vicinity of cells.

To analyse the differences in glycolysis, Seahorse Glycolytic Rate assay was used. In this assay, first, cellular oxygen consumption and extracellular acidification rates are measured in the absence of inhibitors that provides basal oxygen consumption and extracellular acidification rates. Then, the mitochondrial activity is blocked with acute treatment of chemical agents Rotenone/Antimycine A (Electron transport chain-ETC inhibitors). To compensate for the loss of mitochondrial activity, cells are forced to use glycolysis at the maximum capacity that enables measure of maximal cellular glycolytic capacity. Later, glycolysis is blocked with acute treatment of glucose analogue 2-deoxy-D-glucose forcing the glycolysis to decrease to minimal levels. Measurement of oxygen consumption and extracellular acidification in these three different phases allow calculations of both basal and compensatory glycolysis performed in the cells. The results of the Seahorse glycolytic rate assay suggested that PDC69 and PDC80 (primary) and PSN1 (established cells), all classified as QM, present the highest basal and compensatory glycolytic rates. (Figure 3.2.A and Figure 3.2.B)

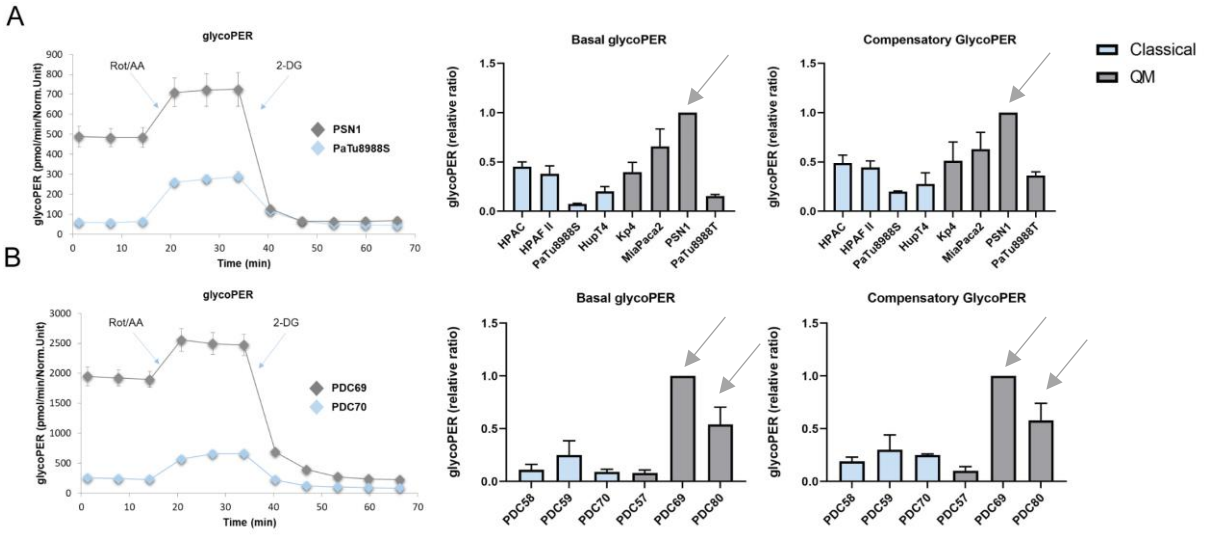

Figure 3.2 **QM cell lines PSN1, PDC69 and PDC80 have highest glycolytic rates.** (A) (Left) Representative graph showing higher glycolytic proton efflux rates in PSN1 (QM) than in classical cell line PaTu8988S (classical). Bar graphs depicting higher basal (middle) and compensatory glycolysis (right) in QM cells, especially in PSN1. (B) (Left) Representative graph showing higher glycolytic proton efflux rates in PDC69 (QM) than in classical cell line PDC70. Bar graphs depicting higher basal (Middle) and compensatory (Right) glycolysis in primary QM cell lines PDC69 and PDC80. The results were normalized by comparing glycolytic rates of each commercial cell lines with the glycolytic rate of PSN1 and by comparing glycolytic rates of each PDCs with the glycolytic rate of PDC69.

To further evaluate glycolysis in these cell lines, gene and protein expression of some known glycolytic enzymes and regulators were analysed with qPCR and Western Blot. In addition to their higher glycolytic rates, PSN1, PDC69 and PDC80 presented highest levels of glycolytic regulators hypoxia-inducible factor 1-alpha (HIF1A) and MYC as well as glycolytic markers lactate dehydrogenase A (LDHA) and monocarboxylate transporter 4 (MCT4/SLC16A3) on both mRNA and protein levels. (Figure 3.3.A and Figure 3.3.B).

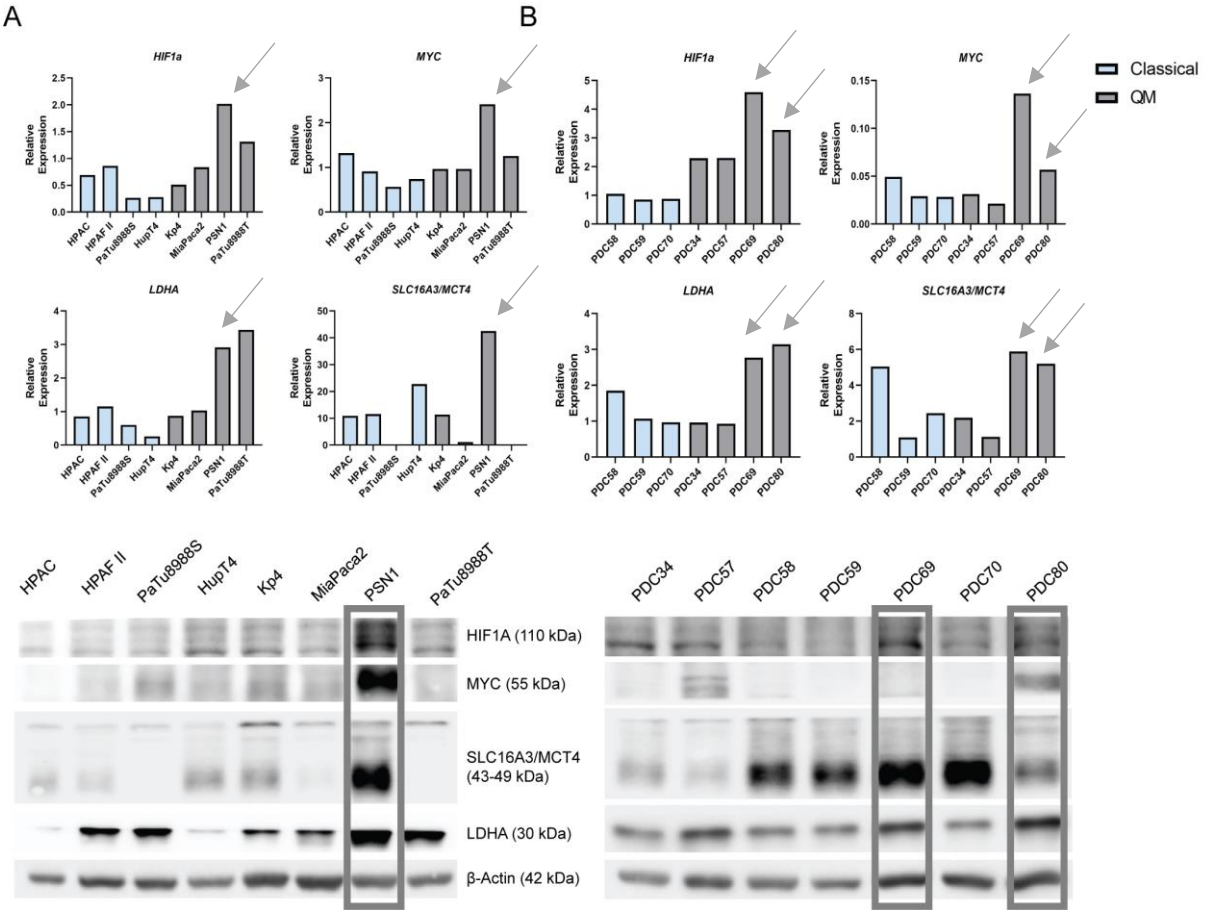

Figure 3.3 **qPCR and western blot analysis for important glycolytic players in established cell lines and PDCs.** Cell lines having higher glycolytic rates also present upregulation of glycolytic regulators HI1Fa and MYC as well as glycolytic markers LDHA and SLC16A3/MCT4. (A) PSN1 (QM) which has the highest basal and compensatory glycolytic rates among established cell lines, also showed the highest expression of glycolytic regulators HIF1A and MYC together with glycolytic markers LDHA and MCT4 on both mRNA (top left) and protein (bottom left) level. (B) PDC69 and PDC80 (both QM) which presented the highest basal and compensatory glycolytic rates in primary cell lines also showed highest mRNA (top right) and protein expression (bottom right) of HIF1A, MYC, LDHA and MCT4. (Ms. Alina Winkelkotte kindly performed primary cell qPCR for HIF1A, LDHA and SLC16A3/MCT4)

Additionally, gene expression analysis of some other important glycolytic enzymes such as Hexokinase 1 and 2 (*HK1, HK2*), Enolase 1 and 2 (*ENO1, ENO2*), Monocarboxylate transporter 1 (*SLC16A1/MCT1*) demonstrated a trend towards higher expression in QM than in classical established PDAC cells (Figure 3.4.A). In PDCs, higher heterogeneity in the expression of glycolytic markers was observed. Again, glycolytic cell lines PDC69 and PDC80 showed the highest expression of glycolytic genes *MCT1, HK1, ENO1* (Figure 3.4.B)

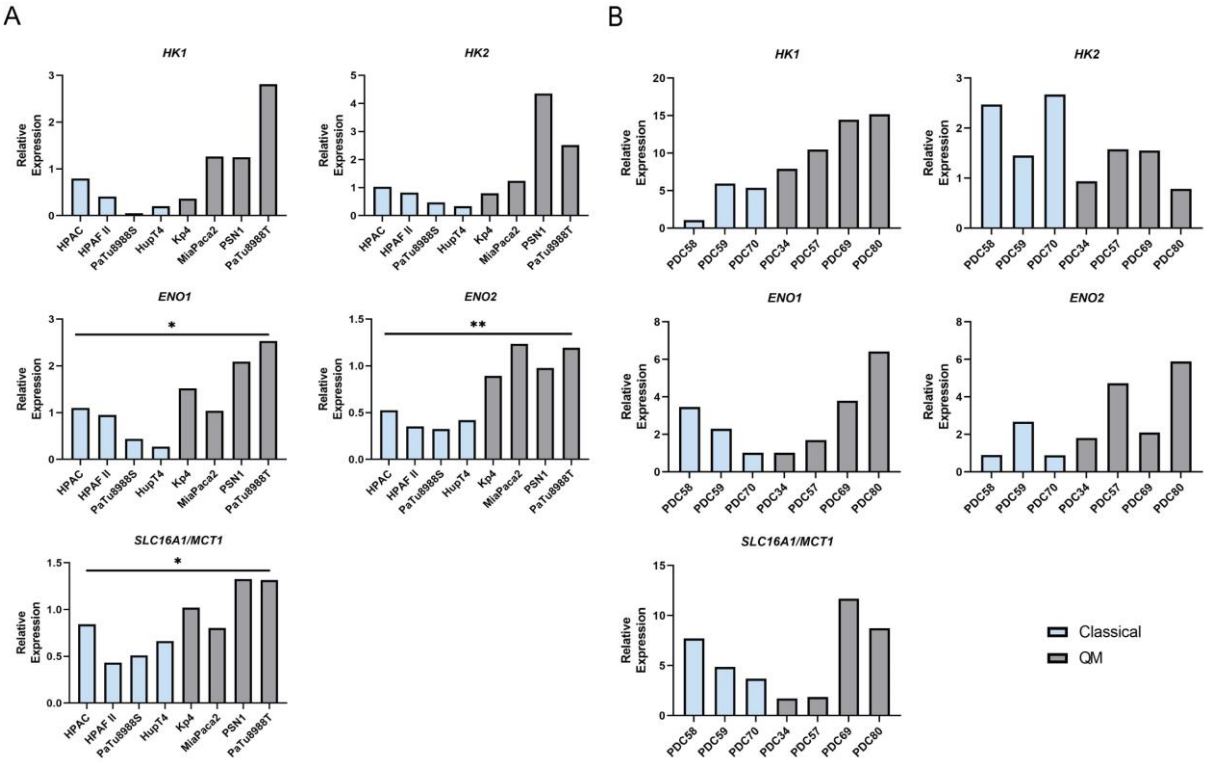

Figure 3.4 **qPCR analysis of important glycolytic players in established PDAC cell lines and PDCs.** (A) Expression of glycolytic genes *HK1/2, ENO1/2* (p=0,034 and p=0,001, respectively) and *MCT1* (p=0,020) is, in general, higher in QM established cell lines, especially in highly glycolytic PSN1, than classical established cell lines. (B) Even though heterogeneity in glycolytic gene expression is more visible in PDCs, highly glycolytic cell lines PDC69 and PDC80 had the highest expression of glycolytic enzymes *HK1, ENO1* and *MCT1*. All p-values were calculated with two-tailed heteroscedastic t-test.

In conclusion, these results support the connection between glycolytic gene expression and glycolytic rate in PDAC cells. A general trend towards higher expression of glycolytic genes in QM then in classical cells has been observed. However, heterogeneity in gene expression even among the members of the same subtype is also present, especially among primary cells.

3.2.2 Glycolytic marker analysis in PDAC patient samples

To evaluate glycolysis and the value of glycolytic enzymes as QM-specific markers in patient samples, single gene expression analysis and immunohistochemical staining were performed with patient data and FFPE patient samples, respectively.

Initially, patient gene expression data (E-MTAB-1791 (Jandaghi et al., 2016)) containing samples from healthy individuals (n=41), pancreatitis (n=59) and PDAC patients (n=204) was used to analyse PDAC specific expression of glucose transporter *GLUT1* and glycolytic enzymes *ENO1,* pyruvate kinase isoform M2 *(PKM2), LDHA*.

The analysis showed that *GLUT1, ENO1, PKM2* and *LDHA* expression was significantly increased in PDAC patients compared to pancreatitis patients and healthy individuals (Figure 3.5.A). Among PDAC patients, all investigated glycolytic genes were higher in QM than in classical PDACs (Figure 3.5.B).

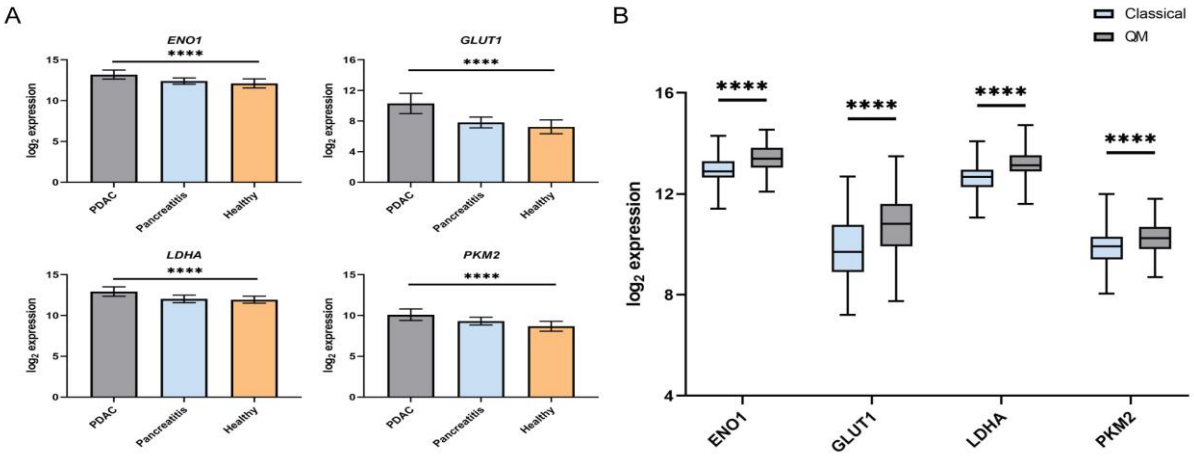

Figure 3.5 **PDAC specific expression of glycolytic enzymes.** (A) The expression of glucose transporter *GLUT1* (PDAC vs Healthy, p<0,000001; PDAC vs Pancreatitis, p<0,000001) and glycolytic enzymes *ENO1* (PDAC vs Healthy, p<0,0001; PDAC vs Pancreatitis, p<0,0001), *LDHA* (PDAC vs Healthy, p<0,0001; PDAC vs Pancreatitis, p<0,0001) and *PKM2* (PDAC vs Healthy, p<0,0001; PDAC vs Pancreatitis, p<0,0001) were significantly increased in PDAC patients compared to healthy pancreata. (B) Among PDAC patients, QM samples showed significantly higher expression of *ENO1* (QM vs Classical, p<0,0001) *GLUT1* (QM vs Classical, p<0,0001), *LDHA* (QM vs Classical, p<0,0001) and *PKM2* (QM vs Classical, p<0,0001). All p-values were calculated with two-tailed heteroscedastic t-test.

Next, PDAC patient FFPE material (9 therapy naïve PDAC patients) were immunohistochemically stained for glycolytic enzymes GLUT1, ENO1, PKM2, LDHA and lactate transporters MCT1, MCT4. First, tissue samples were classified into classical and QM subtype according to the expression of cytokeratin 81 (KRT81), previously identified as QM biomarker and samples with high expression of KRT81 are categorized as QM (classification of FFPE samples into subtype were kindly provided by Dr. Fung-Yi Cheung) (Noll et al., 2016). 5 classical and 4 QM samples were identified and stained against the aforementioned glycolytic enzymes and transporters. The results revealed stronger expression of GLUT1, ENO1, PKM2 and LDHA on cancer cells than stromal cells (Figure 3.6.A). However, differences between classical and QM subtypes were not visually detectable. Thus, each staining was quantified in terms of signal intensity with Definiens Architect Tissue Studio software (explained in

section 2.4.5). Whole-slide quantification of the number of cells with a positive signal of each enzyme showed no dramatic difference in staining intensities among QM and classical samples (Figure 3.6.B).

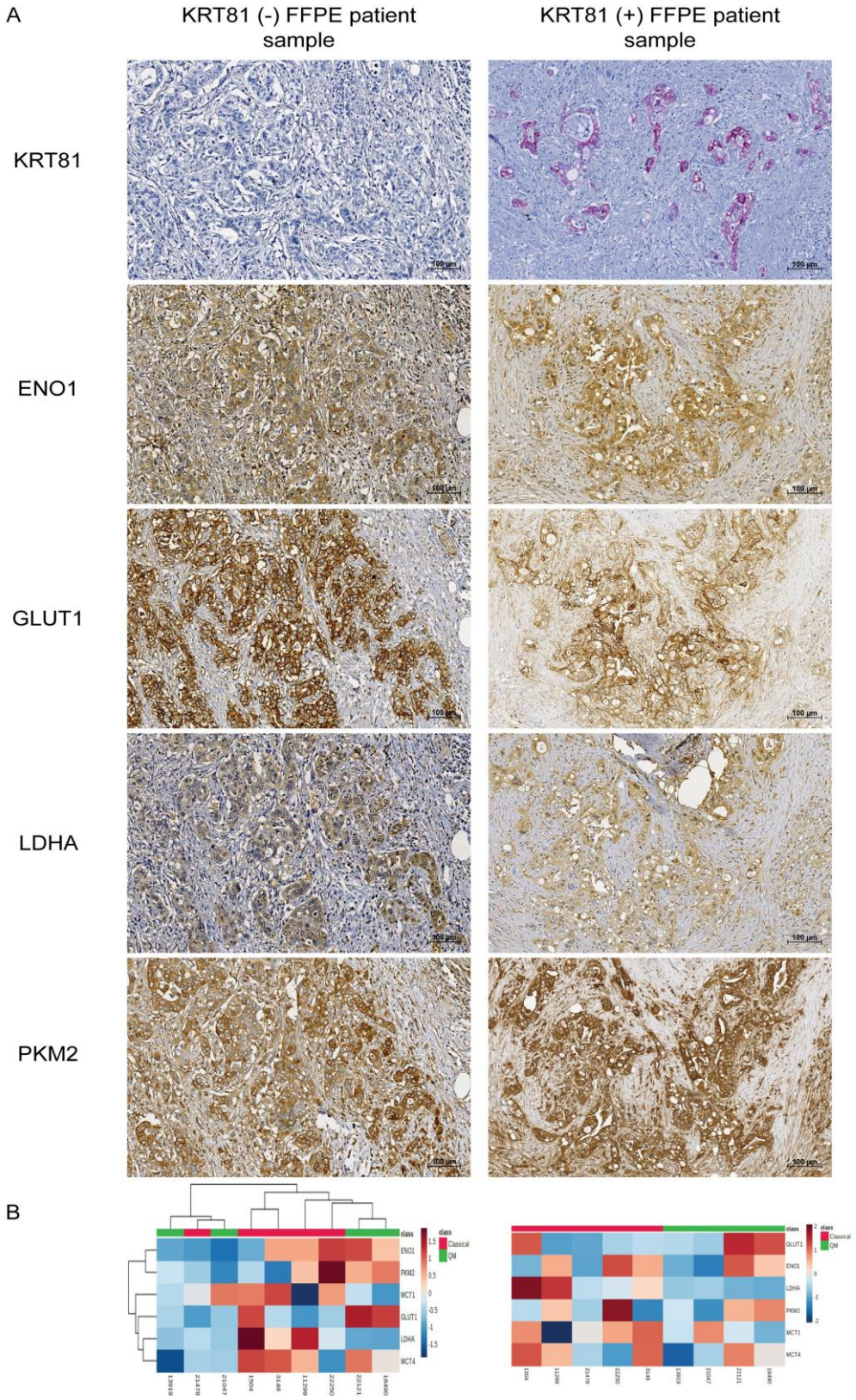

Figure 3.6 **No clear difference observed in intensity of immunohistochemical stainings for glycolytic proteins ENO1, GLUT1, LDHA and PKM2 between Classical (KRT81 negative) and QM (KRT81 positive) FFPE patient samples**. (A) Both KRT81 (-)/classical FFPE samples (first column) and KRT81 (+)/QM FFPE samples (second column) show good expression of respective glycolytic proteins compared to stromal cells. However, no clear difference in the protein expression between subtypes is detected. (B) Both unsupervised (left) and supervised (right) heatmaps present heterogeneous distribution of samples belonging to classical (n=5) and QM (n=4) subtypes. The quantification of signal intensities and the number of positive cells with Definiens Architect Tissue Studio software for each protein in each Classical and QM sample shows also no differences among subtypes.

In addition to glycolytic enzymes, lactate transporters MCT1 and MCT4 which are connected to aggressiveness and higher glycolytic rate in melanoma and PDAC respectively (Baek et al., 2014; Tasdogan et al., 2020), were also evaluated as glycolytic markers for QM subtype. In patient gene expression data, the expression of *MCT4 (SLC16A3)* and *MCT1 (SLC16A1)* were analysed. In general, lower expression of *MCT1* (log_2=5) than *MCT4* (log_2=10) was observed in all samples (normal, pancreatitis, PDAC), indicating a dominant role of *MCT4* in tissue-related context. *MCT4* expression in PDAC patients was significantly higher than in pancreatitis patients and healthy individuals. *MCT1* gene expression was not different among these groups (Figure 3.7.A). Among PDAC patients, QM samples presented higher *MCT4* expression than classical ones. *MCT1* expression was not different among QM and classical PDACs (Figure 3.7.B). In addition to differences in gene expression between subtypes, MCT1 and MCT4 also presented distinct IHC staining pattern in FFPE samples. Although both transporters were expressed by both cancer and stromal cells, MCT1 expression was more prominent on stromal cells whereas MCT4 expression was generally observed on cancer cells (Figure 3.7.C). To confirm these findings, immunohistochemical staining for MCT1 and MCT4 was repeated with more FFPE patient samples (31 therapy naïve PDAC patients) and similar staining pattern was observed (Figure 3.7.C). Furthermore, MCT4 expression seems to correlate with histological QM marker KRT81 (Figure 3.7.C). Therefore, whole-slide quantification of MCT4 signal intensities and the number of cells with positive MCT4 on each FFPE patient samples was performed (explained in section 2.4.5). This quantification revealed that PDACs with high KRT81 expression showed more MCT4 expressing cells compared to slides with lower or no KRT81 expression (Figure 3.7.D).

A

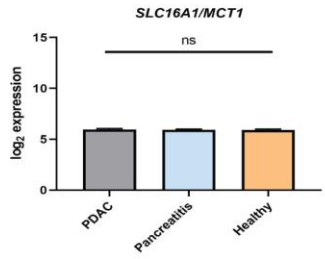
SLC16A1/MCT1
ns
log2 expression
15
10
5
0
PDAC
Pancreatitis
Healthy

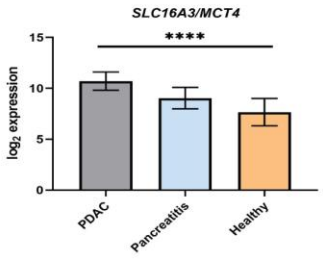
SLC16A3/MCT4
****
log2 expression
15
10
5
0
PDAC
Pancreatitis
Healthy

B

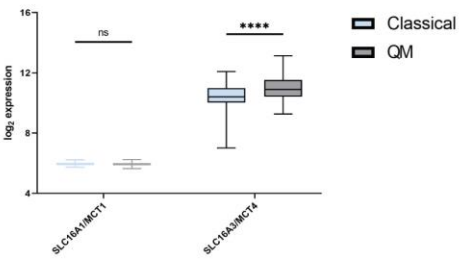
ns
****
log2 expression
16
12
8
4
SLC16A1/MCT1
SLC16A3/MCT4
Classical
QM

C

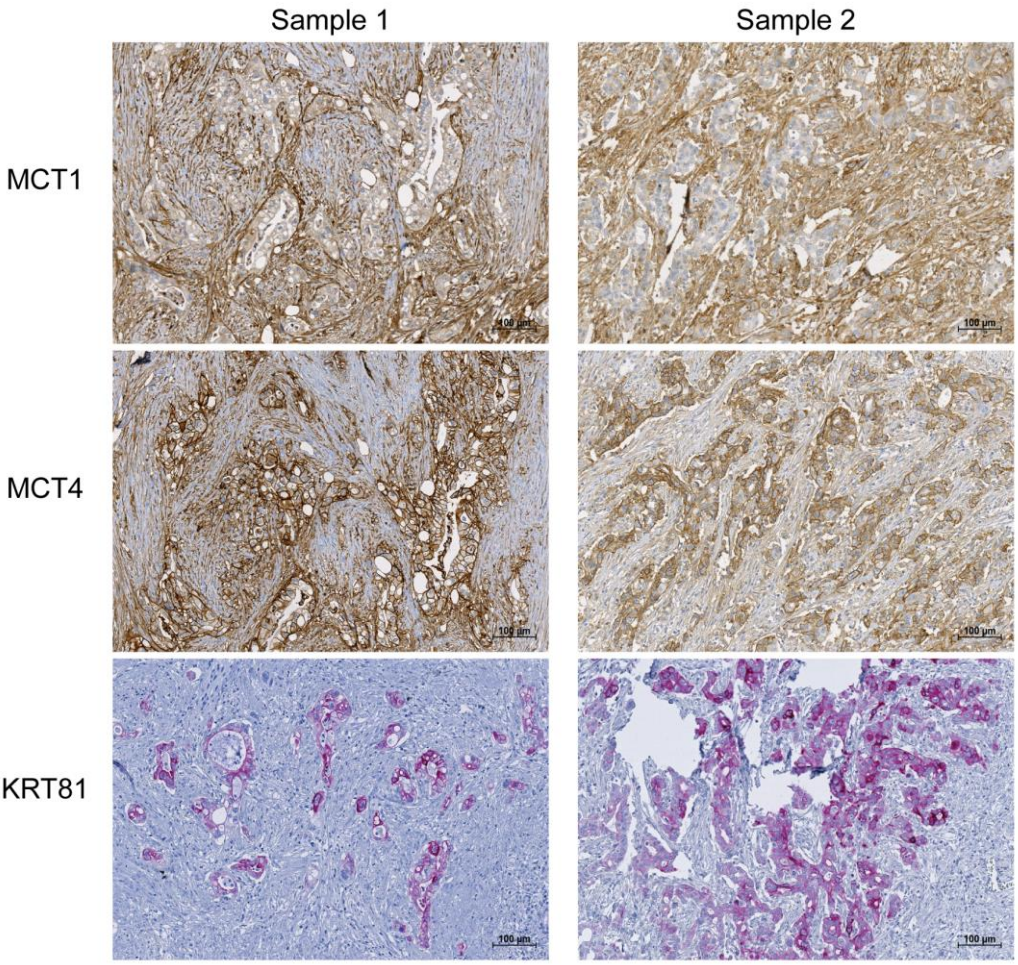
Sample 1
Sample 2
MCT1
MCT4
KRT81
100 µm

D

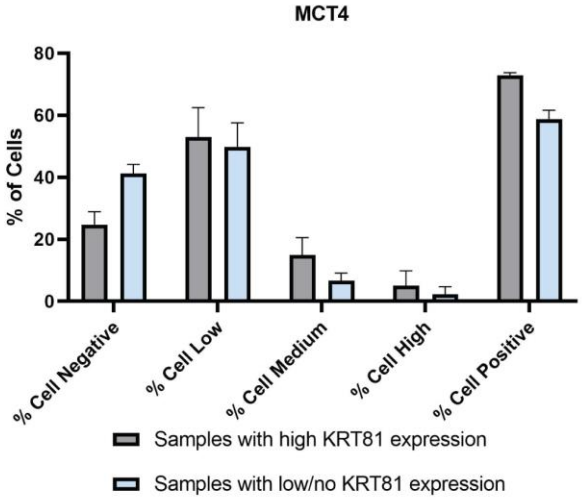
MCT4
% of Cells
80
60
40
20
0
% Cell Negative
% Cell Low
% Cell Medium
% Cell High
% Cell Positive
Samples with high KRT81 expression
Samples with low/no KRT81 expression

Figure 3.7 **Lactate transporters MCT1 and MCT4 represent distinct gene expression and staining patterns in patient samples.** (A) The expression of lactate transporter MCT1 is not changed between healthy individuals and PDAC patients, while MCT4 expression is significantly higher in PDAC patients in comparison to healthy individuals (PDAC vs Healthy, p<0,0001; PDAC vs Pancreatitis, p<0,0001). (B) Similarly, the expression of MCT1 shows no change between subtypes while MCT4 expression is significantly higher in QM patients than classical samples (QM vs Classical, p<0,001). (C) Immunohistochemical analysis of MCT1 and MCT4 expression in FFPE patient cohort (n=40, 25 low/no KRT81 expressing samples, 15 KRT81 expressing samples) reveals that both transporters are expressed on cancer and stromal cells with MCT1 expression detected mostly on stromal cells (first row) and MCT4 expression mostly on cancer cells (second row) in both cohorts. Moreover, KRT81 expressing cells also seem to express MCT4 as well (third row). (D) Higher numbers of MCT4 expressing cells are found on slides with higher KRT81 expression in comparison for KRT81 low expressing/negative slides. All p-values were calculated with two-tailed heteroscedastic t-test.

For further evaluation of MCT4 as a glycolytic marker and its relation with QM cells, six patient FFPE samples were stained against pan-cytokeratin (PanCK, general cancer cell marker), KRT81 (QM marker) and MCT4 with Opal Multiplex immunofluorescence assay (Figure 3.8.A). The co-expression of MCT4 with KRT81 and PanCK was analysed with Definiens Architect Tissue studio software. In all analysed samples, cancer cells expressing KRT81 (PanCK+, KRT81+) are mostly positive for MCT4 (Figure 3.8.A). In average, 73% of KRT81 positive cancer cells were also positive for MCT4, suggesting that most of QM cells also express MCT4 (Figure 3.8.B). 44% of the KRT81 negative cancer cells were also positive for MCT4 (Figure 3.8.B). Analysis of stromal cells showed that only 30% of the stromal cells (PanCK negative cells) were expressing MCT4, supporting cancer-specific expression of MCT4 in PDAC (Figure 3.8.C).

In addition, survival analysis of PDAC patients (www.proteinatlas.org; TCGA data set https://portal.gdc.cancer.gov/) demonstrated that patients with high MCT4 gene expression (n=51) had shorter overall survival in comparison to the patients with low MCT4 gene expression (n=125), fitting well with the worse prognosis of QM patients (Figure 3.8.D). Overall, the data presented here support the premise that PDAC patients with high MCT4 expression are likely to have QM/glycolytic tumour even though the sole MCT4 expression is not enough to unambiguously determine the molecular PDAC subtype.

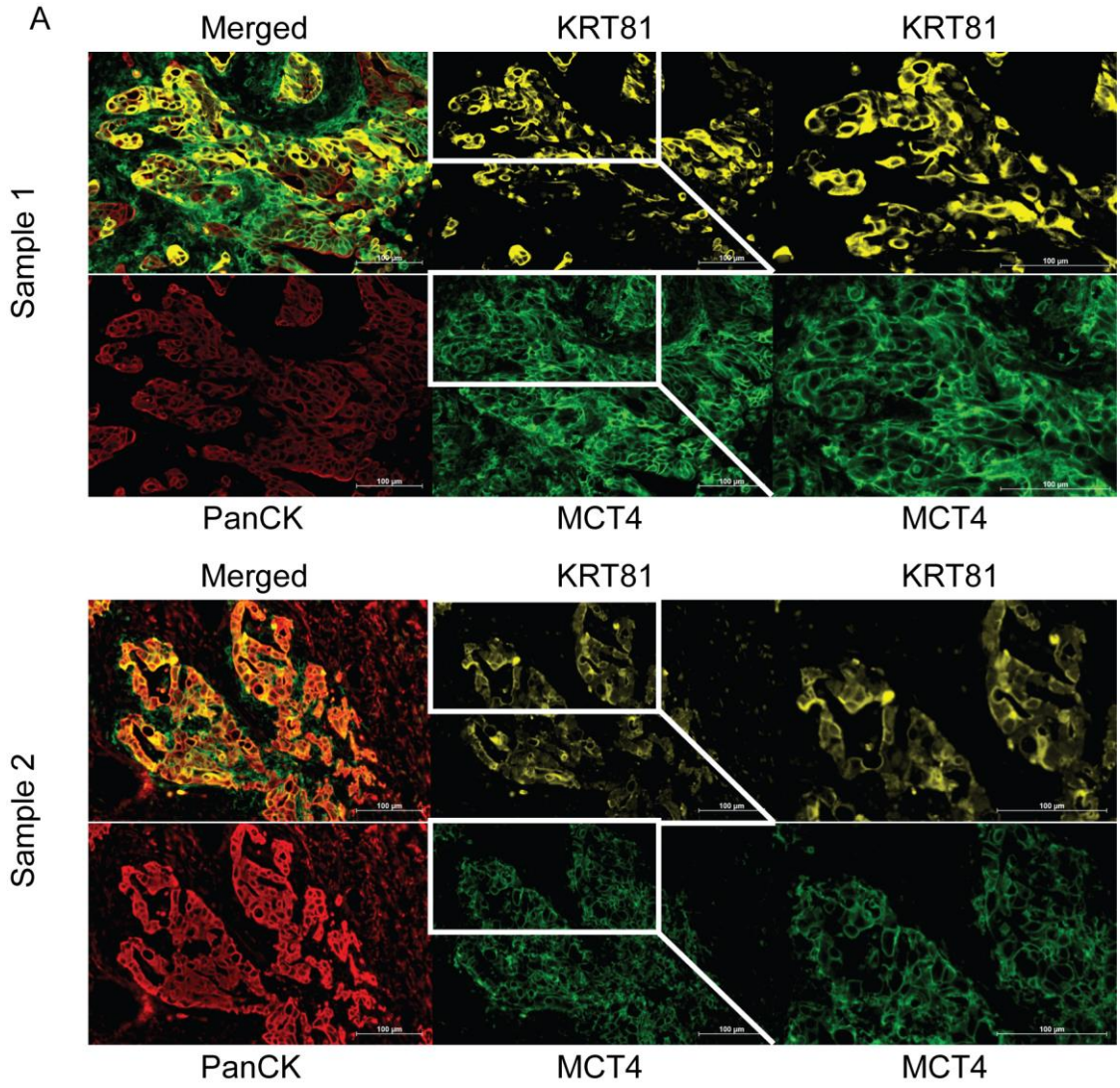
A
Merged
KRT81
KRT81
Sample 1
PanCK
MCT4
MCT4
Merged
KRT81
KRT81
Sample 2
PanCK
MCT4
MCT4

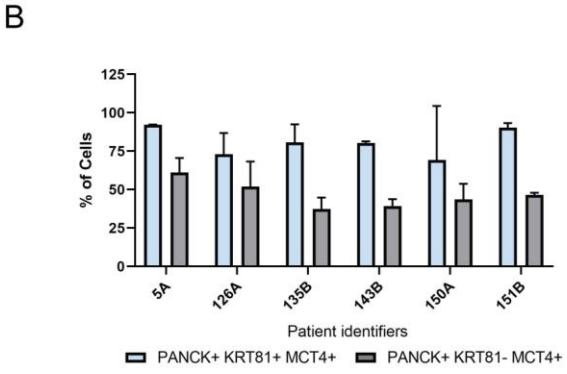
B
% of Cells
125
100
75
50
25
0
5A
126A
135B
143B
150A
151B
Patient identifiers
PANCK+ KRT81+ MCT4+
PANCK+ KRT81- MCT4+

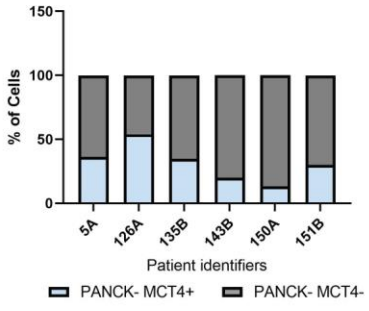
C
% of Cells
150
100
50
0
5A
126A
135B
143B
150A
151B
Patient identifiers
PANCK- MCT4+
PANCK- MCT4-

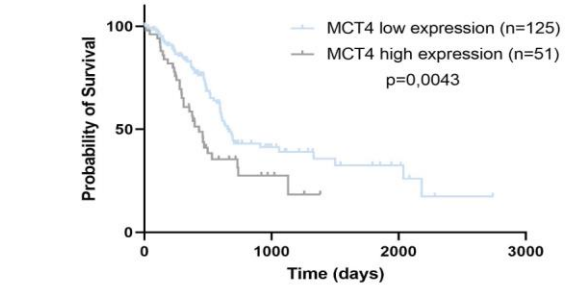
D
Probability of Survival
100
50
0
MCT4 low expression (n=125)
MCT4 high expression (n=51)
p=0,0043
0
1000
2000
3000
Time (days)

Figure 3.8 **Lactate transporter MCT4 co-localizes with KRT81 in QM FFPE patient samples.** (A) Multiplex immunofluorescence staining for MCT4 (green), KRT81 (yellow) and PanCK (red) in FFPE PDAC patient samples showed that KRT81 expressing cancer cells are often express MCT4 as well. (B) In average, 73% of the KRT81 positive cancer cells are also positive for MCT4 whereas only 44% of the KRT81 negative cells express MCT4. (C) Also, MCT4 expression is observed in only 30% of the stromal cells, supporting the premise of predominant MCT4 expression in cancer cells. (D) PDAC patient survival analysis: high expression of MCT4 expression is correlating with worse survival as already observed for QM patients as well.

3.2.3 Inhibition of glycolysis reduces cell viability *in vitro*

To evaluate whether glycolysis is a relevant therapy target especially in the QM PDACs, cell viability assays with established cell lines were performed by using a selection of chemical inhibitors targeting different players/enzymes of the glycolysis: AZD3965 (MCT1/2 inhibitor), syrosingopine (MCT1/4 inhibitor) and shikonin (PKM2 inhibitor). Respective inhibitors were applied to established cells and effects on cell viability were estimated. For this purpose, the optimized number of cells from each cell lines were seeded in 96-well plates and incubated with a concentration range of each inhibitor 1nM to 25 µM) for 72 hours. Shikonin and syrosingopine reduced the cell viability in a dose-dependent manner and both inhibitors showed slightly better effects against QM cell lines (Figure 3.9.A and B). MCT1/2 inhibitor with AZD3965 was not effective on established PDAC cell lines.

A

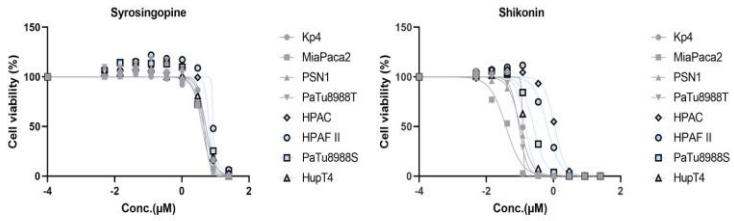

B

Cell lines/Inhibitors	Shikonin/IC50 (µM)	Syrosingopine/IC50 (µM)
HPAC	1.09	6.60
HPAF II	0.65	8.59
PaTu8988S	0.26	5.08
HupT4	0.15	5.10
Kp4	0.12	5.22
MiaPaca2	0.04	3.98
PSN1	0.10	4.54
PaTu8988T	0.09	4.52

Classical
QM

Figure 3.9 **Inhibition of glycolysis reduces cell viability *in vitro.*** (A) MCT1/4 dual inhibition with syrosingopine (left) and PKM2 inhibition with shikonin (right) inhibits cellular growth *in vitro.* (B) Both inhibitors represent slightly lower IC_{50} values in QM cell lines compared to classical cell lines, indicating subtype-specific effect of glycolysis inhibition of cell viability.

3.3 Functional evaluation of lipid metabolism in pre-clinical PDAC models

Gene set enrichment analysis (GSEA) (Figure 3.1) revealed an upregulation of fatty acid/cholesterol/lipid metabolism-related genes in classical subtype in all investigated PDAC models. The enrichment in lipid gene sets in classical subtype could be explained by epithelial feature and well-differentiated morphology of cellular membrane, which demands higher amount of lipids for a proper organisation (Collisson et al., 2011; van, Agnetti, & Gassama-Diagne, 2020). However, lipid metabolism is a large metabolic branch encompassing pathways of fatty acid import, fatty acid synthesis, lipid synthesis and deposition as well as lipid and fatty acid degradation (Snaebjornsson et al., 2020). To explore which of these pathways are functionally active in the classical subtype and thus potentially relevant metabolic target, differences in lipid content and utilization among PDAC subtypes as well as effects of selected lipid metabolism inhibitors were investigated.

3.3.1 Classical subtype is enriched in various lipid classes

To evaluate whether lipid gene sets are translated into functional richness with lipids in the classical subtype, lipid content was investigated in established PDAC cell lines, PDX-derived primary cells using different targeted (Biocrates AbsoluteIDQp180 kit and ultra-performance liquid chromatography-tandem mass spectrometer, UPLC-MS/MS) metabolic profiling platforms.

Firstly, targeted lipid profiling was conducted for established PDAC cell lines (3 classical and 4 QM cells). Total of 80 lipid metabolites, mostly different subclasses of polar membrane lipids such as sphingomyelins, phosphatidylcholines and lysophosphatidylcholines, were detected and quantified at the group of Prof. Dr. Hankemeier in University of Leiden (Table 5-1). In accordance with higher lipid gene expression and previous profiling results from Daemen et al., classical cell lines represented higher levels of analysed phospholipids, sphingomyelins and ceramides (Figure 3.10.A). Concentrations of 77 lipid metabolites were higher in classical group in comparison to QM subtype, among them 3 lipid metabolites reached statistical significance (Figure 3.10.A) (Table 5-2).

A

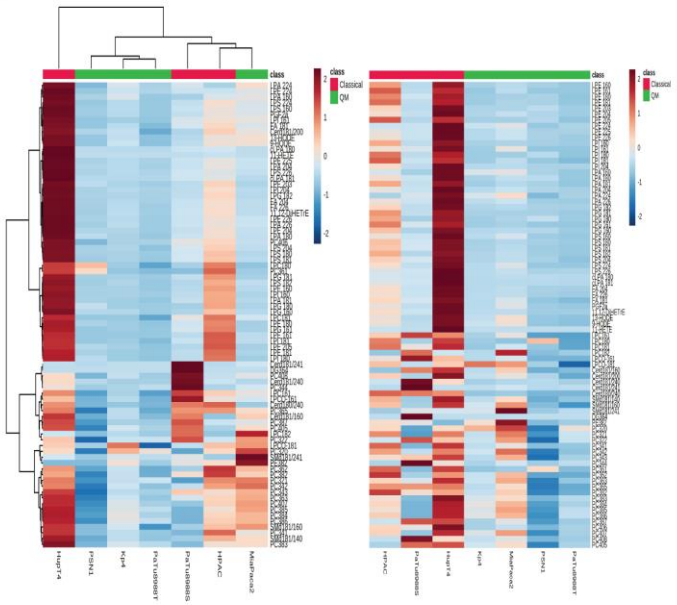

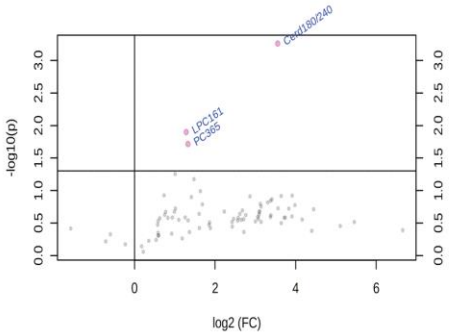

Metabolite/Subtype	Classical	QM
p<0.05	Normalized Response Rates	
PC(36:5)	0.32	0.13
LPC(16:1)	0.15	0.06
Cer(d18:0/24:0)	0.25	0.02

B

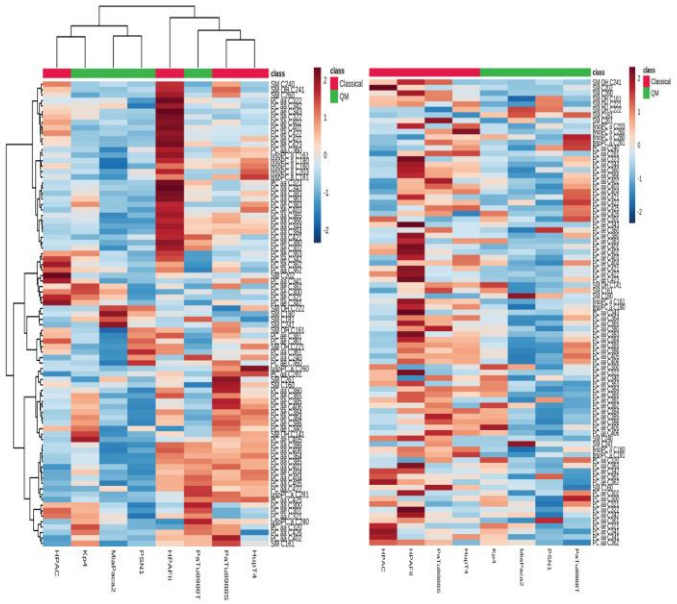

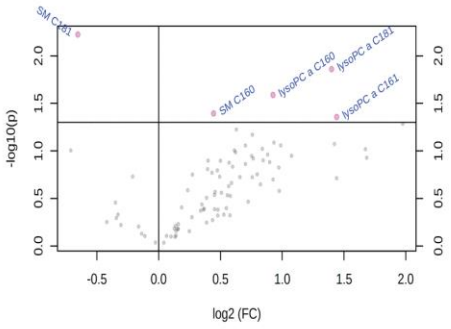

Metabolite/Subtype	Classical	QM
p<0.05	Concentration (pmol/µgprotein)	
lysoPC a C 16:1	1.96	0.72
lysoPC a C 16:0	5.42	2.85
lysoPC a C 18:1	9.58	3.63
SM C 16:0	28.43	20.90
SM C 18:1	0.47	0.74

Figure 3.10 **Classical established cell lines are enriched in various lipid metabolites.** Both targeted metabolite profiling of established PDAC cell lines ((A), Targeted lipid profiling; (B) Biocrates AbsoluteIDQp180 kit) reveal that classical cell lines are enriched in various lipid metabolites. Heatmaps (unsupervised, left; supervised,right) represent the distribution of different lipid metabolites in established PDAC cell lines. Volcano plots show the fold change (x-axis, left side of the threshold is QM area and right side is Classical) and statistical difference (y-axis, the threshold at –log10(0.05)) in the concentration of each lipid metabolite between subtypes. Each grey dot represents a lipid metabolite and pink dots represents the significantly different lipids between subtypes. Tables depict metabolites with significantly different concentrations between subtypes. All p-values were calculated with two-tailed heteroscedastic t-test.

To confirm first targeted lipid profiling results and to investigate lipid distribution also in PDCs, second targeted lipid profiling was performed with Biocrates absoluteIDQ p180 kit. In total, 85 lipid metabolites belonging to lipid subclasses phosphatidylcholines, lysophosphatidylcholines and sphingomyelins were detected and quantified in 8 established (4 classical and 4 QM cells) and 11 PDCs (6 classical and 5 QM cells). Similar results showing higher accumulation of lipid metabolites in classical subtype were observed in both established PDAC cell lines and PDCs, although the distribution of lipids between subtypes was more heterogeneous in PDCs compared to established PDAC cell lines. Concentrations of 73 lipid metabolites were higher in classical established PDAC cell lines than QM cells and 5 lipid concentrations differed significantly between subtypes (Figure 3.10.B). Similarly, classical PDCs have higher concentrations of 48 lipids than QM PDCs while two metabolites were significantly increased in the classical subtype (Figure 3.11).

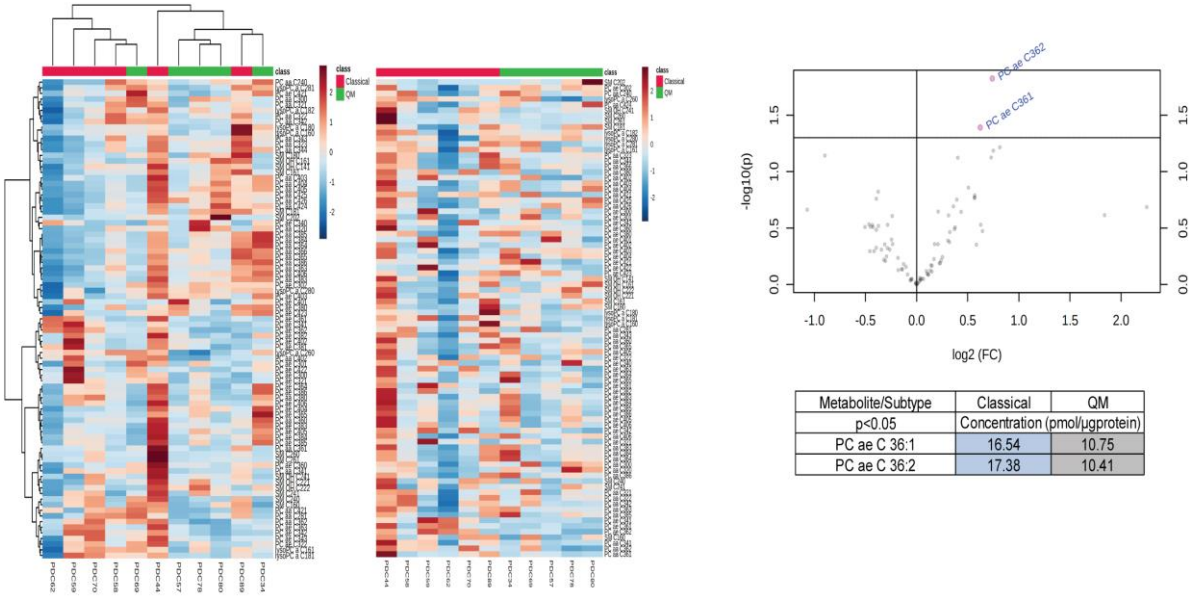

Metabolite/Subtype	Classical	QM
p<0.05	Concentration (pmol/µgprotein)	
PC ae C 36:1	16.54	10.75
PC ae C 36:2	17.38	10.41

Figure 3.11 **Classical PDC lines also show enrichment in various lipid.** Similar to classical established cell lines, classical PDCs also present higher lipid content compared to QM PDCs. Heatmap (unsupervised, left; supervised,right) represents the distribution of different lipid metabolites in primary cell lines. Volcano plot shows the fold change (x-axis, left side of the threshold is QM area, right Classical) and statistical difference (y-axis, threshold at –log10(0.05)) in the concentration of each lipid metabolite between subtypes. Each grey dot represents a lipid metabolite and pink dots represent lipid metabolites significantly different between subtypes. The table depicts metabolites with significantly different concentrations between subtypes. All p-values were calculated with two-tailed heteroscedastic t-test.

Overall, in accordance with the upregulation in the lipid metabolism genes in classical samples throughout different PDAC models, the enrichment of different lipid metabolites from different classes (mostly phospholipids) in samples of classical subtype of established cell lines and PDX derived primary cells have been confirmed with different metabolite profiling methods.

3.3.2 Classical cell lines are more dependent on fatty acid oxidation

In addition to enrichment in lipid metabolism-related transcripts, gene set of fatty acid metabolism was most prominently enriched in classical samples. This large gene set, however, includes around 150 members that belong to processes of fatty acid synthesis and fatty acid oxidation. Thus, it was further investigated to see to which extent different PDAC cells rely on fatty acid metabolism, especially on essential energy-producing process of mitochondrial fatty acid oxidation.

Fatty acids are the main components of lipid metabolism that play key roles in lipid synthesis, degradation, energy production and nutrient storage. However, intracellular fatty acids are toxic in its free form and they are either deposited in lipid droplets in form of triglycerides or shortly available as free fatty acids for direct use by the mitochondria in fatty acid beta-oxidation (Cnop, Hannaert, Hoorens, Eizirik, & Pipeleers, 2001; Gordon, 1977) To evaluate how extensive are fatty acids used in the mitochondrial beta-oxidation in QM and classical subtype, free fatty acid content was quantified. All classical established cell lines presented higher free fatty acids concentrations compared to QM established cells, indicating of higher need for free FA in classical subtype (Figure 3.12.A). Among primary cells, a classical cell line, PDC89, presented the highest free fatty acid content (Figure 3.12.B). Different from the established cells, separation to QM and classical subtype was not clear.

To further substantiate the usage of FA by the mitochondria, Seahorse Mito Fuel Flex Test was performed with established PDAC cell lines. This assay evaluates cell's dependencies on different mitochondrial fuels, glucose, glutamine and fatty acids, by measuring changes in oxygen consumption rates (OCR) in the presence and absence of the inhibitors that block the entry of these fuels into the mitochondria. Contribution of fatty acids to mitochondrial OXPHOS was larger in classical cells than in QM cell lines suggesting higher dependence of classical cell lines on fatty acids for energy production. (Figure 3.12.C). Conversely, QM cell lines showed higher dependency on glucose to fuel mitochondrial energy production.

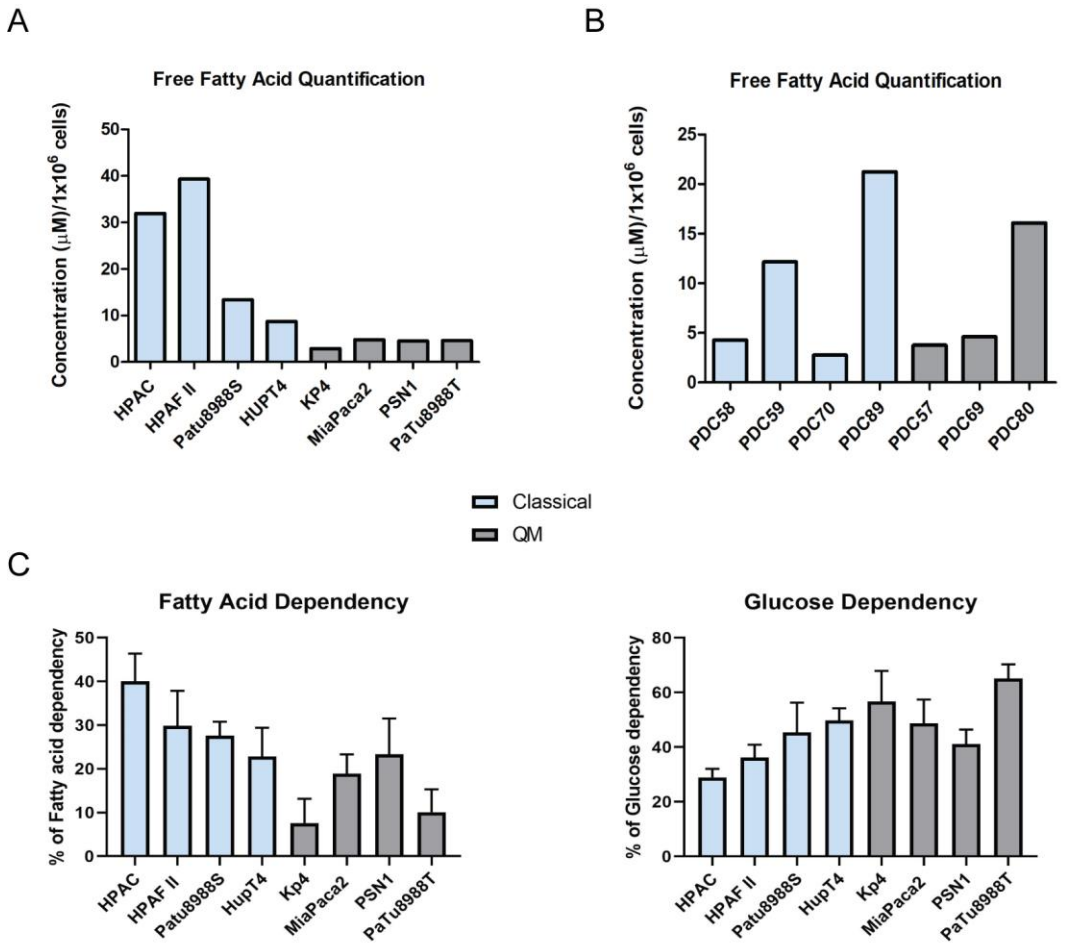

Figure 3.12 **Classical established PDAC cell lines have higher free fatty acid content and higher preference for fatty acids as a mitochondrial fuel**. (A) Classical cells present higher FFA content than the QM established cells. (B) PDC89, a classical cell line, shows the highest content of FFA (C). Seahorse Mitofuel Assay demonstrating higher dependency on fatty acids for mitochondrial energy production in classical established cell lines(bottom left) and higher dependency on glucose for mitochondrial energy production in QM cell lines (bottom right). (100% dependency= % dependency on glucose + % dependency on glutamine + % dependency on fatty acids).

3.3.3 Fatty acid uptake is comparable between cell lines despite different utilization

Intracellular fatty acid demand is satisfied by both fatty acid uptake and *de novo* fatty acid synthesis and both processes are upregulated in PDAC as well as in many other cancer entities (Snaebjornsson et al., 2020). To investigate how much is classical PDAC relying on import of extracellular FA, fatty acid uptake assay was performed. For this purpose, BODIPY (475/572 nm)-labelled palmitate was offered to the cells and fatty acid trafficking was analysed.

Established PDAC cell lines represented comparable uptake of BODIPY-labelled palmitate, suggesting that usage of extracellular FA is not dramatically different among cells and thus subtypes (Figure 3.13.A). However, microscopic analysis revealed that BODIPY signal is localized in lipid droplets in QM cells. In classical cells, more scattered signal with less incorporation into lipid droplets was observed (Figure 3.13.B). The scattered BODIPY fluorescent signals in classical cells may be explained by more active fatty acid metabolism and FA beta-oxidation in this subtype. Also, a higher number of fluorescently labelled lipid droplets was detected in QM cells compared to classical cells. In average, lipid droplets were detected in 52% of QM cells while only 13% of classical cells had BODIPY-labelled lipid droplets (Figure 3.13.C).

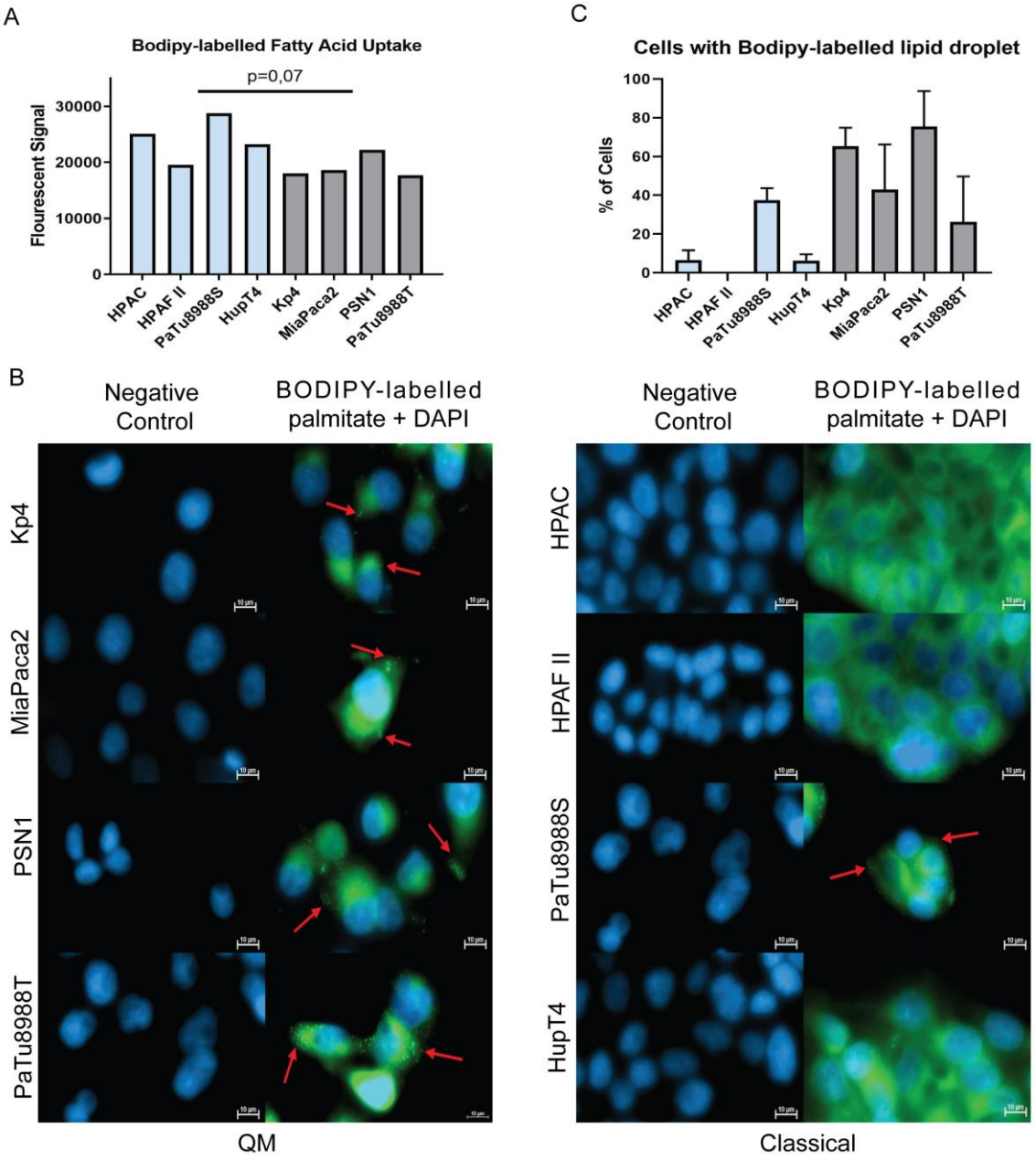

Figure 3.13 **Fatty acid uptake is comparable between subtypes.** (A) Fatty acid uptake assay with Bodipy-labelled palmitate showing no significant difference in fatty acid uptake between classical and QM subtypes. (B) Accumulation of fluorescent BODIPY-labelled palmitate in PDAC cells: QM cells show higher incorporation of imported fatty acids into lipid droplets (red arrows point to fluorescently labelled lipid droplets. DAPI nuclear staining- blue). (C) The quantification of cells containing lipid droplets revealed that more QM cells have bodipy-labelled lipid droplets compared to classical cells. Three microscopical fields of view (40x) were analyzed per cell line. (DAPI staining= total cell number; DAPI+BODIPY= cells containing lipid droplets.) All p-values were calculated with two-tailed heteroscedastic t-test.

3.3.4 Fatty acid oxidation is upregulated in classical PDX and patient samples

Gene set enrichment analyses of PDX and patient data sets also revealed an upregulation in fatty acid metabolism gene set in classical samples (Figure 3.1). However, this gene set contains 158 genes that are involved in different processes such as *de novo* synthesis, fatty acid transport, acylation and incorporation into lipids, lipolysis and beta-oxidation. Therefore, to specifically analyse only fatty acid oxidation, single gene expression analysis of genes closely involved in FAO was performed with PDX and patient data sets. As presented in figure 3.14.A, a majority of the genes (38 and 41 out of 61 genes in patient and PDX samples, respectively) had increased expression in classical samples (Figure 3.14.A) (Table 5-3). Among them, the expression of 11 transcripts (9 in classical, 2 in QM subtype) was significantly different between classical and QM subtypes in both data sets (Figure 3.14.B). The transcripts upregulated in classical samples have important roles in fatty acid oxidation, whereas the genes upregulated in QM subtype have a role in lipid deposition in lipid droplets.

Moreover, custom-made gene sets named fatty acid oxidation 1 (FAO1) and fatty acid oxidation 2 (FAO2) were created. FAO1 gene set consisted of 14 genes involved exclusively in mitochondrial beta-oxidation (from FA entrance into mitochondria until the very last step of Acetyl-CoA generation) whereas FAO2 gene set comprised of 25 genes having a role in fatty acid uptake and transport as well as oxidation (Table 5-4) GSEA demonstrated that both gene sets are significantly enriched in classical subtype in patient data set (Figure 3.14.C). This result indicates that subtype-specific differences in FA handling are also detectable in patient material.

A

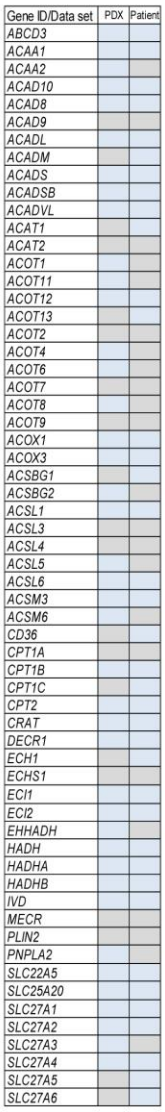

B

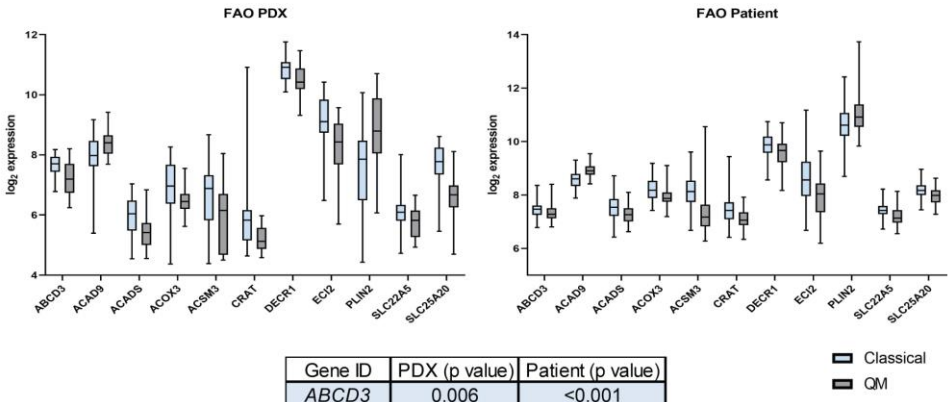

Gene ID	PDX (p value)	Patient (p value)
ABCD3	0.006	<0.001
ACADS	0.004	<0.001
ACOX3	0.034	<0.001
ACSM3	0.028	<0.001
CRAT	0.021	<0.001
DECR1	0.011	<0.001
ECI2	0.006	<0.001
SLC22A5	0.040	<0.001
SLC25A20	<0.01	<0.001
ACAD9	0.009	<0.001
PLIN2	0.005	<0.001

C

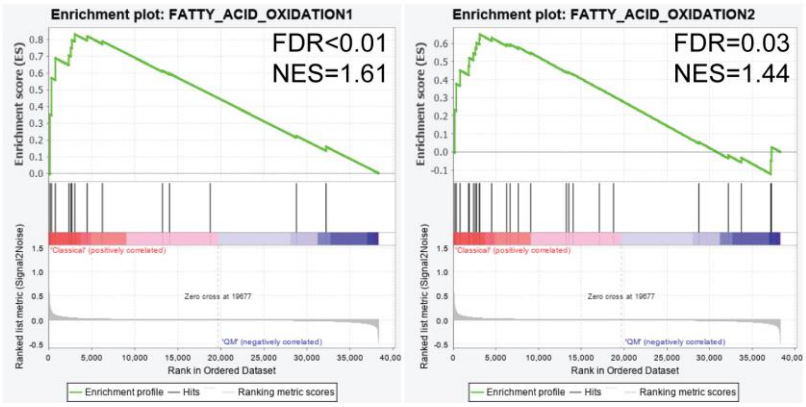

Figure 3.14 **Fatty acid oxidation related genes are upregulated in classical samples of both PDX and patient data sets.** (A) Heatmap shows higher expression of fatty acid oxidation related transcripts in classical subtype in both PDX and patient data sets. Blue indicates higher expression in classical subtype and grey indicates higher expression in QM subtype. (B) Among them, the expression of 11 genes (9 higher in classical, 2 in QM) significantly differs between subtypes in both PDX (right) and patient (left) data sets. The table (middle) presents the P-values for each transcript. The genes with increased expression in classical subtype have a role in mitochondrial oxidation of different types of fatty acids. *PLIN2* with higher expression in QM subtype is essential for lipid accumulation in the lipid droplets. (C) Enrichment plots for custom made FAO1 and FAO2 gene sets in patient cohort reveals that both gene sets are significantly enriched in classical subtype. All p-values were calculated with two-tailed heteroscedastic t-test..

3.3.5 Lipogenic marker analysis in PDAC patient samples

Functional analysis of fatty acid oxidation in established PDAC cell lines and review of fatty acid oxidation related gene expression in PDX and patient data sets revealed that classical subtype represents higher dependency on fatty acid oxidation. Conversely, enhanced *de novo* fatty acid synthesis and upregulation of related gene expression are frequently associated with hypoxia and aggressive phenotype (Munir et al., 2019; Rossi Sebastiano & Konstantinidou, 2019). Therefore, single gene expression analysis and immunohistochemical staining of FFPE patient samples against key components of fatty acid synthesis and oxidation were performed to assess the value of these genes as subtype-specific markers in patient samples. *ACACA, FASN, ACSL4* and *ACSS2* were picked to evaluate fatty acid synthesis due to their key roles in fatty acid synthesis (Snaebjornsson et al., 2020). Carnitine/acyl-carnitine translocase (*SLC25A20*) and ATP binding cassette subfamily D member 3 (*ABCD3*), transporters having a role in fatty acid import to mitochondria and peroxisome, respectively, were selected to assess fatty acid oxidation in patient samples due to observation of highly significant differences in the expression of respective genes between subtypes in previous analyses.

Initially, PDAC specific expression of respective lipogenic enzymes and transporters were determined by using patient gene expression data comprised of samples from healthy individuals, pancreatitis and PDAC patients (E-MTAB-1791, (Jandaghi et al., 2016)). Single gene expression analysis revealed that PDAC patients had increased expression of *ACACA, ACSL4* and *FASN* compared to pancreatitis patients and healthy individuals, possibly indicating increased fatty acid synthesis in PDAC (Figure 3.15.A). The expression of ACSS2, ABCD3 and *SLC25A20* was slightly decreased in PDAC patients in comparison to healthy samples, suggesting downregulation in fatty acid oxidation (Figure 3.15.A). Moreover, comparison of subtype-specific expression of respective genes showed that fatty acid synthesis genes *ACACA, FASN* and *ACSL4* were higher in QM samples indicating induced fatty acid synthesis in this subtype. Conversely, expression of fatty acid oxidation transcripts *SLC25A20* and *ABCD3* together with *ACSS2* were higher in classical samples (Figure 3.15.B).

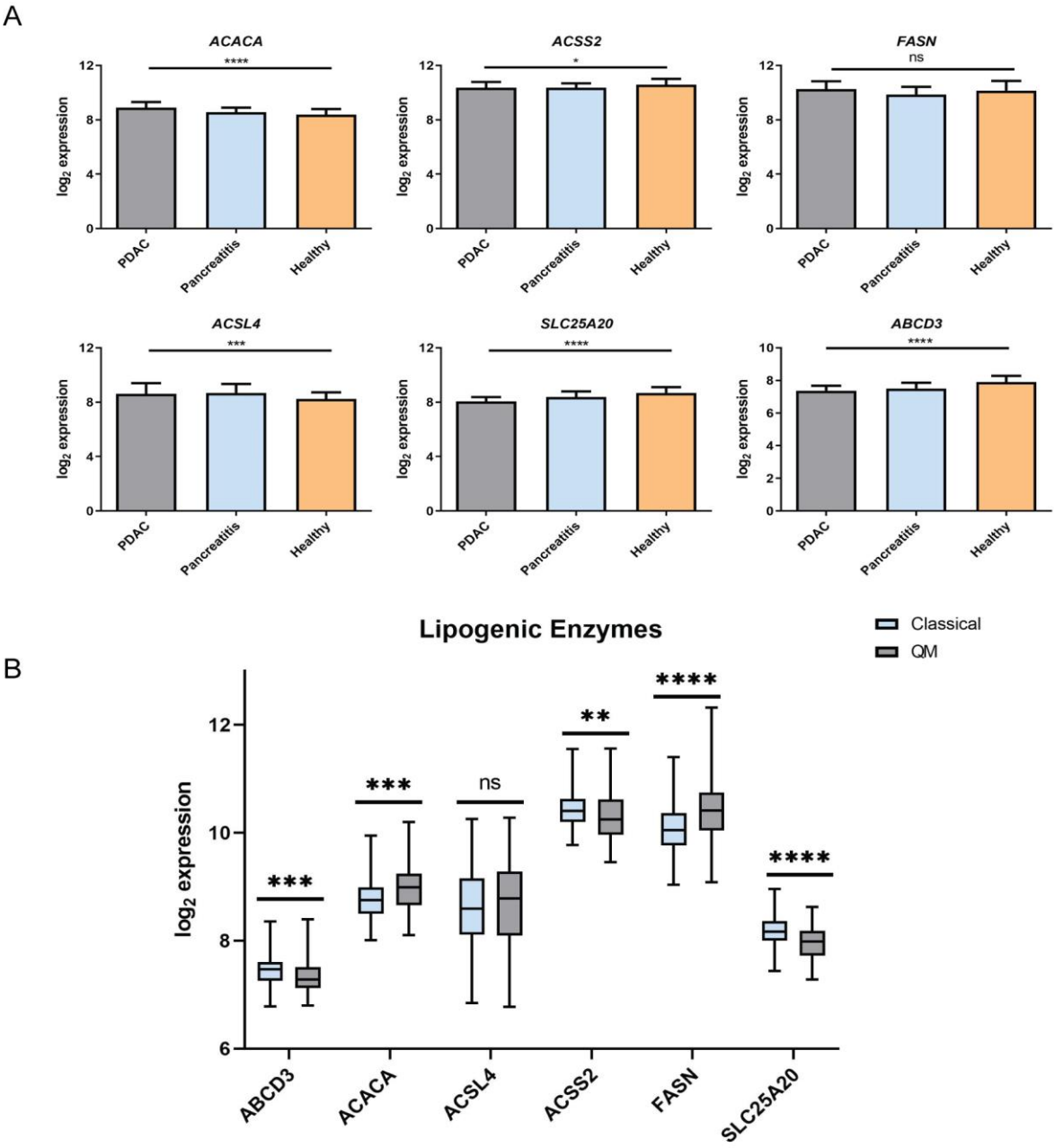

Figure 3.15 **Lipogenic gene expression in patient samples.** (A) PDAC patients show higher gene expression of fatty acid synthesis enzymes *ACACA* (PDAC vs Healthy, p<0,0001; PDAC vs Pancreatitis, p<0,001), *ACSL4* (PDAC vs Healthy, p<0,001; PDAC vs Pancreatitis, not significant) and *FASN* (PDAC vs Healthy, not significant; PDAC vs Pancreatitis, p<0,001) than pancreatitis patients and healthy individuals. *ACCS2* and fatty acid oxidation related *SLC25A20* and *ABCD3* expression are higher in healthy individuals than PDAC and pancreatitis patients. (B) *ACSS2* (QM vs Classical, p<0,01) and *SLC25A20* (QM vs Classical, p<0,0001) and *ABCD3* (QM vs Classical, p<001) expression are significantly higher in classical subtype whereas QM samples show significantly increased expression of *ACACA* (QM vs Classical, p<0,001) and *FASN* (QM vs Classical, p<0,0001) compared to classical subtype. All p-values were calculated with two-tailed heteroscedastic t-test.

Later, to analyse whether observed differences in lipogenic gene expression among subtypes are also visible in FFPE patient material, immunohistochemical staining against respective enzymes were conducted (9 therapy naïve PDAC patients, 4 high KRT81 expressing samples, 5 low/no KRT81 expressing samples). However, the transcriptomic differences between subtypes were not visually detectable on tissue context (Figure 3.16.A). Moreover, whole-slide quantification of signal intensities for each marker and number of cells with positive signal also showed no exceptional differences between high KRT81 expressing and low/no KRT81 expressing samples (Figure 3.16.B).

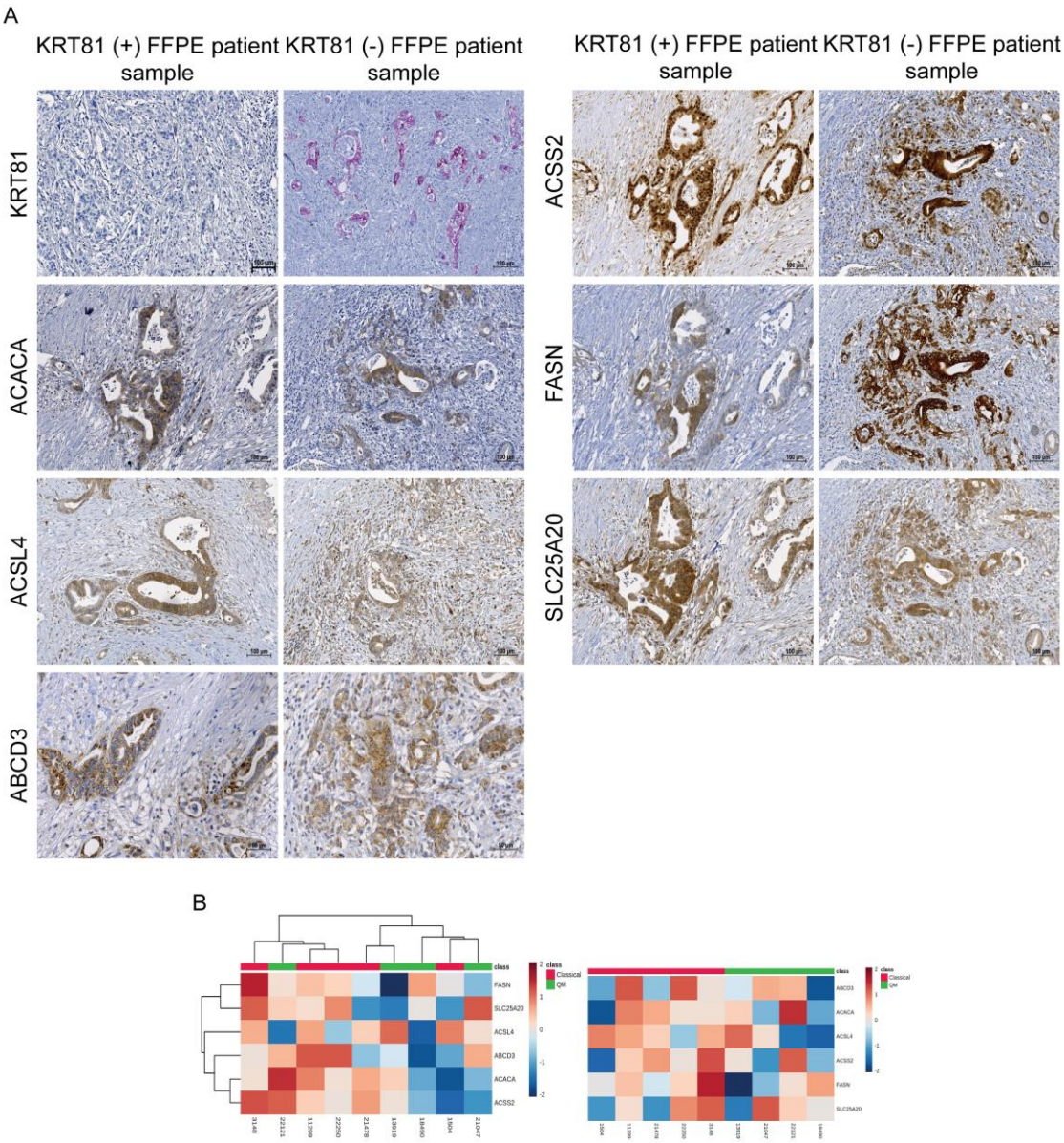

Figure 3.16 **Staining of FFPE patient samples against lipogenic proteins showed no subtype-specific staining patterns.** (A) Patient FFPE samples were stained against fatty acid synthesis and oxidation related proteins. Although, all investigated proteins showed increased expression in cancer cells compared to stromal cells, no difference in staining pattern was detected between KRT81 positive and KRT81 low/negative patient samples. (B) Both unsupervised (left) and supervised (right) heatmaps present heterogeneous distribution of samples belonging to classical (n=5) and QM (n=4) subtypes. The quantification of signal intensities and the number of positive cells with Definiens Architect Tissue Studio software for each protein in each Classical and QM sample shows also no differences among subtypes.

3.3.6 Effects of lipid metabolism inhibitors on PDAC cells

All presented data support the view that lipid metabolism and fatty acid oxidation pathways are more active in the classical subtype. To challenge the value of these processes as targets for classical subtype, different chemical inhibitors of lipid metabolism-related processes (Table 3-4) were used and their effects on PDAC cell viability was evaluated.

Table 3-3 Lipid metabolism inhibitors and their targets

Inhibitor	Inhibited metabolic process / Target
Perhexiline	Fatty acid oxidation / Carnitine palmitoyltransferase 1 and 2, CPT1 and 2
Triacsin C	Fatty acid incorporation into lipids and fatty acid oxidation / Long chain acyl-CoA synthetase, ACSL
Ingenol-3-angelate	Fatty acid oxidation / Carnitine-acyl-carnitine translocase, SLC25A20
Trimetazidine dihydrochloride	Fatty acid oxidation / Mitochondrial long chain 3-ketoacyl-CoA thiolase, ACAA2
Orlistat	Fatty acid synthesis and oxidation / Fatty acid synthase ,FASN and gastric, pancreatic and carboxyl ester lipases
GSK 2194069	Fatty acid synthesis / Fatty acid synthase, FASN
Cerivastatin	Cholesterol synthesis / 3-hydroxy-3-methyl-glutaryl-coenzyme A reductase, HMGCR
Lovastatin	
Simvastatin	

For this purpose, optimized cell numbers of each cell line (8 established and 8 PDCs) were seeded in 96 well plates and incubated with different concentrations of each inhibitor ranging from 1 nM to 50 µM for 72 hours. Among analysed inhibitors,

TriacsinC, perhexiline and statins showed dose-dependent reduction in cell viability of both established and PDC lines (Figure 3.17.A). However, subtype-specific effects were not clear (Figure 3.17.A). TriascinC demonstrated slightly stronger effects on QM established cells; this was however not observed among PDCs (Figure 3.17.A). Cerivastatin presented a similar trend and somewhat higher inhibition of QM established cells, again not observed in the PDC collection.

A

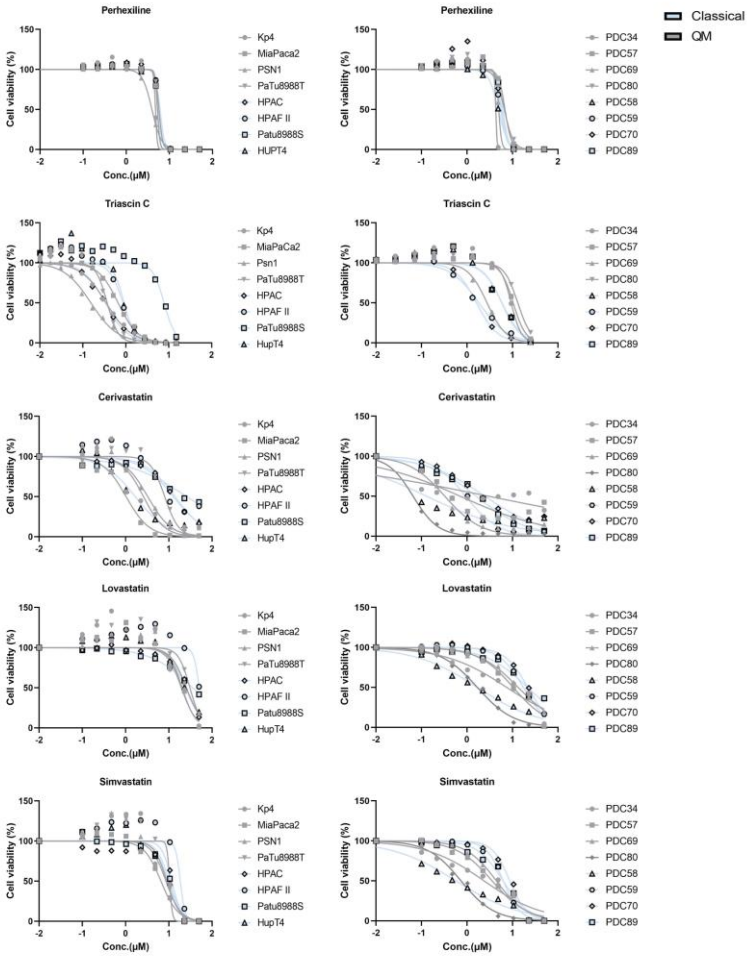

B

Cell lines/Inhibitors	Perhexiline/IC50 (μM)	Triascin C/IC50 (μM)	Simvastatin/IC50 (μM)	Lovastatin/IC50 (μM)	Cerivastatin/IC50 (μM)
HPAC	2.68	0.33	11.74	25.22	12.72
HPAF II	2.80	0.86	18.50	50.38	13.88
Patu8988S	2.46	7.79	10.26	35.62	25.99
HUPT4	2.77	0.91	9.59	24.05	1.67
Kp4	1.98	0.35	9.06	20.44	2.59
MiaPaca2	2.40	0.66	6.59	19.59	1.03
PSN1	1.54	0.15	8.61	25.52	3.25
PaTu8988T	2.53	0.37	10.47	30.79	8.06

Cell lines/Inhibitors	Perhexiline/IC50 (μM)	Triascin C/IC50 (μM)	Simvastatin/IC50 (μM)	Lovastatin/IC50 (μM)	Cerivastatin/IC50 (μM)
PDC58	3.97	5.91	0.57	1.69	0.13
PDC59	4.91	1.82	8.75	21.76	0.94
PDC70	4.85	1.62	6.29	17.32	2.48
PDC89	5.09	5.81	6.24	21.48	1.59
PDC34	4.30	9.35	2.37	7.48	2.97
PDC57	5.47	10.37	3.57	10.41	0.71
PDC69	3.97	2.76	4.43	13.37	0.33
PDC80	4.79	13.11	0.74	1.69	0.07

Figure 3.17 **Effects of lipid metabolism inhibitors on cell viability of established and PDC lines.** (A) Inhibitors of mitochondrial fatty acid transport (Perhexiline), fatty acid acylation (TriacsinC) and cholesterol synthesis (cerivastatin, lovastatin, simvastatin) reduced the cell viability of established (left panel) and primary cell lines (right panel) in a dose-dependent manner. (B) However, an obvious subtype-specific effect on cell viability is not observed with any of the investigated inhibitors. (TriascinC data from primary cells was kindly provided by Ms. Alina Winkelkotte (Winkelkotte, 2018))

4 Discussion

Pancreatic ductal adenocarcinoma (PDAC) is currently the 7th leading cause of cancer related-deaths worldwide due to lack of effective diagnosis and treatment options despite the extensive research during the last decades (Bray et al., 2018). The incidence and mortality rates are expected to be doubled until 2040, if novel effective treatment methods are not introduced into clinical practice (Bray et al., 2018). The current chemotherapeutic options for PDAC are limited to intensified chemotherapy combinations such as FOLFIRINOX and gemcitabine plus nab-paclitaxel (Grasso et al., 2017; Ying et al., 2016). However, none of these therapies is very effective and only 8% of the patients survive for 5 years after diagnosis (Grasso et al., 2017; Ying et al., 2016). Molecular studies showed that oncogenic *KRAS*, which is found in 95% of the patients, is the main driver mutation (Aguirre & Collisson, 2017; Bryant et al., 2014). In addition, other common mutations such as *TP53, CDKN2A* and *SMAD4* have also a role in PDAC initiation and progression (Aguirre & Collisson, 2017; Bryant et al., 2014). In addition, chromosomal structural arrangements, differences in the dosage of mutated genes and epigenetic regulations play an important part in disease prognosis (Waddell et al., 2015). Finally, the accumulation of different combination of these genetic and molecular events renders PDAC very heterogeneous that leads to the failure of current untargeted chemotherapies (Chan-Seng-Yue et al., 2020; Mueller et al., 2018).

In line with the heterogeneous nature of PDAC, different groups identified molecular PDAC subtypes based on gene expression patterns and showed that the identified subtypes were clinically present (Collisson et al., 2019). It has been suggested that molecular subtypes are possibly responsible for the differences in disease prognosis and therapy response between PDAC patients (Collisson et al., 2019). These findings, together with the success in identifying and targeting molecular subgroups with actionable mutations in other cancer entities, make effective patient classification inevitable for successful treatment in PDAC as well (Christenson et al., 2020; Tsimberidou, 2015). Even though the combination of chemotherapy with epidermal growth factor receptor inhibitor (EGFR) in EGFR overexpressing non-small-cell lung cancer patients (Rosell et al., 2012), with BRAF inhibitors in $BRAF^{V600E}$ mutant metastatic melanoma patients (Chapman et al., 2011; Hauschild et al., 2012) and with human epidermal growth factor 2 (HER2) monoclonal antibodies in HER2

overexpressing breast cancer patients (Slamon et al., 2001) show improved therapy response, the only approved targeted therapy for PDAC, chemotherapy plus EGFR inhibitor erlotinib, did not notably change the disease prognosis (Moore et al., 2007). However, the observation of improved response to platinum-based therapies and poly (ADP-ribose) polymerase (PARP) inhibitors in a small subset of PDAC patients with mutations in homologous recombination repair pathway highlighted the importance of tumour subtyping and patient classification for successful treatment (Golan et al., 2019; Golan et al., 2014).

Therefore, in the last decade, tremendous effort has been put on molecular classification and identification of subtype-specific pathways, which are potentially targetable (Collisson et al., 2019). The breakthrough in molecular subtyping of PDAC happened in 2011 when Collisson and his colleagues analysed transcriptome data from a large collection of PDAC cells and patient samples and introduced the following three molecular PDAC subtypes; Classical, quasi-mesenchymal (QM) and exocrine like based on this transcriptomic analysis (Collisson et al., 2011). Classical subtype is characterized with the high expression of adhesion-related genes and QM subtype presents high expression of mesenchymal genes while the high expression of genes related to digestive enzymes seems to the feature of exocrine-like subtype (Collisson et al., 2011). The differences in the clinical presentations of the subtypes were also identified in this first publication (Collisson et al., 2011). The authors showed that QM patients presented worse overall survival than classical patients (Collisson et al., 2011). Moreover, the classical PDAC cells seem to be more sensitive to EGFR inhibitor erlotinib while nucleoside analogue gemcitabine seems to be more effective against the QM cells (Collisson et al., 2011). Following this, molecularly overlapping subtypes with a different nomenclature were also identified by Moffitt et al in 2015 (Moffitt et al., 2015) and Bailey et al in 2016 (Bailey et al., 2016). Conclusively, the Cancer Genome Atlas Network collected all identified subtypes under the umbrella of two main subtypes as QM/Squamous and Classical/Pancreatic progenitor by using the consensus clustering of tumour specific molecular signature, which is defined by all three previous publications (Collisson et al.(Collisson et al., 2011), Moffitt et al.(Moffitt et al., 2015) and Bailey et al (Bailey et al., 2016)) (Cancer Genome Atlas Research Network. Electronic address & Cancer Genome Atlas Research, 2017). Currently, a common classification nomenclature for PDAC describing QM/Squamous/Basal-like and

Classical/Pancreatic progenitor as main subtypes is widely accepted (Collisson et al., 2019). The clinical presence of two main molecular PDAC subtypes, their different prognosis and distinct responses to current chemotherapies were also proven by different research groups (Aung et al., 2018). In COMPASS trial, Aung et al. showed that patients with QM subtype have worse progression-free and overall survival rates compared to the patients with Classical subtype (Aung et al., 2018). Muckenhuber and colleagues demonstrated that patients with QM tumour respond better to therapy with gemcitabine whereas improved respond to FOLFIRINOX was observed in patients with classical PDAC (Muckenhuber et al., 2018).

Though transcriptional subtyping has indisputably improved our understanding of the heterogeneous nature of the PDAC, it did not introduce a novel, more effective therapeutic approaches into the clinical practice. One of the possible explanations for this may be the lack of evaluation of functional and physiological aspects of identified transcriptional differences between PDAC subtypes. Accordingly, analysis of the metabolic gene expression patterns and their relation to clinical outcome in samples from 33 different human cancers showed that upregulation in TCA cycle and lipid metabolism is associated with better prognosis while carbohydrate, nucleotide and vitamin & cofactor metabolism are related to worse prognosis (Peng et al., 2018). Furthermore, integrated analysis of transcriptome and metabolome suggested that the same core metabolic pathways are activated in similar subgroups of various cancers, even though diverse somatic mutations plays role in tumour initiation and progression (Peng et al., 2018), indicating that these core metabolic processes determine cancer behaviour and cancer phenotype. Therefore, it is reasonable to hypothesise that determining the specific metabolic features related to each cancer subtype and targeting them would improve the treatment of cancers including PDAC. In line with this, in 2015, Daemen et al performed the pioneering steps in characterizing the PDAC metabolism (Daemen et al., 2015). Daemen and colleagues performed metabolite profiling of human PDAC cell lines and observed that QM cells accumulate intermediates of the glycolysis while classical cell lines seem to be rich in miscellaneous lipid species (Daemen et al., 2015). These findings prompted the authors to classify the QM PDAC cells as glycolytic and classical PDAC cells as lipogenic (Daemen et al., 2015). However, due to the fact that the majority of the work has been performed on cell lines grown *in vitro* conditions, the translational relevance

of these findings is still under investigation. The problem of the “appropriate” model system and its translational relevance in cancer biology is evident through the fact that many cell culture-based findings have not found their way into the clinical practice (Witkiewicz et al., 2016). Very good number of clinical trials fails already in the first or second phase, as *in vitro* findings are not transferable to the clinic (Witkiewicz et al., 2016). It was the aim of this thesis to investigate the functional metabolic aspects of PDAC in a variety of model systems starting from cell lines over the patient-relevant systems such as Patient-Derived Xenografts and patient samples and identify the functional metabolic niche of the transcriptional subtypes that can eventually be used for the development of novel strategies targeting metabolism. Consequently, in the present work, extensive transcriptional and functional metabolic analyses were performed with different preclinical models of PDAC to identify which metabolic networks are differently regulated among subtypes on gene expression level and whether respective pathways are also translationally active and functional in one and the other subtype.

To investigate the metabolic differences on both molecular and functional level, gene expression data from established PDAC cell lines, primary patient-derived cells, patient-derived xenografts and patient samples were collected and analysed as an initial step. In all four models, samples were successfully separated in two known and dominant transcriptional subtypes, Classical and QM, using the bioinformatics platform developed in our laboratory. The following gene set enrichment analysis (GSEA) with three gene set collections (Hallmark, KEGG and REACTOME) revealed that epithelial-mesenchymal transition gene set (Hallmark_EMT) was mainly correlated with QM subtype whereas gene sets related with cell-cell communication and cellular organization were upregulated in classical subtype (Figure 3.1). In accordance with these observations, the link between classical subtype and high expression of epithelial gene signatures as well as the connection between QM subtype and promoted mesenchymal gene expression has been previously reported by Collisson et al and Bailey et al, supporting the value of our subtyping platform (Bailey et al., 2016; Collisson et al., 2011). These differences in transcriptome between subtypes can be explained by distinct histologic features of classical and QM subtypes. The classical subtype display differentiated tissue morphology, apical-basal polarity and epithelial phenotype. In the epithelial state, cells are in close contact with both neighbouring cells

and basal membrane via cell junctions (Sommariva & Gagliano, 2020) that may be partially explained the positive correlation between classical subtype and cell-cell communication and cellular organization gene sets. By contrast, QM subtype exhibits undifferentiated tissue morphology and fibroblast-like mesenchymal phenotype. During transition from epithelial state to mesenchymal state (epithelial-to-mesenchymal transition, EMT) cells lose their epithelial features such as cell-cell contact and gain mesenchymal features like higher motility and migration capability (Aiello et al., 2018) that may justify the upregulation of mesenchymal transcripts in QM subtype.

Furthermore, extensive analysis of metabolic gene expression was conducted with the same data sets revealed that some metabolic processes are enhanced and preserved in a subtype-specific manner quite stably throughout all four investigated PDAC models (Figure 3.1). The enrichment in ‘glycolysis, hypoxia and MYC targets’ gene sets were commonly detected in QM subtype. Transcripts belong to ‘hypoxia’ gene set was upregulated in QM samples of PDC, PDX and patient data sets whereas ‘glycolysis/glucose metabolism’ and ‘MYC targets’ gene sets were enriched in QM subtype of established PDAC cell lines, PDXs and patient samples. Surprisingly, enrichment in glycolysis related gene sets was not observed in the PDC sample group. The probable explanation for this observation may be the low number of samples and the bigger heterogeneity usually expected and found among patient-derived samples (Figure 3.1).

Differently, classical samples were more associated with the transcripts involved in lipid metabolism. Various gene sets related to lipid metabolism were upregulated in classical samples in all four data sets (Figure 3.1). The gene sets related to the synthesis of membrane lipids e.g. glycerolipid metabolism, glycosphingolipid metabolism were upregulated in classical subtype in almost all data sets. Epithelial and differentiated nature of classical subtype as also noted by Collisson (Collisson et al., 2011) and Bailey (Bailey et al., 2016) that may partly explain the enrichment in phospholipid related transcripts, since epithelial/classical cells need great variety of phospholipids to preserve differentiated morphology and apical-basal polarity requiring different cellular membrane compartments with specific phospholipid composition (van et al., 2020). Furthermore, cholesterol metabolism gene set was also upregulated in classical PDX and patient data sets. Even though cholesterol is an important building

block for cellular membranes, intermediates from cholesterol synthesis (mevalonate) pathway play important roles in different cellular processes ranging from post-translational modification of proteins to energy production and redox balance which are all deregulated in cancer to support tumour cell growth and proliferation (Mullen et al., 2016; Snaebjornsson et al., 2020).

One such example of mevalonate pathway intermediates is farnesylpyrophosphate (FPP) which is a precursor of ubiquinone, an electron transporter necessary for oxidative phosphorylation and precursor for pyrimidine synthesis (Mullen et al., 2016; Snaebjornsson et al., 2020). Accordingly, inhibition of mevalonate pathway shown to promote apoptosis in p53 deficient human colon cancer cell lines due to defect in FPP related pyrimidine synthesis and oxidative stress (Kaymak et al., 2020), supporting the idea that lipids have important functional roles besides being building blocks. In addition to the enrichment of lipid transcripts, fatty acid metabolism gene set was also well enriched in the classical samples of PDX and patient data sets. Although it is not surprising that lipid metabolism and fatty acid metabolism are enriched in the same subtype, it is difficult to say which aspect of fatty acid metabolism is indeed related to classical subtype. Because, fatty acid metabolism gene set contains transcripts that belong to different processes of fatty acid metabolism such as fatty acid import, synthesis, activation and deposition but also oxidation in mitochondria. (Snaebjornsson et al., 2020). As glycolysis was prominently present as a main energetic pathway in the QM subtype, it is reasonable to assume that other energy-producing processes such as fatty acid oxidation would dominate the classical subtype. In accord with this, custom gene sets (FAO1 and FAO2) that included genes exclusively involved in fatty acid transport to the mitochondria and their mitochondrial oxidation were upregulated in classical patient group, supporting the view of fatty acid oxidation being an important energy generating process in this subtype (Figure 3.15).

In line with these observations indicating the connection between glycolysis/hypoxia and QM subtype as well as the link between lipid metabolism and classical subtype, Karasinska et al. have been recently described four different PDAC subtype as glycolytic, quiescent, cholestrogenic and mixed according to the expression of transcripts related to glycolysis and cholesterol biosynthesis (Karasinska et al., 2020). The authors also showed that glycolytic and cholestrogenic subtypes associate with QM and classical subtypes respectively (Karasinska et al., 2020). Further investigation

of metabolic drivers like KRAS and MYC revealed that samples with both KRAS and MYC amplification show increased glycolytic gene expression (Karasinska et al., 2020). Upregulation in the expression of *HIF1A* and its target glycolytic genes *LDHA* and *MCT4* was observed in glycolytic subtype whereas cholestrogenic subtype presented increased expression of sterol regulatory element-binding protein 2 (SREBP2) (Karasinska et al., 2020). Also, cholestrogenic samples showed significantly higher expression of transporters forming mitochondrial pyruvate carrier complex (MPC), mitochondrial pyruvate carrier 1 and 2 (MPC1/2), compared to glycolytic samples suggesting the higher participation of pyruvate in TCA cycle in cholestrogenic subtype (Karasinska et al., 2020). These observations also indicate higher conversion of glucose carbon to lactate in glycolytic samples since the suppression of MPC genes has been shown to increase glycolytic activity and lactate generation leading to more aggressive phenotype (Karasinska et al., 2020). GSEA also showed consistent results that transcripts related with oxidative phosphorylation pathway were positively correlated with high MPC1/2 expression while hypoxia-related genes were negatively correlated with MPC1/2 expression (Karasinska et al., 2020).

Overall, the transcriptional data used in this work revealed that previously identified two major molecular subtypes, QM and classical, were existing in all investigated PDAC models (established cell lines, PDCs, PDXs and patient samples), supporting the view that a) metabolic pathways are relatively stable and functionally independent of the model systems b) patient-relevant model systems such as PDX and PDC preserve the metabolic characteristics of the primary tumour and are usable in preclinical and clinical research. In addition, the data presented here support the preservation of major metabolic pathways at least on the gene expression level, further justifying the use of the PDX and PDCs even in metabolic research and evaluation of metabolic therapies. In accord with this, it has been previously shown that freshly developed primary PDAC cell lines and PDX tumours highly preserve the genetic features and mutational landscape of the primary tumour and the preservation of genetic landscape was visible even in the late passages of primary cells (Knudsen et al., 2018). Furthermore, the authors also indicated that PDX tumours histologically recapitulate primary tumour and metastatic spread as well (Knudsen et al., 2018). Accordingly, the observations of Witkiewicz et al., revealed that primary cell lines and PDXs can be used for high-throughput drug screening and the evaluation of

therapeutic sensitivities due to their resemblance to the primary tumour, indicating the value of PDXs and PDCs in the guidance of personalized precision medicine for PDAC treatment (Witkiewicz et al., 2016).

Even though the analyses of transcriptional data herein show the conservation of glycolysis/hypoxia and lipid/fatty acid metabolism-related transcripts in QM and classical subtype respectively, it is still not clear whether these pathways are indeed functional in the respective subtype. Therefore, a range of functional and metabolic assays was performed to evaluate the physiological roles of glycolysis and lipid metabolism in different PDAC models.

In established cell lines, Seahorse glycolytic rate assay demonstrated somewhat higher glycolytic activity in the QM in comparison to classical cells. The same trend was observed among primary cells. However, detail and close observations rather suggest heterogeneity even in the same subtype. PSN1, a QM established cell line, showed the highest glycolytic rate. Among PDCs, PDC69 and PDC80, represented the highest glycolytic activity while the rest of the primary cells displayed comparable glycolytic rates (Figure 3.2). When specifically analysed, single gene expression analyses of glycolytic genes *ENO1/2*, *HK1/2* in established and primary PDAC cell lines with qPCR depicted the complementary outcome. The highest expression levels of these glycolytic genes, including lactate transporters *MCT1, MCT4* was found in PSN1, PDC69 and PDC80 (Figure 3.2 and 3.3). Similarly, the intra-class heterogeneity was also evident in targeted lipid profiling of established cell lines and PDCs. Even though the higher accumulation of lipid metabolites belonging to different lipid classes including phosphatidylcholines and sphingomyelins was detected in classical samples compared to QM samples, not every single detected lipid metabolite presented higher concentrations in all classical cells (Figure 3.10 and 3.11). The heterogeneity within subtypes was more obvious and separation of cells into subtypes were less clear in PDCs compared to established PDAC cells. These results suggested that both established and primary cell lines are still functionally heterogeneous and a complete simplification of QM subtype to fully glycolytic and classical subtype to non-glycolytic is not possible. A possible explanation for functional heterogeneity observed within the subtypes may be the existence of samples with hybrid transcriptomes, which were recently identified by different groups (Chan-Seng-Yue et al., 2020; Karasinska et al., 2020). Karasinska et al., identified two subgroups with hybrid metabolic gene

expression, mixed and quiescent, which were previously classified under the two major PDAC subtypes (Karasinska et al., 2020). Similarly, Chan-Seng-Yue and colleagues suggested that the two major PDAC subtypes, Classical and QM are still heterogeneous and divided each subtype into two subgroups as classical A/B and basal A/B, respectively (Chan-Seng-Yue et al., 2020). The authors also identified a hybrid subtype based on transcriptome and suggested that both classical and QM gene signatures are expressed in the cells, however, the degree of the expression of these subtype signatures determines the subtype and creates heterogeneity (Chan-Seng-Yue et al., 2020). In accordance with these observations, it is reasonable to think of molecular and metabolic classification of PDAC as a whole spectrum ranging from QM/glycolytic to classical/lipogenic like previously noticed in established PDAC cell lines (Daemen et al., 2015). Accordingly, it is reasonable to suggest that PSN1, PDC69 and PDC80 situate most probably on the highly glycolytic part while PDC89 is on the highly lipogenic side of this spectrum. However, the rest of the cells show variable levels in terms of glycolytic and lipogenic behaviour, indicating the need for better molecular/metabolic markers for PDAC classification.

Even though considerable heterogeneity within the subtypes was observed in investigated models, intra-subtype heterogeneity does not overshadow the transcriptional findings connecting the QM subtype to upregulated expression of the transcripts related to glycolysis and hypoxia gene sets. Because cell lines having the highest glycolytic rates (PSN1, PDC69 and PDC80) also had the highest expression of glycolytic regulators HIF1A and MYC as well as glycolytic markers LDHA and MCT4 on both mRNA and protein levels, confirming the translation of the upregulation in glycolysis and hypoxia gene sets into higher glycolytic activity, as detected by the Seahorse, in respective QM cell lines (Figure 3.2). The concurrent expression of glycolytic regulators MYC and HIF1A together with glycolytic markers LDHA and MCT4 even under normoxic cell culture conditions in highly glycolytic established and primary cell lines indicates the importance of co-operation of glycolysis and hypoxia-related genes for aggressive PDAC phenotype. As it was observed in this study, the relation of high glycolytic rate and hypoxia with aggressive phenotype has been observed mostly in murine systems by different groups both in PDAC and in some other cancer entities (Kalkat et al., 2017).

In PDAC, aerobic glycolysis is mainly controlled by oncogenic *KRAS* together with transcription factor *MYC* through glycolytic gene expression, as it was shown in mouse models (Ying et al., 2012). Similarly, the connection with MYC overexpression and aggressive phenotype and poor prognosis was also confirmed in resected PDAC patient samples by Witkiewicz et al (Witkiewicz et al., 2015). Accordingly, KRAS inactivation leads to downregulation of *MYC* expression and reduced expression of glycolytic genes *LDHA* and *ENO1* in PDAC mouse models, indicating the role of MYC in regulation of the glycolytic gene expression in PDAC (Ying et al., 2012). This further supports the described observation of concurrently high expression of MYC and LDHA on both transcriptome and protein level in highly glycolytic QM cell lines (PSN1, PDC69 and PDC80). Next to MYC, HIF1A, a major transcriptional regulator of cellular response to hypoxia, controls the glycolytic gene expression and promotes cancer cell survival and aggressiveness in various cancers. Consistent with given findings showing increased *HIF1A* and *LDHA* expression in glycolytic QM PDAC cell lines PSN1, PDC69 and PDC80, Guillaumond et al., showed in mouse models that glycolytic genes are mainly co-localizes with hypoxic tumour areas (Guillaumond et al., 2013). The authors also showed that hypoxia increases glycolytic gene expression in PDAC cell lines (Guillaumond et al., 2013). In pancreatic cancer cell lines, PANC-1 and CFPAC-1, hypoxic conditions and HIF1A activation enhanced LDHA expression (Cui et al., 2017). LDHA is responsible for the conversion of pyruvate to L-lactate on the last step of glycolysis (Cui et al., 2017).

Together with high MYC, HIF1A expression most probably enhanced LDHA expression in highly glycolytic QM cell lines PSN1, PDC69 and PDC80 indicating that these cell lines excessively convert glucose into L-lactate creating intracellular and extracellular acidosis. Increased lactate concentrations have been shown to activate HIF1A, regardless of oxygen, further promoting glycolysis and creating positive feedback for continuous glycolysis in aggressive tumour cells (Perez-Escuredo et al., 2016). This may be the explanation of concurrent upregulation of HIF1A and glycolysis in investigated highly glycolytic cell lines. However, intracellular and extracellular lactate concentration should be evaluated to confirm the HIF1A/glycolysis/lactate connection in these cell lines. Moreover, the enhanced expression of lactate transporter MCT4 on both mRNA and protein level was detected in highly glycolytic cell lines PSN1, PDC69 and PDC80. Monocarboxylate transporters, MCT1 and MCT4,

are bidirectional lactate transporters (Halestrap, 2013). MCT1 expression is detected in a wide range of tissues and cell type, whereas MCT4 expression is rather specific to highly glycolytic cells including cancer cells (Halestrap, 2013). Even though both transporters can work in a bidirectional manner, MCT1 is suggested to be mainly involved in the import of lactate while MCT4 is responsible for lactate export (Doherty & Cleveland, 2013). The overexpression of both transporters has been already detected in various cancers and known to associate with the aggressive phenotype (Doherty & Cleveland, 2013). It was shown in breast cancer patient samples that increased expression of MCT1 is correlated with aggressiveness (Gallagher et al., 2020) Similarly, metastatic melanoma cells were shown to be dependent on MCT1 expression and knock-down of MCT1 dramatically reduces the metastatic potential of melanoma cancer cells (Tasdogan et al., 2020). Consistent with findings presented here, high MCT4 expression, but not MCT1, has been suggested as a marker of glycolytic phenotype in PDAC (Baek et al., 2014).

Similar to the heterogeneous glycolytic behaviour detected in QM subtype, the results from lipid profiling presented the intra-subtype heterogeneity. However, the presented functional analysis of fatty acid oxidation, uptake and deposition in established PDAC cell lines revealed the link between classical subtype and fatty acid metabolism and subtype-specific utilization of fatty acids in PDAC. Classical established PDAC cell lines presented higher free fatty acid concentrations and higher preference for fatty acids as a metabolic fuel in Seahorse metabolic flux assays in comparison to QM cells, indicating higher fatty acid usage for energy production in mitochondria in classical subtype (Figure 3.13). Furthermore, the analysis of the expression of fatty acid oxidation genes in PDX and patient data sets revealed that most of the fatty acid oxidation related transcripts were upregulated in classical samples compared to QM samples (Figure 3.15). In line with these results, the upregulation of the fatty acid oxidation related gene expression has recently been shown to associate with better prognosis and longer survival in gastric cancer, lung adenocarcinoma, melanoma, clear cell renal cell carcinoma and breast cancer (Aiderus, Black, & Dunbier, 2018). The lower fatty acid oxidation rates of established QM cell lines can be explained by their hypoxic nature. It has been shown that fatty acid oxidation is reduced in hypoxic cancers in a HIF1A dependent manner to protect cancer cells from mitochondrial beta-oxidation derived reactive oxygen species what further mediated oxidative stress and

apoptosis (Munir et al., 2019). The repression of fatty acid oxidation is regulated by HIF1A through downregulation of acyl-CoA dehydrogenases (*ACADM* and *ACADL*) (Huang et al., 2014) and carnitine palmitoyltransferase 1A (*CPT1A*) (Zhang et al., 2017) in hepatocellular carcinoma (cell lines and patient samples) and clear cell renal carcinoma cell lines, respectively. Moreover, in colorectal and clear cell renal carcinoma cell lines, HIF1A has also been shown to promote the accumulation of fatty acids as triglycerides in lipid droplets to possibly reduce the fatty acid oxidation rates (Bensaad et al., 2014; Zhang et al., 2017). In accordance with this; a higher number of fluorescently-labelled lipid droplets, especially in HIF1A expressing glycolytic cell line PSN1, was observed in established QM cell lines compared to classical cells (Figure 3.14). This may be explained by HIF1A regulated high expression of lipid droplet membrane protein, perilipin 2 (PLIN2). PLIN2 is a major protein located on the membrane of lipid droplets and its function is to prevent the release and use of fatty acids (Munir et al., 2019). In breast cancer and glioma cell lines, HIF1A enhance the lipid droplet formation by upregulating PLIN2 (Bensaad et al., 2014). Though the same trend was observed in this work with increased *HIF1A* and *PLIN2* expression in the same subtype, QM, indicating that HIF1A might play a role in the regulation of fatty acid metabolism in PDAC, this question demands further investigation. However, QM samples of PDX and patient data sets represented significantly higher PLIN2 expression, supporting the view of active fatty acid oxidation in the classical subtype on patient-level as well.

To further evaluate translational significance on the cell-based findings presented here and in hope of identifying a subtype-specific metabolic marker that is usable in clinical practice for identification of highly glycolytic patients, we analysed the expression of selected glycolytic markers in patient samples as well. For this, expression of *GLUT1, ENO1, LDHA, PKM2, MCT1* and *MCT4* was reviewed in the patient data set. The analysis of gene expression data revealed that *GLUT1, ENO1, LDHA, MCT4* and *PKM2* expression were significantly increased in PDAC patients compared to healthy individuals (Figure 3.6 and 3.7). QM samples presented significantly higher expression of respective genes than classical samples. Similar analysis with a variety of here presented genes implicated in FA metabolism was performed and complementary differences were also observed on the molecular level (Figure 3.15 and 3.17). However, immunohistochemical analysis of these markers in 9 FFPE PDAC patient

samples, which were previously separated into QM and classical subtypes, did not substantiate any significant differences among the subtypes and separation of samples into subtypes with any of these proteins was not possible. This may be explained by the low sample size, the imperfect subtyping of tumours using the KRT81 and/or a lower sensitivity of immunohistochemistry as a qualitative method that makes hard to detect differences in the expression levels between cells of different subtypes. In addition, it is most probable that the differences are more present on the activity level rather than on simple protein expression since it is known that transporters and enzymes are mostly regulated post-translationally by substrate availability and microenvironment conditions instead of by changing the mere protein levels. Moreover, as suggested by Chan-Seng-Yue et al., PDAC tumour tissue potentially contains cancer cells belonging to both subtype and the number of cells expressing subtype-specific gene sets determines the subtype of the sample (Chan-Seng-Yue et al., 2020).

Thus, the existence of both classical and QM cells within the same tumour and the same sample may prevent subtype-specific differences in the expression of investigated proteins from being detected with immunohistochemistry. Furthermore, stromal cellularity and number of positive stromal cells may mask the difference between subtypes since whole tissue quantification results quantify all cellular populations, including cancer and stromal cells. To separate the stromal from cancer cells and indeed evaluate the expression of glycolytic and lipogenic markers on cancer cells only, multiplex staining of interested proteins together with a cancer cell marker and subtype marker can be performed. Different from abovementioned proteins, the observed dominance of MCT4 to MCT1 as a lactate transporter in all investigated PDAC models suggested that MCT4 might highlight the glycolytic cells. Accordingly, immunohistochemical analysis of MCT1 and MCT4 expression on PDAC patient FFPE samples revealed that both stromal cells and cancer cells express both transporters but with a different staining pattern. MCT1 expression was more prominent on the stromal cell while MCT4 expression was largely present on cancer cells and mostly correlates with KRT81 (QM marker) expression (Figure 3.7).

In line with this, in murine PDACs, MCT1 expression was detected on both stromal and cancer cells and its expression mostly correlated with normoxic tumour areas (Guillaumond et al., 2013). However, MCT4 expression was shown to be generally restricted to cells in the hypoxic areas (Guillaumond et al., 2013) and high MCT4

expression is related with aggressive phenotype and poor overall survival (Baek et al., 2014). The present results of multiplex staining of PDAC samples for MCT4 together with cancer cell marker pan-cytokeratin and QM marker cytokeratin 81 also showed that MCT4 and KRT81 expression were mostly coincident while KRT81 negative cells were less positive for MCT4, supporting the relation of MCT4 expression and aggressive QM subtype. Therefore, it is acceptable to think that MCT4 has the potential of identifying the glycolytic PDACs and this potential should be exploited in the clinic for identification of such patients. However, its value as a single glycolytic marker is probably questionable and additional markers that will support MCT4 expression are further needed.

Strong presence of glycolysis in the QM subtype renders challenging glycolysis a good strategy to target QM subtype. Therefore, chemical inhibitors targeting different steps and enzymes of glycolysis were used in this study. Pyruvate kinase (PK) converts phosphoenolpyruvate (PEP) to pyruvate with concomitant conversion of ADP to ATP on the last step of glycolysis (Tamada, Suematsu, & Saya, 2012). There are four isoforms of pyruvate kinase encoded by PKM (M1 and M2 isoforms) and PKLR (L and R isoforms) genes (Tamada et al., 2012). The overexpression of M2 isoform (PKM2) has been observed in various cancers including PDAC while most of the healthy cells are expressing PKM1 (Tamada et al., 2012). It is suggested that PKM2 promotes aerobic glycolysis and proliferation in cancer (Tamada et al., 2012). The role of PKM2 in cancer is to slow down the conversion of PEP to pyruvate and thus increase the diversion of glucose carbon to anabolic pathways (Tamada et al., 2012). Even though alternative splicing of PKM2 instead of PKM1 is controlled by MYC, PKM2 also localizes in the nucleus and enhances glycolytic gene expression through activation HIF1A and MYC (Tamada et al., 2012). The cancer-specific expression and important functional and transcriptional roles in glycolysis render PKM2 an important target for the inhibition of aerobic glycolysis in cancer cells (Tamada et al., 2012). The small-molecule inhibitor shikonin has been shown to inhibit PKM2 and therefore reduced to glycolysis in different cancer entities including PDAC (Tamada et al., 2012). A recent study showed that inhibition of PKM2 with shikonin potently reduces cell proliferation and viability as well as promotes apoptosis in pancreatic cancer cell line MiaPaca2 (James et al., 2020). In line with these, the reduction in cell viability in established PDAC cell lines was observed in the presented study. Moreover, shikonin was

somewhat more effective on QM cell lines with calculated IC_{50} values lower than for the classical lines, as would be expected from the higher glycolytic dependence of the QM cells. Blocking lactate transports by inhibiting lactate transporters MCT1 and MCT4 is another strategy that has been used against different cancer entities due to caner specific overexpression of respective genes (Doherty & Cleveland, 2013). Lactate is the mediator of different intracellular and extracellular processes ranging from cellular energy metabolism, angiogenesis to immune suppression and inhibition of lactate transport with AZD3965 (MCT1/2 inhibitor) have been shown to cause growth inhibition and cell death in lymphoma (Beloueche-Babari et al., 2020; Curtis et al., 2017), small cell lung cancer (Polanski et al., 2014) in vitro. However, it has been suggested that glycolytic and MCT4 expressing lymphoma and small cell lung cancer cells are resistant to inhibition of MCT1 with AZD3965 (Beloueche-Babari et al., 2020; Curtis et al., 2017; Polanski et al., 2014). In line with these, no inhibition of cell viability was observed in established PDAC cell lines in this work, supporting the idea that MCT4 plays a more dominant role in lactate transport in PDAC. Most probably, cells overcome the inhibition of MCT1 by using MCT4 for lactate transport. To test the effect of blocking both transporters on cell viability the same cell lines were treated with syrosingopine, MCT1/4 dual inhibitor. Syrosingopine has been shown to sensitize various cancer cells to OXPHOS inhibitor metformin due to dual inhibition of glycolysis and OXPHOS with syrosingopine and metformin what resulted in cell death (Benjamin et al., 2018). In line with these, syrosingopine reduced the cell viability of both QM and classical cell at relatively high concentrations, suggesting that inhibition of lactate transport only is not enough to induce complete apoptosis. QM cell lines did present slightly higher sensitivity against MCT inhibition compared to classical cell lines, as expected due to their generally higher glycolytic dependency. The effects of glycolytic inhibitors are however not prominently different among subtypes and reflect the complexity and the heterogeneity of the metabolic responses observed and described here. Classical subtype, although less glycolytic, is by no means devoid of glycolysis and this metabolic process is essential in this subtype as well. The subtle differences in the IC_{50} values indicate that the QM cells are perhaps somewhat more prone to glycolysis inhibition and perhaps combining chemotherapy plus glycolysis inhibition is the way to go in these patients.

5 Conclusion

Even though two main transcriptional subtypes of PDAC, classical and QM, have been known for almost a decade, functional differences, which determine the clinical phenotype and perhaps offer a targetable niche, are largely not known. Metabolism is the functional link between transcriptome and phenotype. However, subtype-specific metabolic targeting of PDAC is still widely unexplored. Therefore, this thesis aimed to identify the differently regulated metabolic pathways in classical and QM subtypes and explore whether identified pathways are metabolically active in patient-relevant, preclinical PDAC models.

Overall, molecular analysis of four different PDAC models (established PDAC cells, primary cells, PDXs and patient samples) revealed that glycolysis/hypoxia and lipid/fatty acid metabolism transcripts are dominating QM and classical subtype, respectively. However, functional analysis of respective metabolic processes exposed the functional heterogeneity within both subtypes. In the QM subtype, a plethora of samples ranging from high to less glycolytic phenotypes were identified. The same was true for the functional dependence of classical subtype on lipid/fatty acid metabolism. The presented results highlighted that only some representatives of each subtype seem to translate identified molecular differences into specific metabolic activity, potentially indicating the existence of additional metabolic subgroups and the complexity of metabolic actions in a living system. It is reasonable to assume that the fine-tuning between glycolysis and fatty acid metabolism is an adaptive response to the microenvironmental stimuli and stronger implication of one or the other pathway in the metabolic adaptation depends on both molecular and environmental conditions.

Nevertheless, functional identification of prominent representatives of the subtypes is promising and would be the first step of patient stratification for subtype-guided metabolic targeting in PDAC. For example, patients with tumours carrying transcriptional QM signature would be obvious candidates for metabolic targeting of glycolysis if their tumours also demonstrate high glycolytic activity, for example in additional preclinical tests with PDXs or primary cell lines. However, further preclinical and clinical efforts are needed for easier identification of such patients and the development of better metabolic therapies for PDAC.

6 Additional information

Table 6-1 Positive lipids detected and quantified at University of Leiden. Compound names adapted from The Human Metabolome Database (https://hmdb.ca) (Wishart et al., 2018).

Metabolite ID	Metabolite
DG(36:4)	Diacylglycerol with two acyl residue sum 36:4
Cer(d18:0/24:0)	Ceramide with two acyl residue 18:0/24:0
Cer(d18:1/16:0)	Ceramide with two acyl residue 18:1/16:0
Cer(d18:1/20:0)	Ceramide with two acyl residue 18:1/20:0
Cer(d18:1/24:0)	Ceramide with two acyl residue 18:1/24:0
Cer(d18:1/24:1)	Ceramide with two acyl residue 18:1/24:1
SM(d18:1/14:0)	Sphingolipid with two acyl residue 18:1/14:0
SM(d18:1/16:0)	Sphingolipid with two acyl residue 18:1/16:0
SM(d18:1/24:1)	Sphingolipid with two acyl residue 18:1/24:1
PC(32:0)	Phosphatidylcholine with acyl or alkyl residue sum C32:0
PC(32:1)	Phosphatidylcholine with acyl or alkyl residue sum C32:1
PC(32:2)	Phosphatidylcholine with acyl or alkyl residue sum C32:2
PC(34:1)	Phosphatidylcholine with acyl or alkyl residue sum C34:1
PC(34:2)	Phosphatidylcholine with acyl or alkyl residue sum C34:2
PC(34:3)	Phosphatidylcholine with acyl or alkyl residue sum C34:3
PC(34:4)	Phosphatidylcholine with acyl or alkyl residue sum C34:4
PC(36:1)	Phosphatidylcholine with acyl or alkyl residue sum C36:1
PC(36:2)	Phosphatidylcholine with acyl or alkyl residue sum C36:2
PC(36:3)	Phosphatidylcholine with acyl or alkyl residue sum C36:3
PC(36:5)	Phosphatidylcholine with acyl or alkyl residue sum C36:5
PC(38:2)	Phosphatidylcholine with acyl or alkyl residue sum C38:2
PC(38:3)	Phosphatidylcholine with acyl or alkyl residue sum C38:3
PC(38:4)	Phosphatidylcholine with acyl or alkyl residue sum C38:4
PC(38:5)	Phosphatidylcholine with acyl or alkyl residue sum C38:5
PC(38:6)	Phosphatidylcholine with acyl or alkyl residue sum C38:6
PC(38:7)	Phosphatidylcholine with acyl or alkyl residue sum C38:7
PC(40:5)	Phosphatidylcholine with acyl or alkyl residue sum C40:5
PC(40:6)	Phosphatidylcholine with acyl or alkyl residue sum C40:6
PC(40:7)	Phosphatidylcholine with acyl or alkyl residue sum C40:7
PC(40:8)	Phosphatidylcholine with acyl or alkyl residue sum C40:8
PE(38:2)	Phosphatidylethanolamine with residue 38:2
LPC(16:1)	Lysophosphatidylcholine with acyl residue 16:1
LPC(18:0)	Lysophosphatidylcholine with acyl residue 18:0
LPC(18:1)	Lysophosphatidylcholine with acyl residue 18:1
LPC(18:2)	Lysophosphatidylcholine with acyl residue 18:2
LPC(O-16:1)	Lysophosphatidylcholine with fatty alcohol group residue 16:1
LPC(O-18:1)	Lysophosphatidylcholine with fatty alcohol group residue 18:1

Table 6-2 Signalling lipids detected and quantified at University of Leiden.

Metabolite ID	Metabolite
11,12-DiHETrE	(5Z,8Z,14Z)-11,12-Dihydroxyeicosa-5,8,14-trienoic acid
11-HETE	11-hydroxy-5Z,8Z,11E,14Z-eicosatetraenoic acid
13-HODE	13-Hydroxyoctadecadienoic acid
9-HODE	alpha-Dimorphecolic acid
PGF2a	Prostaglandin F2-alpha
FA 18:1	A fatty acid anion with 18 carbons and 1 double bonds
FA 20:4	A fatty acid anion with 20 carbons and 4 double bonds
FA 22:6	A fatty acid anion with 22 carbons and 6 double bonds
cLPA 18:0	Cyclic lysophosphatidic acid with acyl residue 18:0
cLPA 18:1	Cyclic lysophosphatidic acid with acyl residue 18:1
LPA 16:0	Lysophosphatidate with acyl residue 16:0
LPA 18:0	Lysophosphatidate with acyl residue 18:0
LPA 18:1	Lysophosphatidate with acyl residue 18:1
LPA 20:4	Lysophosphatidate with acyl residue 20:4
LPA 22:4	Lysophosphatidate with acyl residue 22:4
LPA 22:6	Lysophosphatidate with acyl residue 22:6
LPE 16:0	Lysophosphatidylethanolamine with acyl residue 16:0
LPE 16:1	Lysophosphatidylethanolamine with acyl residue 16:1
LPE 18:0	Lysophosphatidylethanolamine with acyl residue 18:0
LPE 18:1	Lysophosphatidylethanolamine with acyl residue 18:1
LPE 20:3	Lysophosphatidylethanolamine with acyl residue 20:3
LPE 20:4	Lysophosphatidylethanolamine with acyl residue 20:4
LPE 20:5	Lysophosphatidylethanolamine with acyl residue 20:5
LPE 22:4	Lysophosphatidylethanolamine with acyl residue 22:4
LPE 22:5	Lysophosphatidylethanolamine with acyl residue 22:5
LPE 22:6	Lysophosphatidylethanolamine with acyl residue 22:6
LPG 16:0	Lysophosphatidylglycerol with acyl residue 16:0
LPG 16:1	Lysophosphatidylglycerol with acyl residue 16:1
LPG 18:0	Lysophosphatidylglycerol with acyl residue 18:0
LPG 18:1	Lysophosphatidylglycerol with acyl residue 18:1
LPG 18:2	Lysophosphatidylglycerol with acyl residue 18:2
LPI 16:0	Lysophosphatidylinositol with acyl residue 16:0
LPI 16:1	Lysophosphatidylinositol with acyl residue 16:1
LPI 18:0	Lysophosphatidylinositol with acyl residue 18:0
LPI 18:1	Lysophosphatidylinositol with acyl residue 18:1
LPI 20:4	Lysophosphatidylinositol with acyl residue 20:4
LPS 16:0	Lysophosphatidylserine with acyl residue 16:0
LPS 18:0	Lysophosphatidylserine with acyl residue 18:0
LPS 18:1	Lysophosphatidylserine with acyl residue 18:1
LPS 18:2	Lysophosphatidylserine with acyl residue 18:2
LPS 20:4	Lysophosphatidylserine with acyl residue 20:4
LPS 22:4	Lysophosphatidylserine with acyl residue 22:4
LPS 22:6	Lysophosphatidylserine with acyl residue 22:6

Table 6-3 Metabolites detected and quantified with Biocrates AbsoluteIDQ® p180 Kit. Biocrates Life Sciences AG provided compound names.

Metabolite ID	Metabolite
lysoPC a C16:0	Lysophosphatidylcholine with acyl residue C16:0
lysoPC a C16:1	Lysophosphatidylcholine with acyl residue C16:1
lysoPC a C18:0	Lysophosphatidylcholine with acyl residue C18:0
lysoPC a C18:1	Lysophosphatidylcholine with acyl residue C18:1
lysoPC a C20:3	Lysophosphatidylcholine with acyl residue C20:3
lysoPC a C26:0	Lysophosphatidylcholine with acyl residue C26:0
lysoPC a C28:0	Lysophosphatidylcholine with acyl residue C26:1
lysoPC a C28:1	Lysophosphatidylcholine with acyl residue C28:1
PC aa C24:0	Phosphatidylcholine with diacyl residue sum C24:0
PC aa C28:1	Phosphatidylcholine with diacyl residue sum C28:1
PC aa C30:0	Phosphatidylcholine with diacyl residue sum C30:0
PC aa C32:0	Phosphatidylcholine with diacyl residue sum C32:0
PC aa C32:1	Phosphatidylcholine with diacyl residue sum C32:1
PC aa C32:2	Phosphatidylcholine with diacyl residue sum C32:2
PC aa C32:3	Phosphatidylcholine with diacyl residue sum C32:3
PC aa C34:1	Phosphatidylcholine with diacyl residue sum C34:1
PC aa C34:2	Phosphatidylcholine with diacyl residue sum C34:2
PC aa C34:3	Phosphatidylcholine with diacyl residue sum C34:3
PC aa C34:4	Phosphatidylcholine with diacyl residue sum C34:4
PC aa C36:0	Phosphatidylcholine with diacyl residue sum C36:0
PC aa C36:1	Phosphatidylcholine with diacyl residue sum C36:1
PC aa C36:2	Phosphatidylcholine with diacyl residue sum C36:2
PC aa C36:3	Phosphatidylcholine with diacyl residue sum C36:3
PC aa C36:4	Phosphatidylcholine with diacyl residue sum C36:4
PC aa C36:5	Phosphatidylcholine with diacyl residue sum C36:5
PC aa C36:6	Phosphatidylcholine with diacyl residue sum C36:6
PC aa C38:0	Phosphatidylcholine with diacyl residue sum C38:0
PC aa C38:3	Phosphatidylcholine with diacyl residue sum C38:3
PC aa C38:4	Phosphatidylcholine with diacyl residue sum C38:4
PC aa C38:5	Phosphatidylcholine with diacyl residue sum C38:5
PC aa C38:6	Phosphatidylcholine with diacyl residue sum C38:6
PC aa C40:2	Phosphatidylcholine with diacyl residue sum C40:2
PC aa C40:3	Phosphatidylcholine with diacyl residue sum C40:3
PC aa C40:4	Phosphatidylcholine with diacyl residue sum C40:4
PC aa C40:5	Phosphatidylcholine with diacyl residue sum C40:5
PC aa C40:6	Phosphatidylcholine with diacyl residue sum C40:6
PC aa C42:1	Phosphatidylcholine with diacyl residue sum C42:1
PC aa C42:2	Phosphatidylcholine with diacyl residue sum C42:2
PC aa C42:5	Phosphatidylcholine with diacyl residue sum C42:5
PC aa C42:6	Phosphatidylcholine with diacyl residue sum C42:6
PC ae C30:0	Phosphatidylcholine with acyl-alkyl residue sum C30:0

PC ae C30:1	Phosphatidylcholine with acyl-alkyl residue sum C30:1
PC ae C30:2	Phosphatidylcholine with acyl-alkyl residue sum C30:2
PC ae C32:1	Phosphatidylcholine with acyl-alkyl residue sum C32:1
PC ae C32:2	Phosphatidylcholine with acyl-alkyl residue sum C32:2
PC ae C34:0	Phosphatidylcholine with acyl-alkyl residue sum C34:0
PC ae C34:1	Phosphatidylcholine with acyl-alkyl residue sum C34:1
PC ae C34:2	Phosphatidylcholine with acyl-alkyl residue sum C34:2
PC ae C34:3	Phosphatidylcholine with acyl-alkyl residue sum C34:3
PC ae C36:0	Phosphatidylcholine with acyl-alkyl residue sum C36:0
PC ae C36:1	Phosphatidylcholine with acyl-alkyl residue sum C36:1
PC ae C36:2	Phosphatidylcholine with acyl-alkyl residue sum C36:2
PC ae C36:3	Phosphatidylcholine with acyl-alkyl residue sum C36:3
PC ae C36:4	Phosphatidylcholine with acyl-alkyl residue sum C36:4
PC ae C36:5	Phosphatidylcholine with acyl-alkyl residue sum C36:5
PC ae C38:0	Phosphatidylcholine with acyl-alkyl residue sum C38:0
PC ae C38:1	Phosphatidylcholine with acyl-alkyl residue sum C38:1
PC ae C38:2	Phosphatidylcholine with acyl-alkyl residue sum C38:2
PC ae C38:3	Phosphatidylcholine with acyl-alkyl residue sum C38:3
PC ae C38:4	Phosphatidylcholine with acyl-alkyl residue sum C38:4
PC ae C38:5	Phosphatidylcholine with acyl-alkyl residue sum C38:5
PC ae C38:6	Phosphatidylcholine with acyl-alkyl residue sum C38:6
PC ae C40:1	Phosphatidylcholine with acyl-alkyl residue sum C40:1
PC ae C40:2	Phosphatidylcholine with acyl-alkyl residue sum C40:2
PC ae C40:3	Phosphatidylcholine with acyl-alkyl residue sum C40:3
PC ae C40:4	Phosphatidylcholine with acyl-alkyl residue sum C40:4
PC ae C40:5	Phosphatidylcholine with acyl-alkyl residue sum C40:5
PC ae C40:6	Phosphatidylcholine with acyl-alkyl residue sum C40:6
PC ae C42:1	Phosphatidylcholine with acyl-alkyl residue sum C42:1
PC ae C42:2	Phosphatidylcholine with acyl-alkyl residue sum C42:2
PC ae C42:3	Phosphatidylcholine with acyl-alkyl residue sum C42:3
SM (OH) C14:1	Hydroxysphingomyelin with acyl residue sum C14:1
SM (OH) C16:1	Hydroxysphingomyelin with acyl residue sum C16:1
SM (OH) C22:1	Hydroxysphingomyelin with acyl residue sum C22:1
SM (OH) C22:2	Hydroxysphingomyelin with acyl residue sum C22:2
SM (OH) C24:1	Hydroxysphingomyelin with acyl residue sum C24:1
SM C16:0	Sphingomyelin with acyl residue sum C16:0
SM C16:1	Sphingomyelin with acyl residue sum C16:1
SM C18:0	Sphingomyelin with acyl residue sum C18:0
SM C18:1	Sphingomyelin with acyl residue sum C18:1
SM C20:2	Sphingomyelin with acyl residue sum C20:2
SM C24:0	Sphingomyelin with acyl residue sum C24:0
SM C24:1	Sphingomyelin with acyl residue sum C24:1
SM C26:0	Sphingomyelin with acyl residue sum C26:0
SM C26:1	Sphingomyelin with acyl residue sum C26:1

Table 6-4 Fatty acid oxidation genes and related processes

Gene ID/Data set	Process
ABCD3	Peroxisomal import of fatty acids
ACAA1	Peroxisomal fatty acid oxidation
ACAA2	Mitochondrial fatty acid oxidation
ACAD10	Mitochondrial fatty acid oxidation
ACAD8	Mitochondrial fatty acid oxidation
ACAD9	Mitochondrial oxidation of palmitoyl-CoA and long-chain unsaturated fatty acids
ACADL	Mitochondrial oxidation of straight-chain fatty acids
ACADM	Mitochondrial oxidation of medium-chain fatty acids
ACADS	Mitochondrial oxidation of short-chain fatty acids
ACADSB	Mitochondrial oxidation of short/branched-chain fatty acids
ACADVL	Mitochondrial oxidation of long/very long-chain fatty acids
ACAT1	Mitochondrial fatty acid oxidation
ACAT2	Cholesterol esterification
ACOT1	Mitochondrial and peroxisomal hydrolysis of fatty acyl-CoA
ACOT11	Mitochondrial and peroxisomal hydrolysis of fatty acyl-CoA
ACOT12	Mitochondrial and peroxisomal hydrolysis of fatty acyl-CoA
ACOT13	Mitochondrial and peroxisomal hydrolysis of fatty acyl-CoA
ACOT2	Mitochondrial and peroxisomal hydrolysis of fatty acyl-CoA
ACOT4	Mitochondrial and peroxisomal hydrolysis of fatty acyl-CoA
ACOT6	Mitochondrial and peroxisomal hydrolysis of fatty acyl-CoA
ACOT7	Mitochondrial and peroxisomal hydrolysis of fatty acyl-CoA
ACOT8	Mitochondrial and peroxisomal hydrolysis of fatty acyl-CoA
ACOT9	Mitochondrial and peroxisomal hydrolysis of fatty acyl-CoA
ACOX1	Mitochondrial fatty acid oxidation
ACOX3	Peroxisomal fatty acid oxidation
ACSBG1	Fatty acid esterification for both lipid synthesis and fatty acid oxidation
ACSBG2	Fatty acid esterification for both lipid synthesis and fatty acid oxidation
ACSL1	Fatty acid esterification for both lipid synthesis and fatty acid oxidation
ACSL3	Fatty acid esterification for both lipid synthesis and fatty acid oxidation
ACSL4	Fatty acid esterification for both lipid synthesis and fatty acid oxidation
ACSL5	Fatty acid esterification for both lipid synthesis and fatty acid oxidation
ACSL6	Fatty acid esterification for both lipid synthesis and fatty acid oxidation
ACSM3	Fatty acid esterification for both lipid synthesis and fatty acid oxidation
ACSM6	Fatty acid esterification for both lipid synthesis and fatty acid oxidation
CD36	Cellular fatty acid transport
CPT1A	Mitochondrial fatty acid import
CPT1B	Mitochondrial fatty acid import
CPT1C	Mitochondrial fatty acid import
CPT2	Mitochondrial fatty acid import
CRAT	Mitochondrial and peroxisomal fatty acid import
DECR1	Mitochondrial fatty acid oxidation

ECH1	Peroxisomal fatty acid oxidation
ECHS1	Mitochondrial fatty acid oxidation
ECI1	Mitochondrial oxidation of unsaturated fatty acids
ECI2	Mitochondrial oxidation of unsaturated fatty acids
EHHADH	Peroxisomal fatty acid oxidation
HADH	Mitochondrial fatty acid oxidation
HADHA	Mitochondrial oxidation of long-chain fatty acids
HADHB	Mitochondrial oxidation of long-chain fatty acids
IVD	Mitochondrial hydrolysis of short-chain fatty acyl-CoA
MECR	Mitochondrial fatty acid oxidation
PLIN2	Intracellular lipid storage in lipid droplets
PNPLA2	Hydrolysis of triglycerides in lipid droplets
SLC22A5	Mitochondrial fatty acid import
SLC25A20	Mitochondrial fatty acid import
SLC27A1	Fatty acid esterification for both lipid synthesis and fatty acid oxidation
SLC27A2	Fatty acid esterification for both lipid synthesis and fatty acid oxidation
SLC27A3	Fatty acid esterification for both lipid synthesis and fatty acid oxidation
SLC27A4	Fatty acid esterification for both lipid synthesis and fatty acid oxidation
SLC27A5	Fatty acid esterification for both lipid synthesis and fatty acid oxidation
SLC27A6	Fatty acid esterification for both lipid synthesis and fatty acid oxidation

Table 6-5 Genes comprising FAO1 and FAO2 gene sets

Gene ID	**FAO1 Gene set**
ACAA2	Mitochondrial fatty acid oxidation
ACADL	Mitochondrial oxidation of straight-chain fatty acids
ACADM	Mitochondrial oxidation of medium-chain fatty acids
ACADS	Mitochondrial oxidation of short-chain fatty acids
ACADVL	Mitochondrial oxidation of long/very long-chain fatty acids
ACAT1	Mitochondrial fatty acid oxidation
CPT1A	Mitochondrial fatty acid import
CPT1B	Mitochondrial fatty acid import
CPT1C	Mitochondrial fatty acid import
CPT2	Mitochondrial fatty acid import
ECHS1	Mitochondrial fatty acid oxidation
HADHA	Mitochondrial oxidation of long-chain fatty acids
HADHB	Mitochondrial oxidation of long-chain fatty acids
SLC25A20	Mitochondrial fatty acid import

Gene ID	FAO2 Gene set
ACAA2	Mitochondrial fatty acid oxidation
ACADL	Mitochondrial oxidation of straight-chain fatty acids
ACADM	Mitochondrial oxidation of medium-chain fatty acids
ACADS	Mitochondrial oxidation of short-chain fatty acids
ACADVL	Mitochondrial oxidation of long/very long-chain fatty acids
ACAT1	Mitochondrial fatty acid oxidation
ACSL1	Fatty acid esterification for both lipid synthesis and fatty acid oxidation
ACSL3	Fatty acid esterification for both lipid synthesis and fatty acid oxidation
ACSL4	Fatty acid esterification for both lipid synthesis and fatty acid oxidation
ACSL5	Fatty acid esterification for both lipid synthesis and fatty acid oxidation
ACSL6	Fatty acid esterification for both lipid synthesis and fatty acid oxidation
CD36	Cellular fatty acid transport
CPT1A	Mitochondrial fatty acid import
CPT1B	Mitochondrial fatty acid import
CPT1C	Mitochondrial fatty acid import
CPT2	Mitochondrial fatty acid import
ECHS1	Mitochondrial fatty acid oxidation
HADHA	Mitochondrial oxidation of long-chain fatty acids
HADHB	Mitochondrial oxidation of long-chain fatty acids
SLC25A20	Mitochondrial fatty acid import
SLC27A1	Fatty acid esterification for both lipid synthesis and fatty acid oxidation
SLC27A2	Fatty acid esterification for both lipid synthesis and fatty acid oxidation
SLC27A4	Fatty acid esterification for both lipid synthesis and fatty acid oxidation
SLC27A5	Fatty acid esterification for both lipid synthesis and fatty acid oxidation
SLC27A6	Fatty acid esterification for both lipid synthesis and fatty acid oxidation

7 References

Aguirre, A. J., & Collisson, E. A. (2017). Advances in the Genetics and Biology of Pancreatic Cancer. *Cancer J, 23*(6), 315-320. doi:10.1097/PPO.0000000000000286

Aiderus, A., Black, M. A., & Dunbier, A. K. (2018). Fatty acid oxidation is associated with proliferation and prognosis in breast and other cancers. *BMC Cancer, 18*(1), 805. doi:10.1186/s12885-018-4626-9

Aiello, N. M., Maddipati, R., Norgard, R. J., Balli, D., Li, J., Yuan, S., . . . Stanger, B. Z. (2018). EMT Subtype Influences Epithelial Plasticity and Mode of Cell Migration. *Dev Cell, 45*(6), 681-695 e684. doi:10.1016/j.devcel.2018.05.027

Alizadeh, A. A., Eisen, M. B., Davis, R. E., Ma, C., Lossos, I. S., Rosenwald, A., . . . Staudt, L. M. (2000). Distinct types of diffuse large B-cell lymphoma identified by gene expression profiling. *Nature, 403*(6769), 503-511. doi:10.1038/35000501

Auciello, F. R., Bulusu, V., Oon, C., Tait-Mulder, J., Berry, M., Bhattacharyya, S., . . . Sherman, M. H. (2019). A Stromal Lysolipid-Autotaxin Signaling Axis Promotes Pancreatic Tumor Progression. *Cancer Discov, 9*(5), 617-627. doi:10.1158/2159-8290.CD-18-1212

Aune, D., Greenwood, D. C., Chan, D. S., Vieira, R., Vieira, A. R., Navarro Rosenblatt, D. A., . . . Norat, T. (2012). Body mass index, abdominal fatness and pancreatic cancer risk: a systematic review and non-linear dose-response meta-analysis of prospective studies. *Ann Oncol, 23*(4), 843-852. doi:10.1093/annonc/mdr398

Aung, K. L., Fischer, S. E., Denroche, R. E., Jang, G. H., Dodd, A., Creighton, S., . . . Knox, J. J. (2018). Genomics-Driven Precision Medicine for Advanced Pancreatic Cancer: Early Results from the COMPASS Trial. *Clin Cancer Res, 24*(6), 1344-1354. doi:10.1158/1078-0432.CCR-17-2994

Badea, L., Herlea, V., Dima, S. O., Dumitrascu, T., & Popescu, I. (2008). Combined gene expression analysis of whole-tissue and microdissected pancreatic ductal adenocarcinoma identifies genes specifically overexpressed in tumor epithelia. *Hepatogastroenterology, 55*(88), 2016-2027. Retrieved from https://www.ncbi.nlm.nih.gov/pubmed/19260470

Baek, G., Tse, Y. F., Hu, Z., Cox, D., Buboltz, N., McCue, P., . . . Witkiewicz, A. K. (2014). MCT4 defines a glycolytic subtype of pancreatic cancer with poor prognosis and unique metabolic dependencies. *Cell Rep, 9*(6), 2233-2249. doi:10.1016/j.celrep.2014.11.025

Baenke, F., Peck, B., Miess, H., & Schulze, A. (2013). Hooked on fat: the role of lipid synthesis in cancer metabolism and tumour development. *Dis Model Mech, 6*(6), 1353-1363. doi:10.1242/dmm.011338

Bailey, P., Chang, D. K., Nones, K., Johns, A. L., Patch, A. M., Gingras, M. C., . . . Grimmond, S. M. (2016). Genomic analyses identify molecular subtypes of pancreatic cancer. *Nature, 531*(7592), 47-52. doi:10.1038/nature16965

Bastidas-Ponce, A., Scheibner, K., Lickert, H., & Bakhti, M. (2017). Cellular and molecular mechanisms coordinating pancreas development. *Development, 144*(16), 2873-2888. doi:10.1242/dev.140756

Basturk, O., Hong, S. M., Wood, L. D., Adsay, N. V., Albores-Saavedra, J., Biankin, A. V., . . . Baltimore Consensus, M. (2015). A Revised Classification System and Recommendations From the Baltimore Consensus Meeting for Neoplastic Precursor Lesions in the Pancreas. *Am J Surg Pathol, 39*(12), 1730-1741. doi:10.1097/PAS.0000000000000533

Beloribi-Djefaflia, S., Vasseur, S., & Guillaumond, F. (2016). Lipid metabolic reprogramming in cancer cells. *Oncogenesis, 5*, e189. doi:10.1038/oncsis.2015.49

Beloueche-Babari, M., Casals Galobart, T., Delgado-Goni, T., Wantuch, S., Parkes, H. G., Tandy, D., . . . Leach, M. O. (2020). Monocarboxylate transporter 1 blockade with AZD3965 inhibits lipid biosynthesis and increases tumour immune cell infiltration. *Br J Cancer, 122*(6), 895-903. doi:10.1038/s41416-019-0717-x

Ben, Q., Xu, M., Ning, X., Liu, J., Hong, S., Huang, W., . . . Li, Z. (2011). Diabetes mellitus and risk of pancreatic cancer: A meta-analysis of cohort studies. *Eur J Cancer, 47*(13), 1928-1937. doi:10.1016/j.ejca.2011.03.003

Benjamin, D., Robay, D., Hindupur, S. K., Pohlmann, J., Colombi, M., El-Shemerly, M. Y., . . . Hall, M. N. (2018). Dual Inhibition of the Lactate Transporters MCT1 and MCT4 Is Synthetic Lethal with Metformin due to NAD+ Depletion in Cancer Cells. *Cell Rep, 25*(11), 3047-3058 e3044. doi:10.1016/j.celrep.2018.11.043

Bensaad, K., Favaro, E., Lewis, C. A., Peck, B., Lord, S., Collins, J. M., . . . Harris, A. L. (2014). Fatty acid uptake and lipid storage induced by HIF-1alpha contribute to cell growth and survival after hypoxia-reoxygenation. *Cell Rep, 9*(1), 349-365. doi:10.1016/j.celrep.2014.08.056

Biancur, D. E., & Kimmelman, A. C. (2018). The plasticity of pancreatic cancer metabolism in tumor progression and therapeutic resistance. *Biochim Biophys Acta Rev Cancer, 1870*(1), 67-75. doi:10.1016/j.bbcan.2018.04.011

Blum, R., & Kloog, Y. (2014). Metabolism addiction in pancreatic cancer. *Cell Death Dis, 5*, e1065. doi:10.1038/cddis.2014.38

Boroughs, L. K., & DeBerardinis, R. J. (2015). Metabolic pathways promoting cancer cell survival and growth. *Nat Cell Biol, 17*(4), 351-359. doi:10.1038/ncb3124

Bosetti, C., Lucenteforte, E., Silverman, D. T., Petersen, G., Bracci, P. M., Ji, B. T., . . . La Vecchia, C. (2012). Cigarette smoking and pancreatic cancer: an analysis from the International Pancreatic Cancer Case-Control Consortium (Panc4). *Ann Oncol, 23*(7), 1880-1888. doi:10.1093/annonc/mdr541

Bray, F., Ferlay, J., Soerjomataram, I., Siegel, R. L., Torre, L. A., & Jemal, A. (2018). Global cancer statistics 2018: GLOBOCAN estimates of incidence and mortality worldwide for 36 cancers in 185 countries. *CA Cancer J Clin, 68*(6), 394-424. doi:10.3322/caac.21492

Brissova, M., Fowler, M. J., Nicholson, W. E., Chu, A., Hirshberg, B., Harlan, D. M., & Powers, A. C. (2005). Assessment of human pancreatic islet architecture and composition by laser scanning confocal microscopy. *J Histochem Cytochem, 53*(9), 1087-1097. doi:10.1369/jhc.5C6684.2005

Bryant, K. L., Mancias, J. D., Kimmelman, A. C., & Der, C. J. (2014). KRAS: feeding pancreatic cancer proliferation. *Trends Biochem Sci, 39*(2), 91-100. doi:10.1016/j.tibs.2013.12.004

Burris, H. A., 3rd, Moore, M. J., Andersen, J., Green, M. R., Rothenberg, M. L., Modiano, M. R., . . . Von Hoff, D. D. (1997). Improvements in survival and clinical benefit with gemcitabine as first-line therapy for patients with advanced pancreas cancer: a randomized trial. *J Clin Oncol, 15*(6), 2403-2413. doi:10.1200/JCO.1997.15.6.2403

Buscail, L., Bournet, B., & Cordelier, P. (2020). Role of oncogenic KRAS in the diagnosis, prognosis and treatment of pancreatic cancer. *Nat Rev Gastroenterol Hepatol, 17*(3), 153-168. doi:10.1038/s41575-019-0245-4

Cabrera, O., Berman, D. M., Kenyon, N. S., Ricordi, C., Berggren, P. O., & Caicedo, A. (2006). The unique cytoarchitecture of human pancreatic islets has implications for islet cell function. *Proc Natl Acad Sci U S A, 103*(7), 2334-2339. doi:10.1073/pnas.0510790103

Cairns, R. A., Harris, I. S., & Mak, T. W. (2011). Regulation of cancer cell metabolism. *Nat Rev Cancer, 11*(2), 85-95. doi:10.1038/nrc2981

Camarda, R., Zhou, A. Y., Kohnz, R. A., Balakrishnan, S., Mahieu, C., Anderton, B., . . . Goga, A. (2016). Inhibition of fatty acid oxidation as a therapy for MYC-overexpressing triple-negative breast cancer. *Nat Med, 22*(4), 427-432. doi:10.1038/nm.4055

Cancer Genome Atlas Research Network. Electronic address, a. a. d. h. e., & Cancer Genome Atlas Research, N. (2017). Integrated Genomic Characterization of Pancreatic Ductal Adenocarcinoma. *Cancer Cell, 32*(2), 185-203 e113. doi:10.1016/j.ccell.2017.07.007

Cantor, J. R., & Sabatini, D. M. (2012). Cancer cell metabolism: one hallmark, many faces. *Cancer Discov, 2*(10), 881-898. doi:10.1158/2159-8290.CD-12-0345

Carracedo, A., Cantley, L. C., & Pandolfi, P. P. (2013). Cancer metabolism: fatty acid oxidation in the limelight. *Nat Rev Cancer, 13*(4), 227-232. doi:10.1038/nrc3483

Chan-Seng-Yue, M., Kim, J. C., Wilson, G. W., Ng, K., Figueroa, E. F., O'Kane, G. M., . . . Notta, F. (2020). Transcription phenotypes of pancreatic cancer are driven by genomic events during tumor evolution. *Nat Genet, 52*(2), 231-240. doi:10.1038/s41588-019-0566-9

Chapman, P. B., Hauschild, A., Robert, C., Haanen, J. B., Ascierto, P., Larkin, J., . . . Group, B.-S. (2011). Improved survival with vemurafenib in melanoma with BRAF V600E mutation. *N Engl J Med, 364*(26), 2507-2516. doi:10.1056/NEJMoa1103782

Chong, J., Soufan, O., Li, C., Caraus, I., Li, S., Bourque, G., . . . Xia, J. (2018). MetaboAnalyst 4.0: towards more transparent and integrative metabolomics analysis. *Nucleic Acids Res, 46*(W1), W486-W494. doi:10.1093/nar/gky310

Christenson, E. S., Jaffee, E., & Azad, N. S. (2020). Current and emerging therapies for patients with advanced pancreatic ductal adenocarcinoma: a bright future. *The Lancet Oncology, 21*(3), e135-e145. doi:10.1016/s1470-2045(19)30795-8

Cnop, M., Hannaert, J. C., Hoorens, A., Eizirik, D. L., & Pipeleers, D. G. (2001). Inverse relationship between cytotoxicity of free fatty acids in pancreatic islet cells and cellular triglyceride accumulation. *Diabetes, 50*(8), 1771-1777. doi:10.2337/diabetes.50.8.1771

Cohen, R., Neuzillet, C., Tijeras-Raballand, A., Faivre, S., de Gramont, A., & Raymond, E. (2015). Targeting cancer cell metabolism in pancreatic adenocarcinoma. *Oncotarget, 6*(19), 16832-16847. doi:10.18632/oncotarget.4160

Colegio, O. R., Chu, N. Q., Szabo, A. L., Chu, T., Rhebergen, A. M., Jairam, V., . . . Medzhitov, R. (2014). Functional polarization of tumour-associated macrophages by tumour-derived lactic acid. *Nature, 513*(7519), 559-563. doi:10.1038/nature13490

Collisson, E. A., Bailey, P., Chang, D. K., & Biankin, A. V. (2019). Molecular subtypes of pancreatic cancer. *Nat Rev Gastroenterol Hepatol, 16*(4), 207-220. doi:10.1038/s41575-019-0109-y

Collisson, E. A., Sadanandam, A., Olson, P., Gibb, W. J., Truitt, M., Gu, S., . . . Gray, J. W. (2011). Subtypes of pancreatic ductal adenocarcinoma and their differing responses to therapy. *Nat Med, 17*(4), 500-503. doi:10.1038/nm.2344

Commisso, C., Davidson, S. M., Soydaner-Azeloglu, R. G., Parker, S. J., Kamphorst, J. J., Hackett, S., . . . Bar-Sagi, D. (2013). Macropinocytosis of protein is an amino acid supply route in Ras-transformed cells. *Nature, 497*(7451), 633-637. doi:10.1038/nature12138

Conroy, T., Desseigne, F., Ychou, M., Bouche, O., Guimbaud, R., Becouarn, Y., . . . Intergroup, P. (2011). FOLFIRINOX versus gemcitabine for metastatic pancreatic cancer. *N Engl J Med, 364*(19), 1817-1825. doi:10.1056/NEJMoa1011923

Cui, X. G., Han, Z. T., He, S. H., Wu, X. D., Chen, T. R., Shao, C. H., . . . Xiao, J. (2017). HIF1/2alpha mediates hypoxia-induced LDHA expression in human pancreatic cancer cells. *Oncotarget, 8*(15), 24840-24852. doi:10.18632/oncotarget.15266

Curtis, N. J., Mooney, L., Hopcroft, L., Michopoulos, F., Whalley, N., Zhong, H., . . . Critchlow, S. E. (2017). Pre-clinical pharmacology of AZD3965, a selective inhibitor of MCT1: DLBCL, NHL and Burkitt's lymphoma anti-tumor activity. *Oncotarget, 8*(41), 69219-69236. doi:10.18632/oncotarget.18215

Daemen, A., Peterson, D., Sahu, N., McCord, R., Du, X., Liu, B., . . . Evangelista, M. (2015). Metabolite profiling stratifies pancreatic ductal adenocarcinomas into subtypes with distinct sensitivities to metabolic inhibitors. *Proc Natl Acad Sci U S A, 112*(32), E4410-4417. doi:10.1073/pnas.1501605112

Davidson, S. M., Jonas, O., Keibler, M. A., Hou, H. W., Luengo, A., Mayers, J. R., . . . Vander Heiden, M. G. (2017). Direct evidence for cancer-cell-autonomous extracellular protein catabolism in pancreatic tumors. *Nat Med, 23*(2), 235-241. doi:10.1038/nm.4256

de Bari, L., & Atlante, A. (2018). Including the mitochondrial metabolism of L-lactate in cancer metabolic reprogramming. *Cell Mol Life Sci, 75*(15), 2763-2776. doi:10.1007/s00018-018-2831-y

DeBerardinis, R. J., Lum, J. J., Hatzivassiliou, G., & Thompson, C. B. (2008). The biology of cancer: metabolic reprogramming fuels cell growth and proliferation. *Cell Metab, 7*(1), 11-20. doi:10.1016/j.cmet.2007.10.002

DeBerardinis, R. J., & Thompson, C. B. (2012). Cellular metabolism and disease: what do metabolic outliers teach us? *Cell, 148*(6), 1132-1144. doi:10.1016/j.cell.2012.02.032

Distler, M., Aust, D., Weitz, J., Pilarsky, C., & Grutzmann, R. (2014). Precursor lesions for sporadic pancreatic cancer: PanIN, IPMN, and MCN. *Biomed Res Int, 2014*, 474905. doi:10.1155/2014/474905

Doherty, J. R., & Cleveland, J. L. (2013). Targeting lactate metabolism for cancer therapeutics. *J Clin Invest, 123*(9), 3685-3692. doi:10.1172/JCI69741

Dolensek, J., Rupnik, M. S., & Stozer, A. (2015). Structural similarities and differences between the human and the mouse pancreas. *Islets, 7*(1), e1024405. doi:10.1080/19382014.2015.1024405

Escoll, P., & Buchrieser, C. (2018). Metabolic reprogramming of host cells upon bacterial infection: Why shift to a Warburg-like metabolism? *FEBS J, 285*(12), 2146-2160. doi:10.1111/febs.14446

Fischer, K., Hoffmann, P., Voelkl, S., Meidenbauer, N., Ammer, J., Edinger, M., . . . Kreutz, M. (2007). Inhibitory effect of tumor cell-derived lactic acid on human T cells. *Blood, 109*(9), 3812-3819. doi:10.1182/blood-2006-07-035972

Furuta, E., Pai, S. K., Zhan, R., Bandyopadhyay, S., Watabe, M., Mo, Y. Y., . . . Watabe, K. (2008). Fatty acid synthase gene is up-regulated by hypoxia via activation of Akt and sterol regulatory element binding protein-1. *Cancer Res, 68*(4), 1003-1011. doi:10.1158/0008-5472.CAN-07-2489

Gallagher, F. A., Woitek, R., McLean, M. A., Gill, A. B., Manzano Garcia, R., Provenzano, E., . . . Brindle, K. M. (2020). Imaging breast cancer using hyperpolarized carbon-13 MRI. *Proc Natl Acad Sci U S A, 117*(4), 2092-2098. doi:10.1073/pnas.1913841117

Golan, T., Hammel, P., Reni, M., Van Cutsem, E., Macarulla, T., Hall, M. J., . . . Kindler, H. L. (2019). Maintenance Olaparib for Germline BRCA-Mutated Metastatic Pancreatic Cancer. *N Engl J Med, 381*(4), 317-327. doi:10.1056/NEJMoa1903387

Golan, T., Kanji, Z. S., Epelbaum, R., Devaud, N., Dagan, E., Holter, S., . . . Gallinger, S. (2014). Overall survival and clinical characteristics of pancreatic cancer in BRCA mutation carriers. *Br J Cancer, 111*(6), 1132-1138. doi:10.1038/bjc.2014.418

Gordon, G. B. (1977). Saturated free fatty acid toxicity. II. Lipid accumulation, ultrastructural alterations, and toxicity in mammalian cells in culture. *Exp Mol Pathol, 27*(2), 262-276. doi:10.1016/0014-4800(77)90035-1

Grasso, C., Jansen, G., & Giovannetti, E. (2017). Drug resistance in pancreatic cancer: Impact of altered energy metabolism. *Crit Rev Oncol Hematol, 114*, 139-152. doi:10.1016/j.critrevonc.2017.03.026

Guillaumond, F., Bidaut, G., Ouaissi, M., Servais, S., Gouirand, V., Olivares, O., . . . Vasseur, S. (2015). Cholesterol uptake disruption, in association with chemotherapy, is a promising combined metabolic therapy for pancreatic adenocarcinoma. *Proc Natl Acad Sci U S A, 112*(8), 2473-2478. doi:10.1073/pnas.1421601112

Guillaumond, F., Leca, J., Olivares, O., Lavaut, M. N., Vidal, N., Berthezene, P., . . . Vasseur, S. (2013). Strengthened glycolysis under hypoxia supports tumor symbiosis and hexosamine biosynthesis in pancreatic adenocarcinoma. *Proc Natl Acad Sci U S A, 110*(10), 3919-3924. doi:10.1073/pnas.1219555110

Halbrook, C. J., & Lyssiotis, C. A. (2017). Employing Metabolism to Improve the Diagnosis and Treatment of Pancreatic Cancer. *Cancer Cell, 31*(1), 5-19. doi:10.1016/j.ccell.2016.12.006

Halestrap, A. P. (2013). Monocarboxylic acid transport. *Compr Physiol, 3*(4), 1611-1643. doi:10.1002/cphy.c130008

Hans G. Beger (Editor), A. L. W. E., Ralph H. Hruban (Editor), Markus W. Buchler (Editor), Markus M. Lerch (Editor), John P. Neoptolemos (Editor), Tooru Shimosegawa (Editor), David C. Whitcomb (Editor) (Ed.) (2018). *The Pancreas: An Integrated Textbook of Basic Science, Medicine, and Surgery, 3rd Edition* (3rd ed.): Wiley-Blackwell.

Hauschild, A., Grob, J. J., Demidov, L. V., Jouary, T., Gutzmer, R., Millward, M., . . . Chapman, P. B. (2012). Dabrafenib in BRAF-mutated metastatic melanoma: a multicentre, open-label, phase 3 randomised controlled trial. *Lancet, 380*(9839), 358-365. doi:10.1016/S0140-6736(12)60868-X

Huang, Li, T., Li, X., Zhang, L., Sun, L., He, X., . . . Zhang, H. (2014). HIF-1-mediated suppression of acyl-CoA dehydrogenases and fatty acid oxidation is critical for cancer progression. *Cell Rep, 8*(6), 1930-1942. doi:10.1016/j.celrep.2014.08.028

Hui, S., Ghergurovich, J. M., Morscher, R. J., Jang, C., Teng, X., Lu, W., . . . Rabinowitz, J. D. (2017). Glucose feeds the TCA cycle via circulating lactate. *Nature, 551*(7678), 115-118. doi:10.1038/nature24057

Jacobs, E. J., Chanock, S. J., Fuchs, C. S., Lacroix, A., McWilliams, R. R., Steplowski, E., . . . Zeleniuch-Jacquotte, A. (2010). Family history of cancer and risk of pancreatic cancer: a pooled analysis from the Pancreatic Cancer Cohort Consortium (PanScan). *Int J Cancer, 127*(6), 1421-1428. doi:10.1002/ijc.25148

Jacobs, S. R., Herman, C. E., Maciver, N. J., Wofford, J. A., Wieman, H. L., Hammen, J. J., & Rathmell, J. C. (2008). Glucose uptake is limiting in T cell activation and requires CD28-mediated Akt-dependent and independent pathways. *J Immunol, 180*(7), 4476-4486. doi:10.4049/jimmunol.180.7.4476

James, A. D., Richardson, D. A., Oh, I. W., Sritangos, P., Attard, T., Barrett, L., & Bruce, J. I. E. (2020). Cutting off the fuel supply to calcium pumps in pancreatic cancer cells: role of pyruvate kinase-M2 (PKM2). *Br J Cancer, 122*(2), 266-278. doi:10.1038/s41416-019-0675-3

Jandaghi, P., Najafabadi, H. S., Bauer, A. S., Papadakis, A. I., Fassan, M., Hall, A., . . . Hoheisel, J. D. (2016). Expression of DRD2 Is Increased in Human Pancreatic Ductal Adenocarcinoma and Inhibitors Slow Tumor Growth in Mice. *Gastroenterology, 151*(6), 1218-1231. doi:10.1053/j.gastro.2016.08.040

Kaissis, G., Ziegelmayer, S., Lohofer, F., Steiger, K., Algul, H., Muckenhuber, A., . . . Braren, R. (2019). A machine learning algorithm predicts molecular subtypes in pancreatic ductal adenocarcinoma with differential response to gemcitabine-based versus FOLFIRINOX chemotherapy. *PLoS One, 14*(10), e0218642. doi:10.1371/journal.pone.0218642

Kalkat, M., De Melo, J., Hickman, K. A., Lourenco, C., Redel, C., Resetca, D., . . . Penn, L. Z. (2017). MYC Deregulation in Primary Human Cancers. *Genes (Basel), 8*(6). doi:10.3390/genes8060151

Kamphorst, J. J., Nofal, M., Commisso, C., Hackett, S. R., Lu, W., Grabocka, E., . . . Rabinowitz, J. D. (2015). Human pancreatic cancer tumors are nutrient poor and tumor cells actively scavenge extracellular protein. *Cancer Res, 75*(3), 544-553. doi:10.1158/0008-5472.CAN-14-2211

Karasinska, J. M., Topham, J. T., Kalloger, S. E., Jang, G. H., Denroche, R. E., Culibrk, L., . . . Schaeffer, D. F. (2020). Altered Gene Expression along the Glycolysis-Cholesterol Synthesis Axis Is Associated with Outcome in Pancreatic Cancer. *Clin Cancer Res, 26*(1), 135-146. doi:10.1158/1078-0432.CCR-19-1543

Kaymak, I., Maier, C. R., Schmitz, W., Campbell, A. D., Dankworth, B., Ade, C. P., . . . Schulze, A. (2020). Mevalonate Pathway Provides Ubiquinone to Maintain Pyrimidine Synthesis and Survival in p53-Deficient Cancer Cells Exposed to Metabolic Stress. *Cancer Res, 80*(2), 189-203. doi:10.1158/0008-5472.CAN-19-0650

Kimmelman, A. C. (2015). Metabolic Dependencies in RAS-Driven Cancers. *Clin Cancer Res, 21*(8), 1828-1834. doi:10.1158/1078-0432.CCR-14-2425

Kimmelman, A. C., & White, E. (2017). Autophagy and Tumor Metabolism. *Cell Metab, 25*(5), 1037-1043. doi:10.1016/j.cmet.2017.04.004

Kleeff, J., Korc, M., Apte, M., La Vecchia, C., Johnson, C. D., Biankin, A. V., . . . Neoptolemos, J. P. (2016). Pancreatic cancer. *Nat Rev Dis Primers, 2*, 16022. doi:10.1038/nrdp.2016.22

Klein, A. P., Brune, K. A., Petersen, G. M., Goggins, M., Tersmette, A. C., Offerhaus, G. J., . . . Hruban, R. H. (2004). Prospective risk of pancreatic cancer in familial pancreatic cancer kindreds. *Cancer Res, 64*(7), 2634-2638. doi:10.1158/0008-5472.can-03-3823

Knudsen, E. S., Balaji, U., Mannakee, B., Vail, P., Eslinger, C., Moxom, C., . . . Witkiewicz, A. K. (2018). Pancreatic cancer cell lines as patient-derived avatars: genetic characterisation and functional utility. *Gut, 67*(3), 508-520. doi:10.1136/gutjnl-2016-313133

Larsen, H. L., & Grapin-Botton, A. (2017). The molecular and morphogenetic basis of pancreas organogenesis. *Semin Cell Dev Biol, 66*, 51-68. doi:10.1016/j.semcdb.2017.01.005

Law, H. C., Lagundzin, D., Clement, E. J., Qiao, F., Wagner, Z. S., Krieger, K. L., . . . Woods, N. T. (2020). The Proteomic Landscape of Pancreatic Ductal Adenocarcinoma Liver Metastases Identifies Molecular Subtypes and Associations with Clinical Response. *Clin Cancer Res, 26*(5), 1065-1076. doi:10.1158/1078-0432.CCR-19-1496

Le Large, T. Y. S., Bijlsma, M. F., Kazemier, G., van Laarhoven, H. W. M., Giovannetti, E., & Jimenez, C. R. (2017). Key biological processes driving metastatic spread of pancreatic cancer as identified by multi-omics studies. *Semin Cancer Biol, 44*, 153-169. doi:10.1016/j.semcancer.2017.03.008

Lehninger, A. (2004). *Lehninger Principles of Biochemistry* (4th ed.): W. H. Freeman.

Lerch, M. M., Mayerle, J., Mahajan, U., Sendler, M., Weiss, F. U., Aghdassi, A., . . . Simon, P. (2016). Development of Pancreatic Cancer: Targets for Early Detection and Treatment. *Dig Dis, 34*(5), 525-531. doi:10.1159/000445233

Lunt, S. Y., & Vander Heiden, M. G. (2011). Aerobic glycolysis: meeting the metabolic requirements of cell proliferation. *Annu Rev Cell Dev Biol, 27*, 441-464. doi:10.1146/annurev-cellbio-092910-154237

Lyssiotis, C. A., & Kimmelman, A. C. (2017). Metabolic Interactions in the Tumor Microenvironment. *Trends Cell Biol, 27*(11), 863-875. doi:10.1016/j.tcb.2017.06.003

Ma, Y., Temkin, S. M., Hawkridge, A. M., Guo, C., Wang, W., Wang, X. Y., & Fang, X. (2018). Fatty acid oxidation: An emerging facet of metabolic transformation in cancer. *Cancer Lett, 435*, 92-100. doi:10.1016/j.canlet.2018.08.006

Mann, K. M., Ying, H., Juan, J., Jenkins, N. A., & Copeland, N. G. (2016). KRAS-related proteins in pancreatic cancer. *Pharmacol Ther, 168*, 29-42. doi:10.1016/j.pharmthera.2016.09.003

Marchiq, I., & Pouyssegur, J. (2016). Hypoxia, cancer metabolism and the therapeutic benefit of targeting lactate/H(+) symporters. *J Mol Med (Berl), 94*(2), 155-171. doi:10.1007/s00109-015-1307-x

Maupin, K. A., Sinha, A., Eugster, E., Miller, J., Ross, J., Paulino, V., . . . Haab, B. B. (2010). Glycogene expression alterations associated with pancreatic cancer epithelial-mesenchymal transition in complementary model systems. *PLoS One, 5*(9), e13002. doi:10.1371/journal.pone.0013002

Menendez, J. A., & Lupu, R. (2007). Fatty acid synthase and the lipogenic phenotype in cancer pathogenesis. *Nat Rev Cancer, 7*(10), 763-777. doi:10.1038/nrc2222

Metallo, C. M., & Vander Heiden, M. G. (2013). Understanding metabolic regulation and its influence on cell physiology. *Mol Cell, 49*(3), 388-398. doi:10.1016/j.molcel.2013.01.018

Moffitt, R. A., Marayati, R., Flate, E. L., Volmar, K. E., Loeza, S. G., Hoadley, K. A., . . . Yeh, J. J. (2015). Virtual microdissection identifies distinct tumor- and stroma-specific subtypes of pancreatic ductal adenocarcinoma. *Nat Genet, 47*(10), 1168-1178. doi:10.1038/ng.3398

Moore, M. J., Goldstein, D., Hamm, J., Figer, A., Hecht, J. R., Gallinger, S., . . . National Cancer Institute of Canada Clinical Trials, G. (2007). Erlotinib plus gemcitabine compared with gemcitabine alone in patients with advanced pancreatic cancer: a phase III trial of the National Cancer Institute of Canada Clinical Trials Group. *J Clin Oncol, 25*(15), 1960-1966. doi:10.1200/JCO.2006.07.9525

Muckenhuber, A., Berger, A. K., Schlitter, A. M., Steiger, K., Konukiewitz, B., Trumpp, A., . . . Weichert, W. (2018). Pancreatic Ductal Adenocarcinoma Subtyping Using the Biomarkers Hepatocyte Nuclear Factor-1A and Cytokeratin-81 Correlates with Outcome and Treatment Response. *Clin Cancer Res, 24*(2), 351-359. doi:10.1158/1078-0432.CCR-17-2180

Mueller, S., Engleitner, T., Maresch, R., Zukowska, M., Lange, S., Kaltenbacher, T., . . . Rad, R. (2018). Evolutionary routes and KRAS dosage define pancreatic cancer phenotypes. *Nature, 554*(7690), 62-68. doi:10.1038/nature25459

Mullen, P. J., Yu, R., Longo, J., Archer, M. C., & Penn, L. Z. (2016). The interplay between cell signalling and the mevalonate pathway in cancer. *Nat Rev Cancer, 16*(11), 718-731. doi:10.1038/nrc.2016.76

Munir, R., Lisec, J., Swinnen, J. V., & Zaidi, N. (2019). Lipid metabolism in cancer cells under metabolic stress. *Br J Cancer, 120*(12), 1090-1098. doi:10.1038/s41416-019-0451-4

Nagtegaal, I. D., Odze, R. D., Klimstra, D., Paradis, V., Rugge, M., Schirmacher, P., . . . Board, W. H. O. C. o. T. E. (2020). The 2019 WHO classification of tumours of the digestive system. *Histopathology, 76*(2), 182-188. doi:10.1111/his.13975

Noll, E. M., Eisen, C., Stenzinger, A., Espinet, E., Muckenhuber, A., Klein, C., . . . Sprick, M. R. (2016). CYP3A5 mediates basal and acquired therapy resistance in different subtypes of pancreatic ductal adenocarcinoma. *Nat Med, 22*(3), 278-287. doi:10.1038/nm.4038

Oldfield, L. E., Connor, A. A., & Gallinger, S. (2017). Molecular Events in the Natural History of Pancreatic Cancer. *Trends Cancer, 3*(5), 336-346. doi:10.1016/j.trecan.2017.04.005

Olivares, O., Mayers, J. R., Gouirand, V., Torrence, M. E., Gicquel, T., Borge, L., . . . Vasseur, S. (2017). Collagen-derived proline promotes pancreatic ductal adenocarcinoma cell survival under nutrient limited conditions. *Nat Commun, 8*, 16031. doi:10.1038/ncomms16031

Orth, M., Metzger, P., Gerum, S., Mayerle, J., Schneider, G., Belka, C., . . . Lauber, K. (2019). Pancreatic ductal adenocarcinoma: biological hallmarks, current status, and future perspectives of combined modality treatment approaches. *Radiat Oncol, 14*(1), 141. doi:10.1186/s13014-019-1345-6

Padanad, M. S., Konstantinidou, G., Venkateswaran, N., Melegari, M., Rindhe, S., Mitsche, M., . . . Scaglioni, P. P. (2016). Fatty Acid Oxidation Mediated by Acyl-CoA Synthetase Long Chain 3 Is Required for Mutant KRAS Lung Tumorigenesis. *Cell Rep, 16*(6), 1614-1628. doi:10.1016/j.celrep.2016.07.009

Patra, K. C., & Hay, N. (2014). The pentose phosphate pathway and cancer. *Trends Biochem Sci, 39*(8), 347-354. doi:10.1016/j.tibs.2014.06.005

Pavlova, N. N., & Thompson, C. B. (2016). The Emerging Hallmarks of Cancer Metabolism. *Cell Metab, 23*(1), 27-47. doi:10.1016/j.cmet.2015.12.006

Pei, H., Li, L., Fridley, B. L., Jenkins, G. D., Kalari, K. R., Lingle, W., . . . Wang, L. (2009). FKBP51 affects cancer cell response to chemotherapy by negatively regulating Akt. *Cancer Cell, 16*(3), 259-266. doi:10.1016/j.ccr.2009.07.016

Peng, X., Chen, Z., Farshidfar, F., Xu, X., Lorenzi, P. L., Wang, Y., . . . Liang, H. (2018). Molecular Characterization and Clinical Relevance of Metabolic Expression Subtypes in Human Cancers. *Cell Rep, 23*(1), 255-269 e254. doi:10.1016/j.celrep.2018.03.077

Perez-Escuredo, J., Dadhich, R. K., Dhup, S., Cacace, A., Van Hee, V. F., De Saedeleer, C. J., . . . Sonveaux, P. (2016). Lactate promotes glutamine uptake and metabolism in oxidative cancer cells. *Cell Cycle, 15*(1), 72-83. doi:10.1080/15384101.2015.1120930

Perou, C. M., Sorlie, T., Eisen, M. B., van de Rijn, M., Jeffrey, S. S., Rees, C. A., . . . Botstein, D. (2000). Molecular portraits of human breast tumours. *Nature, 406*(6797), 747-752. doi:10.1038/35021093

Polanski, R., Hodgkinson, C. L., Fusi, A., Nonaka, D., Priest, L., Kelly, P., . . . Morrow, C. J. (2014). Activity of the monocarboxylate transporter 1 inhibitor AZD3965 in small cell lung cancer. *Clin Cancer Res, 20*(4), 926-937. doi:10.1158/1078-0432.CCR-13-2270

Qin, C., Yang, G., Yang, J., Ren, B., Wang, H., Chen, G., . . . Zhao, Y. (2020). Metabolism of pancreatic cancer: paving the way to better anticancer strategies. *Mol Cancer, 19*(1), 50. doi:10.1186/s12943-020-01169-7

Reddy, R. P., Smyrk, T. C., Zapiach, M., Levy, M. J., Pearson, R. K., Clain, J. E., . . . Chari, S. T. (2004). Pancreatic mucinous cystic neoplasm defined by ovarian stroma: demographics, clinical features, and prevalence of cancer. *Clin Gastroenterol Hepatol, 2*(11), 1026-1031. doi:10.1016/s1542-3565(04)00450-1

Rohrig, F., & Schulze, A. (2016). The multifaceted roles of fatty acid synthesis in cancer. *Nat Rev Cancer, 16*(11), 732-749. doi:10.1038/nrc.2016.89

Rosell, R., Carcereny, E., Gervais, R., Vergnenegre, A., Massuti, B., Felip, E., . . . Associazione Italiana Oncologia, T. (2012). Erlotinib versus standard chemotherapy as first-line treatment for European patients with advanced EGFR mutation-positive non-small-cell lung cancer (EURTAC): a multicentre, open-label, randomised phase 3 trial. *Lancet Oncol, 13*(3), 239-246. doi:10.1016/S1470-2045(11)70393-X

Rossi Sebastiano, M., & Konstantinidou, G. (2019). Targeting Long Chain Acyl-CoA Synthetases for Cancer Therapy. *Int J Mol Sci, 20*(15). doi:10.3390/ijms20153624

Ryan, D. P., Hong, T. S., & Bardeesy, N. (2014). Pancreatic adenocarcinoma. *N Engl J Med, 371*(22), 2140-2141. doi:10.1056/NEJMc1412266

Rysman, E., Brusselmans, K., Scheys, K., Timmermans, L., Derua, R., Munck, S., . . . Swinnen, J. V. (2010). De novo lipogenesis protects cancer cells from free radicals and chemotherapeutics by promoting membrane lipid saturation. *Cancer Res, 70*(20), 8117-8126. doi:10.1158/0008-5472.CAN-09-3871

Saiki, Y., & Horii, A. (2014). Molecular pathology of pancreatic cancer. *Pathol Int, 64*(1), 10-19. doi:10.1111/pin.12114

Saung, M. T., & Zheng, L. (2017). Current Standards of Chemotherapy for Pancreatic Cancer. *Clin Ther, 39*(11), 2125-2134. doi:10.1016/j.clinthera.2017.08.015

Schulze, A., & Harris, A. L. (2012). How cancer metabolism is tuned for proliferation and vulnerable to disruption. *Nature, 491*(7424), 364-373. doi:10.1038/nature11706

Shih, H. P., Wang, A., & Sander, M. (2013). Pancreas organogenesis: from lineage determination to morphogenesis. *Annu Rev Cell Dev Biol, 29*, 81-105. doi:10.1146/annurev-cellbio-101512-122405

Singh, S., Hasselluhn, M. C., & Neesse, A. (2019). A tangled tale of molecular subtypes in pancreatic cancer. *Gut, 68*(6), 953-954. doi:10.1136/gutjnl-2018-318086

Slamon, D. J., Leyland-Jones, B., Shak, S., Fuchs, H., Paton, V., Bajamonde, A., . . . Norton, L. (2001). Use of chemotherapy plus a monoclonal antibody against HER2 for metastatic breast cancer that overexpresses HER2. *N Engl J Med, 344*(11), 783-792. doi:10.1056/NEJM200103153441101

Snaebjornsson, M. T., Janaki-Raman, S., & Schulze, A. (2020). Greasing the Wheels of the Cancer Machine: The Role of Lipid Metabolism in Cancer. *Cell Metab, 31*(1), 62-76. doi:10.1016/j.cmet.2019.11.010

Sommariva, M., & Gagliano, N. (2020). E-Cadherin in Pancreatic Ductal Adenocarcinoma: A Multifaceted Actor during EMT. *Cells, 9*(4). doi:10.3390/cells9041040

Son, J., Lyssiotis, C. A., Ying, H., Wang, X., Hua, S., Ligorio, M., . . . Kimmelman, A. C. (2013). Glutamine supports pancreatic cancer growth through a KRAS-regulated metabolic pathway. *Nature, 496*(7443), 101-105. doi:10.1038/nature12040

Sousa, C. M., Biancur, D. E., Wang, X., Halbrook, C. J., Sherman, M. H., Zhang, L., . . . Kimmelman, A. C. (2016). Pancreatic stellate cells support tumour metabolism through autophagic alanine secretion. *Nature, 536*(7617), 479-483. doi:10.1038/nature19084

Sunami, Y., Rebelo, A., & Kleeff, J. (2017). Lipid Metabolism and Lipid Droplets in Pancreatic Cancer and Stellate Cells. *Cancers (Basel), 10*(1). doi:10.3390/cancers10010003

Tamada, M., Suematsu, M., & Saya, H. (2012). Pyruvate kinase M2: multiple faces for conferring benefits on cancer cells. *Clin Cancer Res, 18*(20), 5554-5561. doi:10.1158/1078-0432.CCR-12-0859

Tasdogan, A., Faubert, B., Ramesh, V., Ubellacker, J. M., Shen, B., Solmonson, A., . . . Morrison, S. J. (2020). Metabolic heterogeneity confers differences in melanoma metastatic potential. *Nature, 577*(7788), 115-120. doi:10.1038/s41586-019-1847-2

Tsimberidou, A. M. (2015). Targeted therapy in cancer. *Cancer Chemother Pharmacol, 76*(6), 1113-1132. doi:10.1007/s00280-015-2861-1

van, I. S. C. D., Agnetti, J., & Gassama-Diagne, A. (2020). Mechanisms behind the polarized distribution of lipids in epithelial cells. *Biochim Biophys Acta Biomembr, 1862*(2), 183145. doi:10.1016/j.bbamem.2019.183145

Vander Heiden, M. G., Locasale, J. W., Swanson, K. D., Sharfi, H., Heffron, G. J., Amador-Noguez, D., . . . Cantley, L. C. (2010). Evidence for an alternative glycolytic pathway in rapidly proliferating cells. *Science, 329*(5998), 1492-1499. doi:10.1126/science.1188015

Von Hoff, D. D., Ervin, T., Arena, F. P., Chiorean, E. G., Infante, J., Moore, M., . . . Renschler, M. F. (2013). Increased survival in pancreatic cancer with nab-paclitaxel plus gemcitabine. *N Engl J Med, 369*(18), 1691-1703. doi:10.1056/NEJMoa1304369

Waddell, N., Pajic, M., Patch, A. M., Chang, D. K., Kassahn, K. S., Bailey, P., . . . Grimmond, S. M. (2015). Whole genomes redefine the mutational landscape of pancreatic cancer. *Nature, 518*(7540), 495-501. doi:10.1038/nature14169

Warburg, O. (1956). On the origin of cancer cells. *Science, 123*(3191), 309-314. doi:10.1126/science.123.3191.309

Winkelkotte, A. (2018). *Metabolic sensitization of Pancreatic Ductal Adenocarcinoma for chemotherapy.* (Master of Science). University of Duisburg-Essen, Essen.

Wishart, D. S., Feunang, Y. D., Marcu, A., Guo, A. C., Liang, K., Vazquez-Fresno, R., . . . Scalbert, A. (2018). HMDB 4.0: the human metabolome database for 2018. *Nucleic Acids Res, 46*(D1), D608-D617. doi:10.1093/nar/gkx1089

Witkiewicz, A. K., Balaji, U., Eslinger, C., McMillan, E., Conway, W., Posner, B., . . . Knudsen, E. S. (2016). Integrated Patient-Derived Models Delineate Individualized Therapeutic Vulnerabilities of Pancreatic Cancer. *Cell Rep, 16*(7), 2017-2031. doi:10.1016/j.celrep.2016.07.023

Witkiewicz, A. K., McMillan, E. A., Balaji, U., Baek, G., Lin, W. C., Mansour, J., . . . Knudsen, E. S. (2015). Whole-exome sequencing of pancreatic cancer defines genetic diversity and therapeutic targets. *Nat Commun, 6*, 6744. doi:10.1038/ncomms7744

Yang, A., Rajeshkumar, N. V., Wang, X., Yabuuchi, S., Alexander, B. M., Chu, G. C., . . . Kimmelman, A. C. (2014). Autophagy is critical for pancreatic tumor growth and progression in tumors with p53 alterations. *Cancer Discov, 4*(8), 905-913. doi:10.1158/2159-8290.CD-14-0362

Yang, L., Venneti, S., & Nagrath, D. (2017). Glutaminolysis: A Hallmark of Cancer Metabolism. *Annu Rev Biomed Eng, 19*, 163-194. doi:10.1146/annurev-bioeng-071516-044546

Yang, S., Wang, X., Contino, G., Liesa, M., Sahin, E., Ying, H., . . . Kimmelman, A. C. (2011). Pancreatic cancers require autophagy for tumor growth. *Genes Dev, 25*(7), 717-729. doi:10.1101/gad.2016111

Yao, W., Maitra, A., & Ying, H. (2020). Recent insights into the biology of pancreatic cancer. *EBioMedicine*, 102655. doi:10.1016/j.ebiom.2020.102655

Ye, H., Zhou, Q., Zheng, S., Li, G., Lin, Q., Wei, L., . . . Chen, R. (2018). Tumor-associated macrophages promote progression and the Warburg effect via CCL18/NF-kB/VCAM-1 pathway in pancreatic ductal adenocarcinoma. *Cell Death Dis, 9*(5), 453. doi:10.1038/s41419-018-0486-0

Ying, H., Dey, P., Yao, W., Kimmelman, A. C., Draetta, G. F., Maitra, A., & DePinho, R. A. (2016). Genetics and biology of pancreatic ductal adenocarcinoma. *Genes Dev, 30*(4), 355-385. doi:10.1101/gad.275776.115

Ying, H., Kimmelman, A. C., Lyssiotis, C. A., Hua, S., Chu, G. C., Fletcher-Sananikone, E., . . . DePinho, R. A. (2012). Oncogenic Kras maintains pancreatic tumors through regulation of anabolic glucose metabolism. *Cell, 149*(3), 656-670. doi:10.1016/j.cell.2012.01.058

Zamboni, G., Hirabayashi, K., Castelli, P., & Lennon, A. M. (2013). Precancerous lesions of the pancreas. *Best Pract Res Clin Gastroenterol, 27*(2), 299-322. doi:10.1016/j.bpg.2013.04.001

Zdralevic, M., Brand, A., Di Ianni, L., Dettmer, K., Reinders, J., Singer, K., . . . Kreutz, M. (2018). Double genetic disruption of lactate dehydrogenases A and B is required to ablate the "Warburg effect" restricting tumor growth to oxidative metabolism. *J Biol Chem, 293*(41), 15947-15961. doi:10.1074/jbc.RA118.004180

Zhang, X., Saarinen, A. M., Hitosugi, T., Wang, Z., Wang, L., Ho, T. H., & Liu, J. (2017). Inhibition of intracellular lipolysis promotes human cancer cell adaptation to hypoxia. *Elife, 6*. doi:10.7554/eLife.31132

Zhou, Q., & Melton, D. A. (2018). Pancreas regeneration. *Nature, 557*(7705), 351-358. doi:10.1038/s41586-018-0088-0

Acknowledgements

First of all, I would like to pay my special regards to Prof. Jens T. Siveke for giving me this once-in-a-lifetime opportunity by accepting me as a PhD student in his group, for his scientific and financial support during the project.

I would like to express my deepest appreciation to Dr. Marija Trajkovic-Arsic for enlightening my way through the project, for sharing her scientific expertise and knowledge and for amazing personal and professional guidance through my time in the lab.

I would like to extend my sincere thanks to Dr. Smiths S. Lueong, Dr. Phyllis Fung-Yi Cheung and Dr. Sven T. Liffers for sharing their scientific expertise and practical suggestions.

I am also grateful to Prof. Dr. Alexander Rösch and Prof. Dr. Björn Scheffler, who joined the Thesis Advisory Committee, for their supervision, helpful advice and time.

I am extremely grateful to my colleagues and friends, Chris, Anna, F.Glenamann, Alina, Tim, Kostas, Svenja, Ben, Desiree, Corinna, Yang, F.Lang and Laura for their support and for making me feel home every day.

Also, I would like to thank all the members of our group for the welcoming and pleasant environment in the lab.

I am also thankful to my friends back in Turkey, Talha, Özge, Ali İhsan, Ata, Onur, Serhat, Eren, Burcin, İpek, Kagan, Hakan who never make me feel alone by calling, listening and visiting me during my stay in Germany.

Additionally, I am also extremely grateful to my friend, Dr. Yasemin Furtun Uçal, for encouraging me to apply to the position and for her invaluable and constructive advice on metabolic data analysis.

Finally, I am deeply indebted to my parents, my sisters as well as my girlfriend for their love, support and faith since the beginning of my doctoral studies.

Declaration:

In accordance with § 6 (para. 2, clause g) of the Regulations Governing the Doctoral Proceedings of the Faculty of Biology for awarding the doctoral degree Dr. rer. nat., I hereby declare that I represent the field to which the topic "*Metabolic subtyping and targeting of pancreatic ductal adenocarcinoma"* is assigned in research and teaching and that I support the application of Sinan Karakaya.

Essen, date _____ _____ _____

Name of the scientific supervisor/member of the University of Duisburg-Essen	Signature of the supervisor/ member of the University of Duisburg-Essen

Declaration:

In accordance with § 7 (para. 2, clause d and f) of the Regulations Governing the Doctoral Proceedings of the Faculty of Biology for awarding the doctoral degree Dr. rer. nat., I hereby declare that I have written the herewith submitted dissertation independently using only the materials listed, and have cited all sources taken over verbatim or in content as such.

Essen, date _____ _____

Signature of the doctoral candidate

Declaration:

In accordance with § 7 (para. 2, clause e and g) of the Regulations Governing the Doctoral Proceedings of the Faculty of Biology for awarding the doctoral degree Dr. rer. nat., I hereby declare that I have undertaken no previous attempts to attain a doctoral degree, that the current work has not been rejected by any other faculty, and that I am submitting the dissertation only in this procedure.

Essen, date _____ _____

Signature of the doctoral candidate

Curriculum Vitae

Personal Information

Aus datenschutzrechtlichen Gründen ist der Lebenslauf in der Online-Version nicht enthalten.

For data protection reasons, the CV is not included in the online version

Publications

Karakaya S., Heid I., Münch C., Winkelkotte A., Lueong S. S., Liffers T. S., Trajkovic-Arsic M. and Siveke T. J. Glycolysis is a hallmark of quasi-mesenchymal PDAC subtype and can be detected *in vivo.* (Manuscript in preparation)

Honours & Awards

02/2020	European Association for Cancer Research (EACR) - Worldwide Cancer Research Meeting Bursary
06/2017-06/2020	German Cancer Research Center International PhD Program Studentship
07/2011	University of Nottingham Turkey Masters' Scholarship

Talks & Poster Presentations

02/2020	5th EACR conference on A Matter of Life or Death, Bergamo, Italy, Flash talk & Poster,
02/2020	Essener Translational Oncology Symposium 2020, Essen, Germany, Poster
11/2019	Science Day 2019, Essen, Germany, Poster
02/2019	39th Annual meeting of German Pancreas Club, Gottingen, Germany, Poster
02/2019	Essener Translational Oncology Symposium 2019, Essen, Germany, Poster
11/2018	WTZ Research Meeting, Essen, Germany, Scientific talk
07/2018	German Cancer Consortium (DKTK) Retreat Essen/Dusseldorf, Raesfeld, Germany, Scientific talk
01/2018	Essener Translational Oncology Symposium 2018, Essen, Germany, Poster
10/2017	Summer School in Translational Cancer Research, Albufeira, Portugal, Poster